Catamaran Wetdeck Slamming – A Numerical and Experimental Investigation

by

Ahmed Abdelwahab Swidan

BSc (Mechanical Engineering) (Hons), MSc (Marine Engineering), P.Eng

National Centre for Maritime Engineering and Hydrodynamics

Australian Maritime College

Submitted in fulfilment of the requirements for the degree of Doctor of Philosophy

University of Tasmania

June 2016

Statement of Co-authorship

Chapters 2 - 6 of this thesis have been written as scientific (peer-reviewed) papers. All numerical simulation, experimental design, data analysis and manuscript preparations were the primary responsibility of the candidate. However the following people contributed to the publication of work undertaken as part of this thesis:

Candidate		Ahmed A. Swidan	University of Tasmania
Author 1	Professor	Giles Thomas	University College London
Author 2	Professor	Dev Ranmuthugala	University of Tasmania
Author 3	Associate Professor	Irene Penesis	University of Tasmania
Author 4	Dr	Walid Amin	University of Tasmania
Author 5	Dr	Tom Allen	University of Auckland
Author 6	Professor	Mark Battley	University of Auckland

Publication list and proportion of work details:

Chapter 2 – (Paper 1 – Published in World Journal of Mechanics)

Numerical prediction of symmetric water impact loads on wedge shaped hull form using CFD (2013).

Candidate was the primary author. Authors 1, 2, 3 and 4 contributed to the design of the analysis, its formulation and development. Authors 1, 2, 3 and 4 provided top level of consultancy advice and manuscript preparation assistance.

[Candidate: 80%, Author 1: 5%, Author 2: 5%, Author 3: 5%, Author 4: 5%]

Chapter 3 – (Paper 2 – In proceedings of the 10th Symposium on high-speed marine vessels (HSMV))

Numerical investigation of water slamming loads on wave-piercing catamaran hull model (2014).

Candidate was the primary author. Authors 1, 2, 3 and 4 contributed to the design of the analysis, its formulation and development. Authors 1, 2 and 3 provided top level of consultancy advice and manuscript refinement assistance.

[Candidate: 75%, Author 1: 8%, Author 2: 7%, Author 3: 5%, Author 4: 5%]

Chapter 4 – (Paper 3 – Published in Ocean Engineering)

Experimental drop test investigation into wetdeck slamming loads on a generic catamaran hullform (2016).

Candidate was the primary author. Author 1 provided lead consultancy advice, technical input and contributed in the design of analysis its formulation and development. Authors 5 and 6 provided the opportunity to conduct experiments using their advanced controlled speed test facility with top level technical assistance during experiments and manuscript preparation. Authors 2, 3 and 4 provided top level consultancy advice and manuscript refinement assistance.

[Candidate: 75%, Author 1: 10%, Author 2: 3%, Author 3: 3%, Author 4: 3%, Author 5: 3%, Author 6: 3%]

Chapter 5 - (Paper 4 – Published in Ships and Offshore Structures)

Wetdeck slamming loads on a developed catamaran hullform - Experimental investigation (2016).

Candidate was the primary author. All co-authors provided consultancy advice and contributed in the design of analysis its formulation and development. Authors 1, 2, 3, 4 and 5 provided manuscript refinement assistance.

[Candidate: 76%, Author 1: 10%, Author 2: 3%, Author 3: 3%, Author 4: 3%, Author 5: 3%, Author 6: 2%]

Chapter 6 - (Paper 5 - In proceedings of the 13th international conference on fast sea transportation (FAST)

Prediction of slamming loads on catamaran wetdeck using CFD (2015).

Candidate was the primary author. Authors 1, 2 and 3 contributed to the design of the analysis its formulation and development. Authors 1, 4, 5 and 6 provided top level of consultancy advice and manuscript refinement assistance.

[Candidate: 81%, Author 1: 6%, Author 2: 6%, Author 3: 3%, Author 4: 1%, Author 5: 1%, Author 6: 1%]

DECLARATIONS

Authority of Access

The publishers of the papers comprising Chapters 2 – 6 hold the copyright for that content, and access to the material should be sought from the respective journals/proceedings. The remaining non published content of this thesis may be made available for loan and limited copying and communication in accordance with the Copyright Act 1968.

Statement of Originality

This thesis contains no material which has been accepted for a degree or diploma by the University or any other institution, except by way of background information and duly acknowledged in the thesis, and to the best of my knowledge and belief no material previously published or written by another person except where due acknowledgement is made in the text of the thesis, nor does the thesis contain any material that infringes copyright.

Signed: ……... Date: 23/06/2016

Name: Ahmed Abdelwahab Wahby Swidan

We the undersigned agree with the above stated "proportion of work undertaken" for each of the above published peer-reviewed manuscripts contributing to this thesis

Signed:

Signature: ……... Date: 24/06/2016

Associate Professor Irene Penesis

Principal Supervisor

National Centre for Maritime Engineering and Hydrodynamics, University of Tasmania

---

Signature: ……... Date: 24/06/2016

Professor Giles A. Thomas

Co-Supervisor

Department of Mechanical Engineering, University College London

---

Signature: ……... Date: 24/06/2016

Professor Dev Ranmuthugala

Co-Supervisor

National Centre for Ports and Shipping, University of Tasmania

---

Signature: ……... Date: 24/06/2016

Dr Walid Amin

Co-Supervisor

National Centre for Maritime Engineering and Hydrodynamics, University of Tasmania

---

Signature: ……... Date: 14/04/2016

Dr Tom Allen

Signature: ……... Date: 14/04/2016

Professor Mark Battley

[Academic partners]

National Centre for Advanced Composite Materials, University of Auckland

---

[Page intentionally left blank]

ABSTRACT

High-speed catamarans have, over the past two decades, extended their service areas from protected waters to the open ocean where impacts with waves can result in structural damage. The work detailed in this thesis investigates the hydrodynamic loads experienced by wave-piercer catamarans during water impacts using a combination of experimental and numerical techniques. This work is aimed at addressing the lack of high-quality three-dimensional (3D) experimental data suitable for benchmarking catamaran vessels impacting with water in a 3D regime, as well as establishing an understanding of the key elements influencing the severity of wetdeck slamming loads. It also aims to evaluate the accuracy of numerical techniques by utilising Computational Fluid Dynamics (CFD) simulations to predict the magnitude of wetdeck slamming forces and pressure distributions, thus allowing ship designers to improve catamaran hull designs.

A quasi two-dimensional (quasi-2D) simulation of a wedge shaped hullform impacting with water was validated against existing free-fall experimental data and compared to previously published numerical simulations using Smoothed Particle Hydrodynamics (SPH), with the CFD results showing better agreement with the experimental data than the SPH predictions. CFD simulations were then used to investigate the behaviour of a quasi-2D catamaran hull section with a centrebow during water-entry. The computed 2D vertical acceleration and slamming pressures are comparable to previously published drop test experimental data. With the lack of existing 3D water-impact experimental validation data for wave-piercer catamaran hullforms, two series of water-impact experiments were performed to investigate the hydrodynamic loads experienced by a generic wave-piercer catamaran hullform with two interchangeable centrebow sections during water impacts. The experiments, which focused on the characterisation of the unsteady slam loads on an arched wetdeck, were conducted using a Servo-hydraulic Slam Testing System (SSTS) allowing the model to penetrate a body of water at a range of constant speeds and two trim angles.

The systematic and random uncertainties associated with the controlled speed test results are quantified in detail. These experiments therefore provide a new dataset for the slam pressure distributions and forces on the arched wetdeck structure of catamaran vessels.

Strong relationships between slam force peaks and impact velocity are observed as a function of relative impact angle and centrebow geometry, with a possible reduction for a newly-developed centrebow. The three dimensionality of the water flow in these slam test events is characterised. It was also found that the limited pressure measurements along the archway were not representative of wetdeck slamming loads. High localised pressure is affected by jet formation or localised flow effects. Total slamming load is governed by the relative impact velocity and the rate of change of added mass and is not necessarily strongly related to localised pressure distributions.

The 3D CFD simulations provide information on the different techniques and settings required to accurately model such unsteady events. The CFD simulations were able to accurately characterise 3D wetdeck slamming loads of catamaran vessels and quantify the splitting force (i.e. the component of slamming force that mainly acts on demihulls and centrebow in the transverse direction) that occurs concurrently with the wetdeck slamming event.

[Page intentionally left blank]

ACKNOWLEDGMENTS

I would like to thank my friends and colleagues at the University of Tasmania, University of Auckland, Incat Tasmania and Revolution Design for the support they have provided during the course of this project. With a great pleasure I would like to acknowledge and thank the following people.

The Brains Trust

I am sincerely grateful to my academic supervisors:

- Professor Giles Thomas at the University College London; communicating via Skype and email, for his project direction, contributions to the thesis, lead consultancy advice, technical input and top level of support throughout my PhD study. I have learned from Professor Giles Thomas many valuable things, so thank you.
- Professor Dev Ranmuthugala for his technical input, top level of consultancy advice, contributions to the thesis, valuable support and brilliant suggestions. Professor Dev's advices on both research and career have been priceless, so thank you.
- Associate Professor Irene Penesis for her aspiring guidance, time, valuable support and consultancy advice throughout my PhD study.
- Dr Walid Amin for his support, time and consultancy advice.

The Australian Maritime College, University of Tasmania

For awarding a full-time scholarship to the author and for providing cutting edge technology and financial support throughout my PhD journey, i.e. to conduct series of experiments in collaboration with University of Auckland in New Zealand and to present my results at two prestigious international conferences .

The University of Auckland (academic partner)

The presented experimental data were recorded at the Industrial Research Limited (IRL) in Auckland, New Zealand under the supervision of Professor Mark Battley and Dr Tom Allen at the Centre for Advanced Composite Materials, University of Auckland.

I am grateful to Dr Tom Allen and Professor Mark Battley for their time, humour, technical input and extensive support.

Revolution Design and Incat (industry partner)

The author acknowledges the ongoing support of Revolution Design and Incat for the research undertaken in collaboration with AMC, UTAS.

The Arab Academy for Science, Technology and Maritime Transport (AAST)

I would like to express my gratitude to the Arab Academy for Science, Technology and Maritime Transport for financial support during my PhD study leave. I have always appreciated belonging to the Maritime College, AAST, but never more so than like now.

I have been particularly grateful for Prof. Ismail Abdel-Ghaffar the President of AAST for his extensive support to researchers at AAST. Many thanks also go to Professor Gamal Ibrahim Selim, Dr. Mohi Elsayeh, Dr Nasr Abdel-Rahaman, Professor Said Abdel-Kadder, Eng Mohamed Eweda, Professor Saad Eldin Mesbah and Professor Amr Ali for the administrative support they provided.

I am also thankful to my supervisors during my MSc study (Professor M. Kotb, Professor E. Hegazy and Assoc. Professor A. Naguib). I have been particularly grateful to Associate Professor Ahmed Naguib, your kindness goes along way and makes this world a beautiful and a better place to live. Without your recommendation and support this journey would have never been started, so thank you.

My family

"I wholeheartedly thank mighty God for the family He graciously provided".

To my Dad Abdelwahab Wahby, my Mum Khadija, my Sister Dr Heba and my Brothers Dr Mohamed and Captain Alaa; this dissertation is dedicated to all of you with my love.

This research project was in collaboration between the Australian Maritime College, University of Tasmania, Revolution Design, Incat Tasmania and the University of Auckland.

CONTENTS

1 INTRODUCTION 1

1.1 BACKGROUND 1
1.2 PROBLEM DEFINITION 4
1.3 WETDECK SLAMMING PREDICTION 5
1.4 RESEARCH QUESTIONS AND OBJECTIVES 8
1.5 METHODOLOGY 9
1.6 CFD APPROACHES 10
1.7 EXPERIMENTAL APPROACHES 11

2 VERIFICATION AND VALIDATION OF CFD METHOD 15

2.1 INTRODUCTION 16
2.2 NUMERICAL SIMULATION OF FREE FALLING WEDGE ENTRY 16
2.3 SPH METHOD 23
2.4 MODEL TESTS 23
2.5 RESULTS AND DISCUSSIONS 24
2.6 CONCLUSIONS 27
2.7 NEXT STEPS 28

3 PREDICTIONS OF QUASI-2D WETDECK SLAM LOADS 29

3.1 INTRODUCTION 30
3.2 NUMERICAL SIMULATION 31
3.3 COMPUTATIONAL SET-UP 32
3.3.1 Grid generation 32
3.3.2 Initial and boundary conditions 34
3.3.3 Governing equations 35
3.3.4 Uncertainty analysis 36
3.4 RESULTS AND DISCUSSION 41
3.5 CONCLUSIONS 46
3.6 NEXT STEPS 47

4 EXPERIMENTAL INVESTIGATION INTO WETDECK SLAMMING LOADS 48

4.1 INTRODUCTION 49
4.2 MODEL AND EXPERIMENTAL SETUP 49
4.2.1 The controlled speed test system 49
4.2.2 The test model 50
4.2.3 Instrumentation 52
4.2.4 Test conditions 54
4.3 UNCERTAINTY ANALYSIS 55
4.3.1 Random uncertainties 55
4.3.2 Systematic uncertainties 59
4.3.3 Velocity variations 59
4.3.4 Filtering 60
4.4 RESULTS AND DISCUSSION 61
4.4.1 Time history results 61
4.4.2 Influence of impact velocity 67
4.4.3 Three-dimensional effect 69
4.5 CONCLUSIONS 71

4.6 NEXT STEPS 73
5 CHARACTERISTICS OF WETDECK SLAM EVENTS 74
5.1 INTRODUCTION 75
5.2 MODEL AND EXPERIMENTAL SETUP 76
5.2.1 The test system 76
5.2.2 Instrumentation 76
5.2.3 The test model 77
5.2.4 Test conditions 79
5.3 RESULTS AND DISCUSSION 80
5.3.1 Slamming force 80
5.3.2 Pressure distributions 86
5.4 CONCLUSIONS 89
5.5 NEXT STEPS 90
6 PREDICTION OF 3D WETDECK SLAM LOADS 91
6.1 INTRODUCTION 92
6.1 NUMERICAL METHOD 92
6.2 GRID INDEPENDENCE STUDY 95
6.3 RESULTS AND DISCUSSION 97
6.4 CONCLUSIONS 101
7 CONCLUSIONS AND FUTURE WORK 102
7.1 SUMMARY 102
7.2 CONCLUSIONS 103
7.3 IMPLICATIONS TO THE INDUSTRY 105
7.4 FUTURE WORK 106
APPENDICES 117
I CFD TESTED PARAMETERS 117
II REPEATABILITY 120
III PRESSURE COEFFICIENTS 123
IV SIMULATED FLOW BEHAVIOUR 126
V INSTRUMENTATION DATA SHEETS 129

LIST OF FIGURES

Fig. 1.1: *Kat Express 2,* high-speed wave-piercing catamaran, LOA = 112m (Incat, 2013).1

Fig. 1.2: Tassie Devil 2001, the original wave-piercing catamaran fitted with centrebow, LOA = 31m (Incat, 1986). 2

Fig. 1.3:Schematic diagram of bow section for an Incat wave-piercing catamaran. 2

Fig. 1.4: Fore section of an Incat wave-piercing catmataran, LOA = 112m showing the protected and unprotected structures at the bow section with approximately 20% of LOA. 3

Fig. 1.5: Structural damage due to wetdeck slamming on *HSS Stena Discovery*, in 1997 (Thomas, 2003). 4

Fig. 2.1: Schematic drop test diagram. 17

Fig. 2.2: 2D computational domain (wedge shaped hull model) 18

Fig. 2.3: The scalar fields for the background and overset regions. 19

Fig. 2.4: Half of the transducer geometry. (a) Shows a course grid with 1.2 mm (b) Shows a fine grid with 0.3 mm. 20

Fig. 2.5: Symmetry view of the free falling wedge's grids. 20

Fig. 2.6: The effect of grid size on the computed pressure at pressure transducer No.1. 22

Fig. 2.7: The effect of time step (Δs) on the computed pressure at pressure transducer No.1. 22

Fig. 2.8: The effect of two time steps in predicting P2. 22

Fig. 2.9: The effect of two time steps in predicting P4. 22

Fig. 2.10: Quasi-2D free-falling drop test tank at the University of Tasmania. 24

Fig. 2.11:Shifting positions of pressure transducer No.3 by ±1.9 mm. 25

Fig. 2.12: The effect of the location of pressure transducers on the computed pressure. 25

Fig. 2.13: 25° deadrise angle wedge shaped hullform during water-entry. Showing subplot (a) pressure contours and subplot (b) illustrates corresponding jet evolution that concurrent with P3 pressure peak. 25

Fig. 2.14: Wedge vertical translation with respect to time. 26

Fig. 2.15: Wedge vertical velocity with respect to time. 26

Fig. 2.16: Wedge vertical acceleration with respect to time. 27

Fig. 2.17: Pressure time-histories at P3. Showing computed pressures using CFD and SPH (Shahraki et al., 2011) in relation to past experimental data recorded by Whelan (2004). 27

Fig. 3.1: Incat 112m high-speed catamaran fitted with centrebow (Maritime Denmark, 2013) 30

Fig. 3.2: Positions of four pressure transducers on the wave piercer model. 31

Fig. 3.3: Wave piercer model and tank dimensions. 32

Fig. 3.4: Symmetry, side and perspective, views of initial general arrangement of the numerical model and the tank side. 33

Fig. 3.5: Two perspective views of (a) cross-section in grids of quarter wave piercer numerical model and (b) transparent grid showing the overlap region. 34

Fig. 3.6: A transverse section in the grid of the computational domain; showing the boundary conditions and one quarter of the numerical tested model of quasi-2D catamaran. 35

Fig. 3.7: Sensitivity to the grid resolution at 5 mm venting clearance. 37

Fig. 3.8: Venting clearance error study and corresponding time record uncertainty of vertical acceleration and slamming pressures distribution. 38

Fig. 3.9: Sensitivity grid study vs. drop test data 39

Fig. 3.10: Computed free surface elevations as a function of time (on left) versus experimental water-entry of catamaran model (on right), as recorded by high-speed photography by Whelan (2004). 40

Fig. 3.11: Vertical acceleration of Incat model as a function of time. 42

Fig. 3.12: Computed velocity profiles for the Incat model against experimental data..... 42

Fig. 3.13: Simulation on impact after 80ms involving locations of the four pressure probes and jet forming around probe P2 43

Fig. 3.14: Time histories of measured and computed pressures around the archway at four defined locations (i.e., from P1 to P4 respectively)..... 45

Fig. 4.1: Profile view of hydraulic test installation (dimensions in mm). 49

Fig. 4.2: Body lines of generic catamaran hull form, also showing the locations of the five pressure transducers. 51

Fig. 4.3: Test model instrumented with three load cells and five pressure transducers. All spaces were filled with expanding foam prior to testing. 51

Fig. 4.4: Test model installed on the centreline of the moving test fixture. 52

Fig. 4.5: The experimental test setup instrumentation; showing 1 = LVDT and hydraulic ram cylinder, 2 = Load Cell and 3 = Pressure transducer and fitting surface. 52

Fig. 4.6: The instrumented test model and spatial distribution of gauges (P = pressure transducer while LC = load cell). 56

Fig. 4.7: Repeatability of three tests for target velocity of 4.5m/s; (a) immersion, (b) velocity profile, (c) pressure transducer and (d) hydrodynamic load. 56

Fig. 4.8: Immersion and velocity time histories of repeated tests at target velocity equal to 4m/s. 57

Fig. 4.9: Total hydrodynamic load time histories of repeated tests at target velocity equal to 4m/s. 57

Fig. 4.10: Hydrodynamic pressure time-series of P1 at target velocity equal to 4m/s. 58

Fig. 4.11: Evolution of water-jets from the centrebow and demihull prior to wetdeck slamming event for a target velocity of 4m/s. 58

Fig. 4.12: Error bound of water impact velocity for the target velocity. 60

Fig. 4.13: Comparison of raw load signals from three load cells during 4m/s water-entry with filtered data with a cut-off frequency of 500 Hz. 60

Fig. 4.14: Time-history of measured data (target velocity of 5m/s), (a) immersion, (b) velocity, (c) total hydrodynamic load and measured forces from three load cells, (d) pressure trace from P1 to P5. 62

Fig. 4.15: Time-history of measured data (target velocity of 4.5m/s), (a) immersion, (b) velocity, (c) total hydrodynamic load and measured forces from three load cells, (d) pressure trace from P1 to P5. 63

Fig. 4.16: Time-history of measured data (target velocity of 4m/s), (a) immersion, (b) velocity, (c) total hydrodynamic load and measured forces using three load cells, (d) pressure trace from P1 to P5, while '^' marker corresponds to images in Fig. 4.17. 64

Fig. 4.17: Frames taken by high-speed camera 3000 fps (frame per second) correspond to 'Δ' markers in Fig. 16 (c). 65

Fig. 4.18: Bow view of model showing immersions (130 and 159 mm) that correspond to the peaks of slam pressure and slam force respectively (4m/s water-entry) in relation to the original water-surface. Also shown on the starboard side are the locations of the five pressure transducers. 66

Fig. 4.19: Relationship between slam force peak and the square of the velocity at the instant of impact. 67

Fig. 4.20: The measured slam force peak error bounds corresponding to the square of instantaneous impact velocities against the slam load prediction equation, as illustrated in Fig. 4.19. 67

Fig. 4.21: Pressure peaks for the five pressure transducers plotted against the square of corresponding impact velocities. Subplots from (a) to (e) are for P1 to P5 respectively. ... 68

Fig. 4.22: Mean pressure peaks corresponding to six relative target velocities against the distance y in reference to the centrebow aft truncation. Vertical bars indicate standard deviation. 70

Fig. 4.23: Profile view of model showing immersions corresponding to the slam pressure peaks. Also shown on the archway are the locations of the five pressure transducers. 70

Fig. 4.24: Mean model immersions correspond to slam pressure peaks of all test conditions against the distance y in reference to the centrebow truncation. 71

Fig. 4.25: Mean timings that correspond to the peak slam pressures of five pressure transducers at six relative velocities against the distance y in reference to the centrebow truncation. 71

Fig. 5.1: General test arrangement. Showing the main components of SSTS and the instrumented model (dimensions in mm). 75

Fig. 5.2: Tested model installation at 5° angle of trim (bow-down), showing two wedges between the rig and a stiffened support. 76

Fig. 5.3: Schematic diagram of profile and bow views of the parent model at θ = 0°, showing locations of the used pressure transducers and load cells (LCi). 76

Fig. 5.4: Catamaran body lines with two interchangeable centrebows; showing the parent centrebow lines illustrated in orange on the right and the amended centrebow lines presented in green on the left. 77

Fig. 5.5: Catamaran test-model, showing the two interchangeable centrebows. 77

Fig. 5.6: Schematic chart showing the five pressure transducers (red surface) on the starboard side and the anticipated flow behaviour on one side during water penetration of; (a) parent centrebow and (b) amended centrebow.....78

Fig. 5.7: Bow and profile views of model at trim angles of 0 and 5 degrees corresponding to two relative impact angles (β) of 11 and 6 degrees. It shows the red reference line on the archway that represents the highest section along the top of the arch way. z_w (θ°) is the vertical distance between the initial calm water-surface and the highest point on the wetdeck at the aft end of the centrebow and z_F (θ°) which corresponds to the immersion at which the maximum slam force occurs. 81

Fig. 5.8: Comparison between using parent against amended centrebows for a target relative velocity of 4m/s at θ = 5°. Subplots illustrate time histories of (a) measured velocities, (b) total slam force. 82

Fig. 5.9: Flow visualisation time history for; parent and amended centrebows hull at θ = 5° and impact velocity of 4m/s.....82

Fig. 5.10: Relationships of slam force peaks against the relative impact angles and the corresponding relative velocity for both centrebows. 83

Fig. 5.11: Time histories of; LC1= load cell No.1, LC2 = load cell No.2 and LC3 = load cell No.3 for a target velocity of 5m/s and at two relative impact angles. 84

Fig. 5.12: Total hydrodynamic load time-histories for; (a) parent hull at θ = 0°, (b) amended hull at θ = 0°, (c) parent hull at θ = 5°, (d) amended hull at θ = 5°.....85

Fig. 5.13: Cross plot of slam force peaks against dimensional z_F/z_w for; (a) parent hull at θ = 0°, (b) amended hull at θ = 0°, (c) parent hull at θ = 5°, (d) amended hull at θ = 5°. 86

Fig. 5.14: The peak pressure distributions for all test conditions.....88

Fig. 6.1: Overview of generic catamaran hullform model, (a) Geometry with five pressure sensors' locations, (b) Generated grid and (c) Computational domain. 93

Fig. 6.2: Computed vertical slamming forces by applying three different grid sizes for, (a) fixed grid and (b) for the overset grid.....96

Fig. 6.3: Experimental immersion and velocity data, for the target velocity of 4m/s. 98

Fig. 6.4: Comparison of total slam force data against the CFD results using both the overset grid and the fixed grid methods. 98

Fig. 6.5: Pressure distributions along arched way of catamaran wetdeck time histories. Subplots (a-e) present the measured pressure time histories against computed results using overset and fixed grid methods from P1-P5 respectively.....100

Fig. 6.6: Total transverse force acting on demihulls during model-water impact.....101

LIST OF TABLES

Table 2-1: Main Particulars of the 2D Model (Whelan, 2004). 17

Table 2-2: Grid Size Study. 21

Table 2-3: Details of Instrumentation (Whelan, 2004). 23

Table 4-1: Details of Gauges. 52

Table 4-2: Location of Pressure Transducers. 53

Table 4-3: Summary of Test Conditions. 55

Table 4-4: Summary of Systematic Errors. 59

Table 5-1: Test Model Main Particulars. 78

Table 5-2: Test Conditions. 79

Table 5-3: Summary of Results 80

Table 5-4: Summary of Expressions Derived for Maximum Slam Forces Based on Relative Impact Angles and Impact Velocities. 84

Table 6-1: Summary of Numerical Independence Study with Associated Uncertainty against Experimental Data. 97

Table 6-2: Summary of Results. 98

Nomenclature

B	Maximum beam (m)
F	Force (N)
F_{max}%	Force peak differences %
Fr	Froude number (-) = $v/\sqrt{g.L}$
F_t	Total force (N)
F_y	Transverse splitting force (N)
F_z	Vertical force (N)
G	Gravitational acceleration (m/s^{-2})
H	Height (m)
L	Length (m)
m*	Mass number
m_m	Mass of the model (kg)
P	Pressure (Pa)
Δs	Time step (s)
T	Time (ms)
t_o	Time at which model touches the free-surface (-)=0s
V	Velocity ($m.s^{-1}$)
v_{impact}	Relative impact velocity ($m.s^{-1}$)
v_{target}	Input target velocity to the control system ($m.s^{-1}$)
v_{std}	standard deviation
x, y, z	Body axis Cartesian coordinates in the x,y,z-direction (m)
Δx	Venting clearance (m)
y+	Non-dimensional wall distance (-) = $(u_* y_{wall})/v$
z_F	Immersion correspond to slam force peaks (m)
z_w	Immersion (m)
B	Relative impact angle
∇	Volumetric displacement (m^3)
Θ	Trim angle
P	Fluid density ($kg.m^{-3}$)

Abbreviations

2D	Two-dimensional
3D	Three-dimensional
ABS	American Bureau of Shipping
AMC	Australian Maritime College
BEM	Boundary Element Method
CDAQ	Compact Data Acquisition
CFD	Computational Fluid Dynamics
CIP	Constrained Interpolation Profile
CNC	Computer Numerically Controlled
DFBI	Dynamic Fluid Body Interaction
DNV-GL	Det Norske Veritas- Germanischer Lloyd
DOF	Degree of Freedom
FDM	Finite Difference Method
FEM	Finite Element Method
FVM	Finite-Volume Method
HSMV	High-Speed Marine Vehicles
ITTC	International Towing Tank Conference
LCi	Load cell number i
MS	Merchant Ship
NZ	New-Zealand
Pi	Pressure transducer number i
RINA	Royal Institution of Naval Architects
RO-PAX	RORO-Passenger
SIMPLE	Semi-Implicit Method for Pressure-Linked Equations
SNAME	Society of Naval Architecture and Marine Engineering
SPH	Smoothed Particle Hydrodynamics
SSC	Ship Structure Committee
SST	Shear Stress Transport
SSTS	Servo-hydraulic Slam Testing System

URANS	Unsteady Reynolds Averaged Navier-Stokes
UTAS	University of Tasmania
VOF	Volume of Fluid

Chapter 1
Introduction

This thesis presents a detailed investigation into wetdeck slamming, one of the principal mechanisms for wave induced loads on catamaran ships. A catamaran experiences this type of slamming when operating in large waves as the wetdeck, the exposed deck area between the two demi hulls of the catamaran, impacts the water surface with a high relative vertical velocity (see Fig. 1.1). Wetdeck slamming is a significant design issue for catamarans since it can cause major structural damage and avoiding its occurrence is one of the main reasons a vessel's master will reduce speed or change course in heavy weather, adversely affecting the vessel's operation and schedule.

Fig. 1.1: *Kat Express 2*, high-speed wave-piercing catamaran, LOA = 112m (Incat, 2013).

1.1 Background

Over the past three decades there has been increased military and commercial interest in lightweight high-speed catamarans, mainly due to their ability to provide fast sea transportation with large deck areas and relatively high payload capacity.

Fig. 1.2: Tassie Devil 2001, the original wave-piercing catamaran fitted with centrebow, LOA = 31m (Incat, 1986).

Australia is an acknowledged world leader in the innovative design and construction of large high-speed aluminium catamarans, such as the vessels developed by Incat Tasmania. In 1986, Incat Tasmania introduced the first wave-piercing catamaran with a centrebow located between the two demihulls (Figs. 1.2 - 1.4). The length of the centrebow is typically between 20% to 33% of the vessel's overall length (LOA) (see Fig. 1.4), and is designed to avoid deck diving in following seas and to reduce pitching by providing additional reserve buoyancy at the bow. Incat vessels have two arched wetdecks between the demihulls and the centrebow in the forward part, which is followed by a flat wetdeck extending aft to the transom.

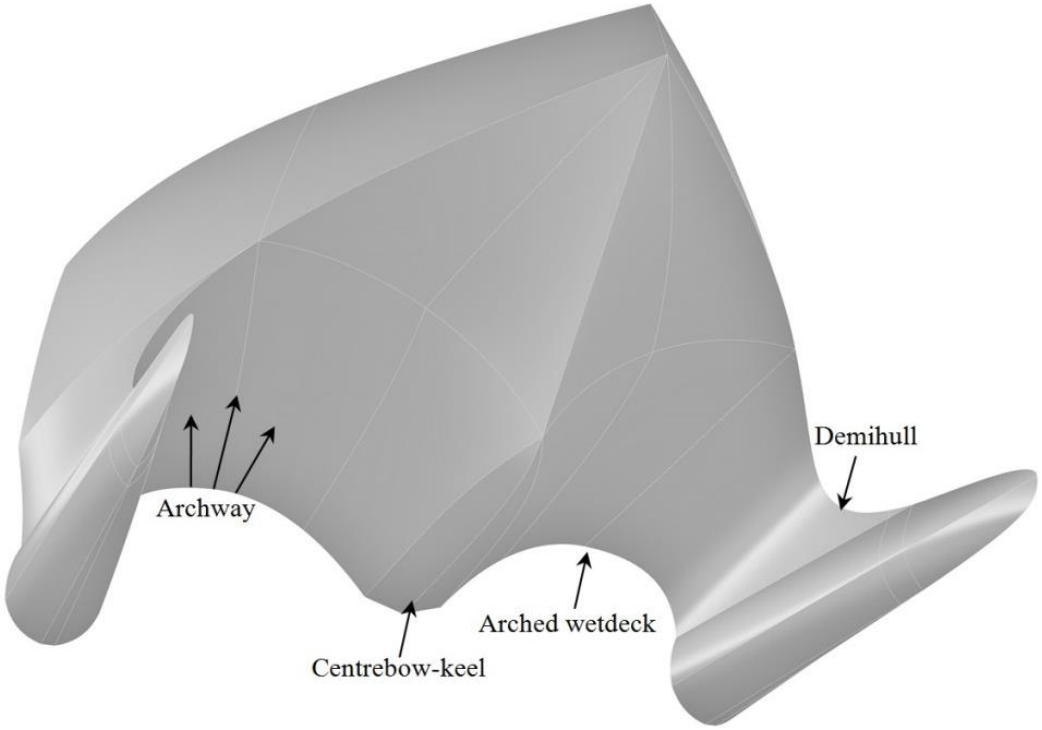

Fig. 1.3:Schematic diagram of bow section for an Incat wave-piercing catamaran.

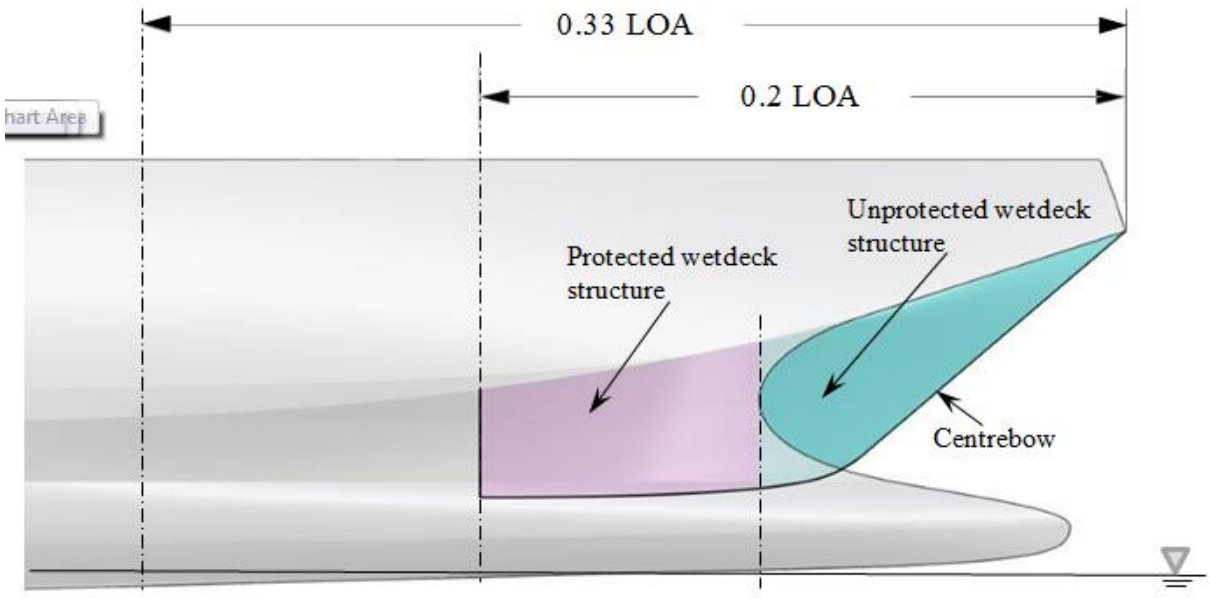

Fig. 1.4: Fore section of an Incat wave-piercing catmataran, LOA = 112m showing the protected and unprotected structures at the bow section with approximately 20% of LOA.

In 1990, Incat launched the first RO-PAX high-speed wave-piercing catamaran vessel to carry a combination of passengers and vehicles, with an LOA of 74m. The success of these medium-sized RO-PAX high-speed wave-piercing catamarans led to the development of larger, faster, lightweight vessels up to 112m in length (see Fig. 1.1).

A major challenge in designing high-speed wave-piercing catamarans is to increase the ratio of deadweight to lightship weight, whilst ensuring safe structural design and maintaining high operational speeds. Structural optimisation relies on the accurate prediction of the wave loads, which for a high-speed catamaran are generally dominated by wetdeck slamming (French, 2012; Kaplan, 1987; Kvålsvold & Faltinsen, 1995) that is centred in the vicinity of the bow section (American Bureau of Shipping [ABS], 2016; Amin, 2009; Davis & Whelan, 2007; Det Norske Veritas [DNV], 2015; French et al., 2015; He et al., 2013; Lloyd's Register [LR], 2016).

The bow section includes both protected and unprotected structures, as illustrated in Fig. 1.4. The protected structure is the wetdeck section that is enclosed between the demihull on one side and the centrebow structure on the adjacent side, while the unprotected structure is the section that is not enclosed, and thus facilitates water outflow to escape during water impacts (LR, 2016).

1.2 Problem definition

The main area of interest in the design of large wave-piercing catamarans is the impact loading in the vicinity of the centrebow (i.e. the wetdeck and adjacent structures) during immersion (Davidson et al., 2006; Faltinsen, 2006). Several large high-speed catamarans have suffered damage due to wetdeck slamming, although these vessels were designed to classification society rules (Rothe et al., 2001; Steinmann et al., 1999; Thomas et al., 2002, 2003). Some prominent examples of damage due to wetdeck slam events are:

- extensive structural damage to the bow of *HSS Stena Discovery* during operations in the North Sea, (Fig. 1.5, (Thomas, 2003));
- local plastic deformation on the loaded region on the 67m oceanographic research catamaran *USN Hayes* (Hadler et al., 1974);
- localised buckling of plates, stiffeners and distortion of centrebow T-shaped stiffeners of Incat Hull 050 during ferry operations in New Zealand (Thomas, 2003); and
- longitudinal cracking in the flat wetdeck of *MS Sollifjell* (Fricke & Bronsart, 2012).

Fig. 1.5: Structural damage due to wetdeck slamming on *HSS Stena Discovery*, in 1997 (Thomas, 2003).

To eliminate the prospect of structural damage and to secure insurance cover in case of damage, high-speed craft are designed to rule-based design loads. Currently classification societies (ABS, 2016; DNV, 2015; LR, 2016) provide designers with a range of empirical formulae that are based on quasi-static pressure predictions due to impact on high-speed catamaran's wetdeck, which in reality may over or underestimate the actual impact pressure distributions (Paik & Shin, 2006).

Thus, there is a need to provide designers and classification societies with an accurate means to predict impact load magnitudes and distributions, based on reliable experimental work and validated computational tools.

The wetdeck slamming problem is significantly more complex than that for monohull slamming as it involves rapid changes of local loads in time and space, air inclusions, and the compressibility of mixing fluids (water and air) over a non-uniform surface in three dimensions.

1.3 Wetdeck slamming prediction

The majority of research into slamming has focussed on monohull vessels (Kapsenberg, 2011; Luo & Soares, 2012). The four main theoretical/numerical approaches previously used to predict impact loads are described below.

- Analytical methods can provide approximate solutions of hydrodynamic impact loads on simplified 2D shapes. However it is impossible to accurately predict the 3D wetdeck slamming loads on complex shapes with disturbed water surfaces (Bertram, 2000).
- Panel methods, based on the Boundary Element Method (BEM), are potential flow solvers that discretise the boundaries of the fluid domain to solve the pressure field using Bernoulli's equation. These are more suitable for predicting slamming loads on simplified hull shapes (Zhao & Faltinsen, 1993). One of the obvious limitations in applying BEM for non-uniform geometries is the arrangement of the panels around 3D hull forms to capture free-surface deformations and the water jet evolution during water-entry, an extremely complicated and time consuming exercise (Kapsenberg, 2011; Yang & Qiu, 2012).

- Computational Fluid Dynamics (CFD) using volumetric methods have solved some of the more complex flow problems in engineering by utilising either Euler equations (for inviscid flow) (Batina, 1991; Wendt, 2009) or Navier-Stokes equations (Mørch et al., 2008; Wang & Guedes Soares, 2013). The Volume-of-Fluid (VOF) method developed by Hirt & Nichols (1981) has been extensively used to accurately capture complex free-surface deformations due to sudden shock (Bozorgnia & Lee, 2012; Brizzolara et al., 2012; Chen & Yu, 2008; Sun & Faltinsen, 2009).
- One of the advanced numerical methods to predicting wave impact behaviour is Smoothed Particle Hydrodynamics (SPH), which is a meshless Lagrangian computational method. In the SPH method, distributed particles represent the domain and each particle represents the fluid's physical properties. SPH predictions have shown to be capable of predicting hydrodynamic impact loads for 2D and 3D bodies, with comparable results to experimental data (Oger et al., 2006; Veen & Gourlay, 2012). However SPH pressure, force and motion predictions show large oscillations, which often happen when applying particle methods to water-impact problems (Chen & Yu, 2008; Fricke & Bronsart, 2012). Shahraki et al. (2011) used SPH to predict the behaviour of a 2D wedge shaped hull form during water-entry. The predictions showed a variation of around 40% against experimental data (Whelan, 2004), with large oscillations around the mean values.

The lack of accurate and stable numerical models to predict wetdeck slamming is a strong motivation to develop validated CFD models in order to assist ship designers and relevant classification authorities.

The main techniques used to collect data to validate numerical methods are full-scale sea trials or model-scale experiments.

Full-scale measurements can provide valuable data on the loads experienced by vessels in realistic sea conditions and allow the characterisation of the parameters that influence slam severity (Roberts et al., 1997; Thomas, 2003). However due to a range of factors, such as associated costs, inability to control the test environment and difficulties in isolating the actual slam load measurements from complex strain gauge records, full-scale tests are not always the preferred method to obtain validation data for wave slam load predictions.

There are two model-scale experimental techniques that are generally used to obtain impact loads: seakeeping tests and drop tests. Seakeeping tests of high-speed wave-piercing catamaran models can provide valued data and knowledge with regard to global and local loads (French et al., 2015; He et al., 2013; Lavroff et al., 2011; Thomas et al., 2011b). Although tests in irregular seas are recommended to test catamaran operational limits, in order to measure extreme phenomena, such as local slam pressures in irregular waves, a run length of 100 slam events is recommended (International Towing Tank Conference [ITTC], 1999), which incurs time and cost penalties. The complexity of the experimental set-up and the un-avoidable differences in wave amplitudes lead to scattered data that may present challenges in the validation process (Amin, 2009; Dessi & Ciappi, 2013; Lavroff et al., 2013).

The drop test technique is used extensively to characterise slam loads in a more controlled environment. However there is limited data available in the public domain for multihull vessels. An exception is the study conducted by Whelan (2004), where a series of 2D drop tests was conducted to evaluate the behaviour of seven catamaran model hull forms during the water-impact phase. The limitations of assuming that the wetdeck slam event is a 2D phenomenon were highlighted by the results of a computational study conducted by Davis & Whelan (2007), where the impact loading magnitudes of the 2D simulations were found to be significantly larger than those when the three dimensionality of the section was included.

To date, no 3D water impact tests of catamaran hullforms have been conducted and as such it is not currently possible to validate numerical predictions for 3D catamaran hullforms impacting water. To assess slam load severity on monohull vessels, extensive research has been conducted to directly quantify pressure peak measurements on tested models using a limited number of pressure transducers (Alaoui et al., 2015; Engle & Lewis, 2003; Hermundstad & Moan, 2007; Okada & Sumi, 2000; Panciroli & Porfiri, 2013; Pistani & Thiagarajan, 2012; Rosén, 2005; Van Nuffel et al., 2013; Yettou et al., 2007). Several researchers have developed methods for mapping the complete pressure distributions using limited number of pressure measurements (Razola et al., 2014; Rosén, 2005; Yettou et al., 2007). However Payne (1988) highlighted a major disagreement between eight methods to quantify design impact loads of high-speed crafts in relation to pressure peak measurements.

Recently Fricke & Bronsart (2012) raised the issue of the relationship (if it exists) between local pressure measurements and slamming load. To date no strong/accurate relationships have been observed between local pressure measurements and design loads (i.e. lack of connection between slam loads and slam pressures), even for small vessels.

In conclusion, there is currently a lack of knowledge with regard to wetdeck slamming problem due to its complexity and the limitations in the published data. Thus at present it is not possible to characterise wetdeck slamming loads nor validate numerical prediction methods for catamarans. Consequently there is a lack of an accurate method for predicting 3D wetdeck slamming loads.

1.4 Research questions and objectives

As prefaced within the above sections, the specific research questions are:

1. How well can various CFD modelling methods predict wetdeck slamming loads, especially when air inclusion and complex hull shapes forming water jets are entrapped in a semi-enclosed void?
2. What are the key factors and considerations influencing the characteristics and magnitudes of wetdeck slam events?

To answer these two overriding research questions, the work is divided into four main parts, which are the global project aims:

(a) To provide ship designers with a verified/validated numerical method to accurately predict wetdeck slamming loads on catamarans (i.e. a practical tool with an accuracy of ±5% in relation to measured data).

(b) To address the lack of benchmark data for catamarans slam impacts in 3D flow regimes.

(c) To investigate the 3D fluid flow effects on the slam impact characteristics including the wetdeck slam force and pressure distribution magnitudes.

(d) To determine the relationship between local pressure measurements and slam loads (if existing), in particular identify whether the local pressure peak magnitudes are

principally dependent on the changes in flow behaviour and jet evolution or the hydrodynamic load magnitudes.

1.5 Methodology

The following approach was utilised to achieve the main project objectives:

Phase 1: A review of the literature pertaining to fluid-structure interaction, CFD modelling methods, water-impact experimental work, sea-load characteristics and in particular transient hydrodynamic impact loads on floating structures.

Phase 2: CFD prediction of impact pressure distributions and corresponding motions of a 2D simple rigid hull form; and validation against past numerical simulations and free-fall test results.

Phase 3: Development of a verified and validated CFD simulation model to capture local pressure distributions and corresponding motions of 2D rigid catamaran hull sections impacting a quasi-2D body of water.

Phase 4: Designing and conducting a series of controlled-speed 3D water impact experiments at a range of impact velocities and trim angles. The 3D test model was developed based on a generic wave-piercing catamaran with two interchangeable centrebows. The aim was to characterise wetdeck slam events and provide high-quality experimental data suitable for validation and benchmarking.

Phase 5: Development, evaluation and validation (i.e. against 3D experimental data presented in phase 3) of two 3D CFD modelling methods. These methods, using the outcomes from phases 1 and 2, implemented actual (unsteady) velocity traces and predicted impact pressure distributions and hydrodynamic loads on generic wave-piercing catamaran hulls impacting water in 3D flow regimes.

1.6 CFD approaches

The Finite Volume (FV) grid-based CFD method was employed in this work to predict the behaviour and slamming loads of 2D, quasi-2D and 3D hull models impacting with the water surface.

Over the past three decades several techniques have been developed to simulate moving bodies through multiphase flows. The three main approaches are grid re-meshing, grid deformation and overlapping/overset grid.

In the overlapping or overset grid method (Starius, 1977) the numerical domain consists of two grids, one around the moving body that follows the time history of the body motion referred to as the overset grid, and the other a stationary grid representing the total domain, referred to as the background grid. The main advantage of this meshing technique is that it enables large body motion without deleting the old grid and regenerating a new grid which is called re-meshing method such as discussed by Zhu et al., 2012) or by dynamically deform the grid (discussed by Demirzic & Peric, 1990). For transient applications that require updating the grid at every time step, re-meshing technique consumes time and high CPU power. For applications that require capturing pressure spikes, where the pressure output signals are localised in space and time, that requires high quality of established cells in the vicinity of pressure sensors where deforming cells at such finite regions would lead to in accurate predictions of the impulse loads due to the probability of low cell quality at the instant at which pressure peaks. Thus, overset grid offers higher flexibility and lower computational time as opposed to the other two methods (Bodony et al., 2011; Chen & Yu, 2008; Mørch et al., 2009; Panahi & Shafieefar, 2010; Zagaris et al., 2010).

For the catamaran wetdeck slamming problem, an Unsteady Reynolds Averaged Navier-Stokes (URANS) based CFD simulation, with an overlapping grid and the VOF method, was therefore deemed one of the most promising methods. However, CFD predictions can exhibit large variations when compared against experimental data depending on the quality of measured data, grid quality of the numerical model, simulation settings, and the experience of the analyst in carrying out the simulations (Fricke & Bronsart, 2012).

The CFD simulation model setup for water impact problems involves the development of an adequate computational grid, setting of boundary and initial conditions, selection of turbulence models, development of motion simulation techniques in order to accurately predict free-surface deformations and to compute sudden local pressures on relatively small sensing areas over short time durations (full details on this aspect of the work are contained in Appendix I). However, to provide confidence in the computational approach it is vital that the numerical model is firstly verified and the computed results are then validated against high-quality experimental data.

1.7 Experimental approaches

Among the experimental techniques presented in section 1.2, there are two vertical water impact experimental techniques that are generally used to characterise slamming loads, i.e. drop tests and controlled speed tests.

Drop tests allow the test model to fall under gravitational forces onto the water surface. Since the vertical velocity of the test section (for free-falling condition) is not controlled during the impact, the impact velocity profile may not be relevant to that experienced by vessels in real slamming conditions. Early examples of drop tests are found in Chuang (1966) and Ochi & Motter (1971) to predict design pressures of flat-bottomed and simplified monohull shape models respectively. Many references to 2D and 3D free fall monohull experiments are found in the literature of Chuang & Milne (1971), De Backer et al. (2009), Engle & Lewis (2003, Jalalisendi et al. (2015), Lewis et al. (2010), Ochi & Motter (1973), Panciroli & Porfiri (2013), Van Nuffel et al. (2013), (2014) and Yettou et al. (2007).

Controlled-speed water-impact experiments require a more sophisticated experimental set-up in order to allow the model-water impact to occur at constant or given velocities, i.e. implementing a variable velocity profile (Alaoui et al., 2015; 2012; Battley & Allen, 2012; Battley et al., 2005; Campbell & Weynberg, 1980; Stenius et al., 2013; 2011; Tassin et al., 2012). This technique can provide qualified data for parameters influencing wetdeck slam load severity and occurrences whilst ignoring mass scaling effects (i.e. constant speed-water entry) or the rapid deceleration of velocity profiles during water impacts.

The three main factors involved in determining the type of experiment to use were: reproducing realistic conditions, degree of control over the tested model and the degree of statistical fluctuation. These were all met by the controlled-speed tests. However, the presented work focused on the slam pressure distributions and hydrodynamic impact loads acting on rigid bodies; i.e. neglecting the corresponding hydroelastic effects due to the high-rigidity of the tested model that allowed this assumption is to be valid. In the present study, the motions of the model were restricted in all degrees of freedom except for the vertical motion. This technique is widely used to provide high-quality data for validation of numerical techniques to predict impact loads (Alaoui et al., 2015; Lewis et al., 2010; Stenius et al., 2013; Tassin et al., 2012; Van Nuffel et al., 2014).

All measured peaks of pressure distributions and impact loads were presented for the actual corresponding velocities. Thus results would be comparable against data from drop tests, seakeeping experiments and even full-scale trials following scaling of the results.

A minimum gap between the model and the tank walls of at least double the model's overall beam was considered sufficient to minimise boundary condition effects and the possibility of wave reflections. The conducted experimental set-up is discussed in detail in chapters 4 and 5.

The water impact experiments were conducted at a range of controlled water-impact velocities, with the speeds primarily selected based on full scale impact values presented by Jacobi et al. (2014). Consideration was also given to ensure that the ratio of measured loads to the maximum range of employed load cells was sufficient to provide a good signal to noise ratio.

The second series of controlled speed tests was performed at two trim angles by bow of 0 and 5 degrees, which were based on the measured seakeeping experimental data from Lavroff (2009).

1.8 Thesis Structure

This thesis comprises a collation of published refereed scientific papers presented in chapters 2 to 6. The relevant publishing details are given at the beginning of each chapter, which also includes a review of the current literature pertaining to each study. Noting that to avoid repetition in the thesis each original paper has been somewhat modified. An outline of the thesis is given below:

Chapter 2: A comparative numerical study was performed to evaluate URANS-based CFD, VOF and 2D overset meshing method against both past SPH simulations and experimental measurements for predicting vertical acceleration and slamming pressure distributions on a wedge shaped hull-form impacting with water under gravitational acceleration. The computed results provide confidence in the applied numerical simulation setup and the ability of CFD to accurately predict transient impact loads, i.e. pressure traces and magnitudes, with better agreement with experimentally measured data than currently possible with SPH. The study also demonstrates the ability of the overset meshing method in reproducing the same velocity profile and vertical acceleration measured during the drop tests. The parameters tested in the convergence study for this 2D simulation (given in Appendix I) formed the basis for the validation study conducted in Chapter 3.

Chapter 3: Presents a numerical investigation into the free-falling wave-piercing catamaran model into still water, with restrictions on the outflow of water and air from the impact region. The magnitude and occurrence of slamming loads, corresponding motions and flow visualisation show good agreement with existing experimental data. The numerical setup discussed in Chapter 2 was used for this work, with the additional inclusion of compressibility of the trapped air to accurately predict slamming pressures and corresponding motions. The maximum computed pressure was close to the highest point of arched wetdeck. The results and recommendations from these numerical simulations were vital for the design of the physical generic catamaran bow section model and the water-impact experimental set up discussed in Chapter 4. In addition, the methodology and key findings from this modelling were used to develop the CFD capabilities for simulating a generic wave-piercing catamaran bow section impacting with water in a 3D flow regime, as described in Chapter 6.

Chapter 4: The work presented in this chapter was motivated by the lack of non-proprietary dataset of catamaran vessels during water impacts. The chapter includes the first series of 3D water impact experiments that were conducted to investigate the hydrodynamic loads (pressure distributions and slamming forces on the entire bow model) experienced by a generic wave-piercer catamaran hullform impacting with the water. The experiments were conducted in collaboration with the University of Auckland using a Servo-hydraulic Slam Testing System (SSTS) that allows the model to enter the water at a range of constant speeds. The data presented in this chapter were used to characterise the slam impacts and validate the 3D numerical simulations described in Chapter 6.

Chapter 5: The work presented in this chapter extends the 3D controlled speed tests presented in Chapter 4 using the SSTS and two interchangeable centrebows. The investigation centred on the influence of flow separation using an amended centrebow and the effect of the relative impact angle and relative vertical velocity on slamming loads and pressure distributions. This study presents a new dataset for the pressure distributions along the archway of the wetdeck and the entire slamming forces as the arched wetdeck impacts the water. The pressure peaks were found to be more dependent on the localised flow behaviour than the applied hydrodynamic loads.

Chapter 6: This chapter assesses two CFD numerical simulation techniques against experimental data from Chapter 4. The work also evaluates the proposed numerical method for predicting local and entire wetdeck slamming loads on a 3D generic wave-piercer catamaran. Numerical results of the slam force peak and pressure magnitudes from five pressure transducers distributed along the archway of the wetdeck compared (quantitatively and qualitatively) well with the experimental data presented in Chapter 4. The transverse splitting force due to wetdeck slamming was also quantified and the CFD simulation model was shown to be an accurate tool to predict wetdeck slam event effects.

Chapter 7: The concluding chapter provides an overall summary of the project, bringing together the findings of the individual chapters. It also concludes on the findings and outcomes, as well as discussing the implications and limitations of the work, and provides recommendations for future work.

Chapter 2

Verification and validation of CFD method

This research was originally published, after peer review, as:

Swidan, A., Amin, W., Ranmuthugala, D., Thomas, G. & Penesis, I. Numerical Prediction of Symmetric Water Impact Loads on Wedge Shaped Hull Form Using CFD. World Journal of Mechanics, vol. 3, pp.1-8. 2013.

(http://dx.doi.org/10.4236/wjm.2013.38033)

For the avoidance of repetition the original paper has been modified for this thesis.

2.1 Introduction

Many researchers have developed and/or applied numerical approaches to simulate the behaviour of ships during water entry, including Finite-Volume Method (FVM) (Mørch et al., 2009), Finite-Element Method (FEM) (Wagner, 1932), Finite-Difference Method (FDM) (Kapsenberg, 2011), Smoothed Particle Hydrodynamics (SPH) (Veen & Gourlay, 2012) and Boundary Element Method (BEM) (Sun & Faltinsen, 2010). Validation of these methods has usually been carried out through benchmark model tests results (DNV, 2010).

This present work is devoted to predicting the behaviour of wedge-shaped hull forms during slam events including the local slam loads as the wedge impacts the water. This paper outlines work to predict the motions response and local slam loads of quasi-2D wedge shaped hull form impacting water, using finite-volume CFD method. The computed results were verified to ensure stable numerical results and compared to a set of SPH predictions performed by Shahraki et al. (2011) for the same test conditions. In addition, the results were validated against drop test data from a series of experiments conducted by Whelan (2004). Whelan (2004) has conducted quasi two-dimensional symmetrical drop tests of nine scaled models (wedges and catamaran hull forms) to capture the essential features of slam events.

2.2 Numerical simulation of free falling wedge entry

The present work is devoted to the numerical simulation of a quasi 2D 25° deadrise wedge dropped from above the water surface with a given initial velocity equivalent to the experimental data, see Table 2.1 and Fig. 2.1. The numerical simulations were conducted using the CFD software STAR-CCM+ Version 7.06.

To assist the validation of the CFD results and to enable comparisons with the experimental data the entire domain was given the dimensions of the University of Tasmania (UTAS) drop test tank. Length 2.4m, width 0.3m and water depth 1m, as shown in Fig. 2.1.The symmetry of the geometry about y-z plane and symmetric water entry condition enabled the domain to be reduced in half. The domain thickness was simulated by 25mm, one cell in the “y” direction in most of the domain, to reduce the calculation time, as shown in Fig. 2.2.

Table 2-1: Main Particulars of the 2D Model (Whelan, 2004).

Type	Mass (Kg)	Experimental drop height (m)	Impact velocity (m/s)
Wedge	21	0.081	1.22

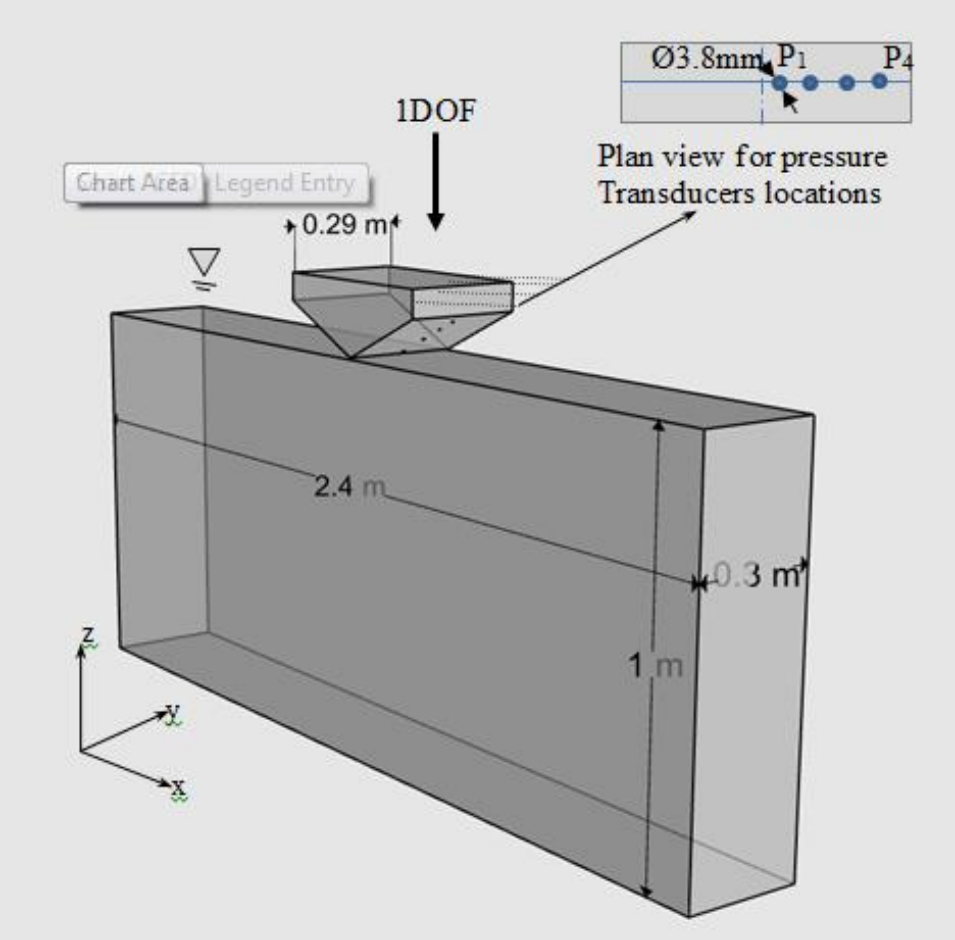

Fig. 2.1: Schematic drop test diagram.

The computational domain and the boundary conditions for the CFD simulations are shown in Fig. 2.2. A multiphase segregated fluid model is employed to solve the conservation equations for mass, momentum, and energy for each phase. This model solves the flow equations for the velocity components and pressure in an un-coupled manner (Appendix I).

The employed CFD code uses a Semi-Implicit Method for Pressure-Linked Equations (SIMPLE) algorithm to resolve the pressure-velocity coupling, while the linkage between the momentum and continuity equations is achieved through predictor and corrector stages. The laminar flow is considered sufficient to capture the local slamming loads, as the high pressure strikes are localised in time and space, see Appendix I (Faltinsen, 2005; Johannessen, 2012).

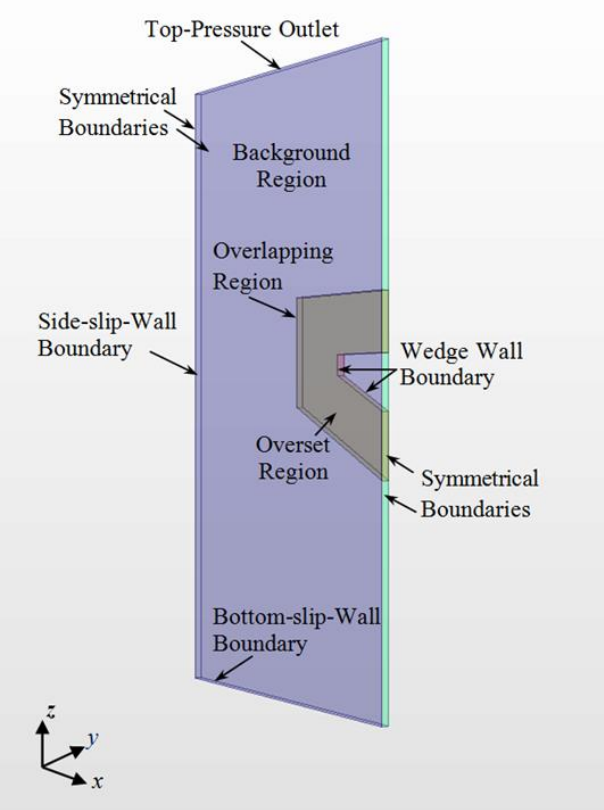

Fig. 2.2: 2D computational domain (wedge shaped hull model).

The free surface was modelled using the Volume of Fluid (VOF) method based on fluid volume fraction for solving the equations in both air and water and capturing the interface between them. The free surface was considered to be the region between cells comprised entirely of each of the two fluids, or where the volume fraction of either fluid is one half and these cells sum to one. The two fluids mix at their interface and the physical properties are taken as averages, weighted by the volume fraction of each of the fluids in these cells. A point on the water surface defined the free surface position.

In order to preserve the sharpness (i.e. avoid smearing) of the interface between the water and air, the High Resolution Interface Capturing (HRIC) scheme is used for the discretisation of the non-linear convective term in the momentum equation of the volume fraction (Wacławczyk & Koronowicz, 2008). This scheme is activated by default in the code for Courant number[1] less than 0.5.

[1] Courant number = velocity (m/s) *x* time step (s)/cell size (m)

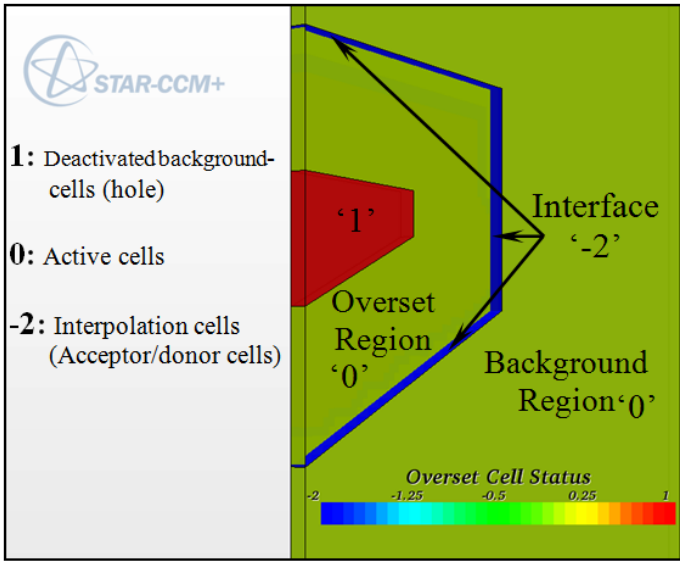

Fig. 2.3: The scalar fields for the background and overset regions.

The drop motion of the wedge was achieved by activating the vertical motion only in the 6-DOF DFBI (dynamic fluid body interaction) rotation and translation model in STAR-CCM+, which solves the equations of rigid body motion for all 6-DOF bodies. However in this case it was reduced to solve it in the vertical direction only.

The computational domain consisted of overset grids, which are arbitrarily assembled blocks that overlap covering the following regions, see Figs. 2.2 and 2.3.

- Background region containing the far-field flow domain and covered by stationary grid components.
- Overset region, extend to some distance from the moving wedge. The overset grid is attached to the moving wedge and covered the overset.

Figs. 2.2 and 2.3 illustrate the interface between the overset grid and the background grid. This region contains three main types of cells namely active cells, interpolation (acceptor / donor) cells and inactive (passive) cells. The overset grid follows the time history of the body motions and is influenced by the gravity and fluid resistance; details can be found in Johannessen (2012).

The grid was constructed using STAR-CCM+ CFD software, the calculations were carried out on two hexahedral grids, see Fig. 2.4.

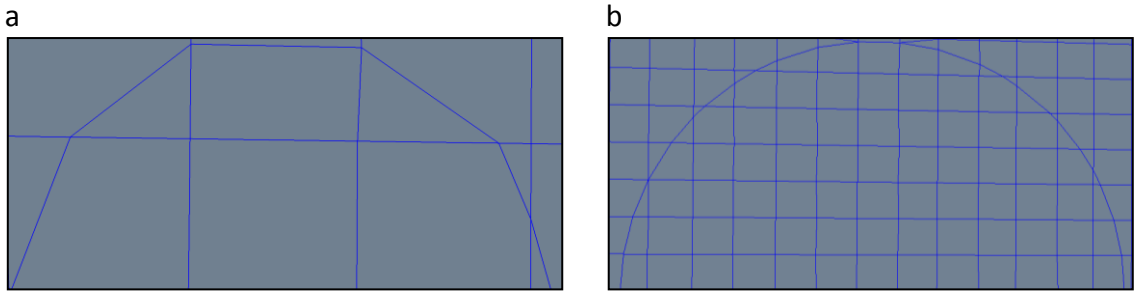

Fig. 2.4: Half of the transducer geometry. (a) Shows a course grid with 1.2 mm (b) Shows a fine grid with 0.3 mm.

First, the overset grid which was refined around each pressure transducer to capture the rapid slamming pressure instead of refining the whole bottom of the wedge. Fig. 2.4 shows the effect of grid size on the transducer geometry. The cell sizes of 0.3 x 0.3 x 0.3 mm at the four pressure transducers was considered the minimum sufficient cell size, see Fig. 2.4b; using a coarser grid would distort the transducer geometry, see Fig. 2.4a, and consequently, will affect the surface average pressure.

The background grid was refined at the overlapping region by using assembled blocks, called volumetric grid controls. For accuracy, the cell size in the overlapping region, see Fig. 2.5, was similar on all grids that overlap since if cells sizes are different the accuracy of interpolation on the coarser grid will determine the accuracy of grid coupling.

Linear interpolation was used among each moving acceptor cell centroid and four donor cells' centroids for 3D cases. The fluxes through the cell face between the last active cell and the acceptor cells were approximated in the same way as between two active cells. While parts of the background grid lying on the moving wedge were deactivated, see Figs. 2.3 and 2.5.

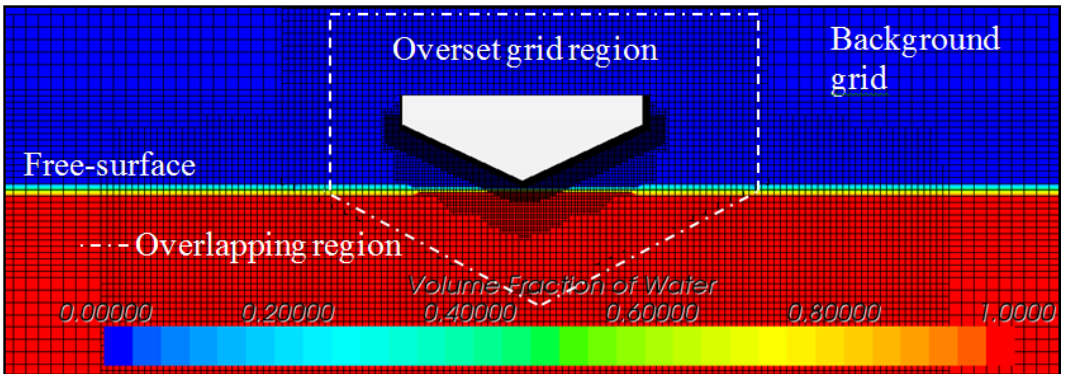

Fig. 2.5: Symmetry view of the free falling wedge's grids.

To ensure smooth transition between neighbouring cells, cell sizes in the vicinity of pressure transducers are equal to 0.25 x cell sizes at water surface. A sensitivity study was carried out to analyse the effect of varying the grid density in the vicinity of the pressure transducers at a constant time step of 0.5 ms. The selected time step considered that Courant number is less than 0.5 for conducted simulations. The CFD uncertainty was approximated by increasing the grid density systematically from 47,628 to 578,132 cells, as presented in Table 2-2. The grid independence study demonstrated that using grid number 2 results in stable calculations when compared with grid numbers 1 and 3, however grid number 3 is approximately four times the number of total cells in grid number 2. Thus grid number 2 is selected for the presented simulations in this chapter.

A further sensitivity study was performed to analyse the effect of three different time steps on computed results. In Fig. 2.7 the pressure at P1, was under predicted by 24% when compared to the experimental data (at Δs of 0.5 ms), however was found to significantly increase (uncertain by 10%) and shown more stability as the time step was reduced to 0.05ms. This was attributed to the rapid change in pressure distributions during water impacts, in particular at P1 (Johannessen, 2012; Lewis, 2010; Lewis and Turnock, 2008), see Fig. 2.7.

The pressure at P2 shows also good agreement with the experimental result by using Δs equal to 0.05ms, see Fig. 2.8. At this location the time step had an insignificant effect on the calculated pressure. Higher up the deadrise at location P4, the predicted pressure was found to be 10% greater than the experimental measurements. While the change in time step only resulted in a change in pressure of 5%, see Fig. 2.9.

Table 2-2: Grid Size Study.

	Grid1	Grid 2	Grid 3
Cells	47628	148344	578132
Δx (at the vicinity of pressure sensors)	0.003	0.0015	0.00075
Δy (at the vicinity of pressure sensors)	0.003	0.0015	0.00075
Δz (at the vicinity of pressure sensors)	0.003	0.0015	0.00075
Time steps [Δ sec]	0.0005	0.0005	0.0005
Wall clock Time ($\approx$ hours)	0.33	1.8	8.3
Random access memory	4 Gb		

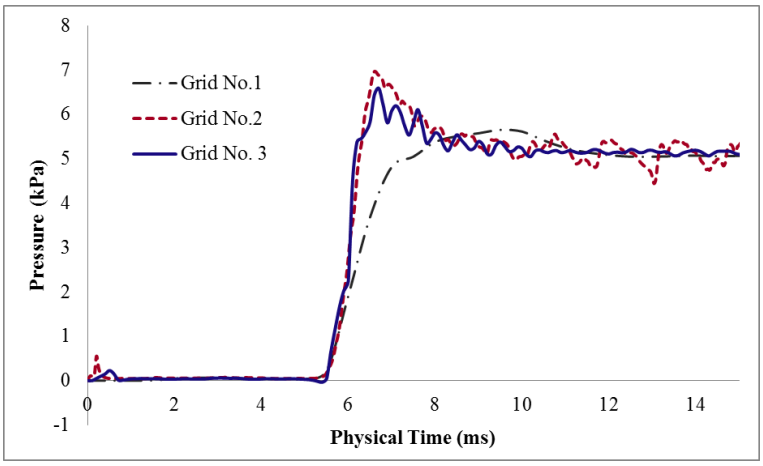

Fig. 2.6: The effect of grid size on the computed pressure at pressure transducer No.1.

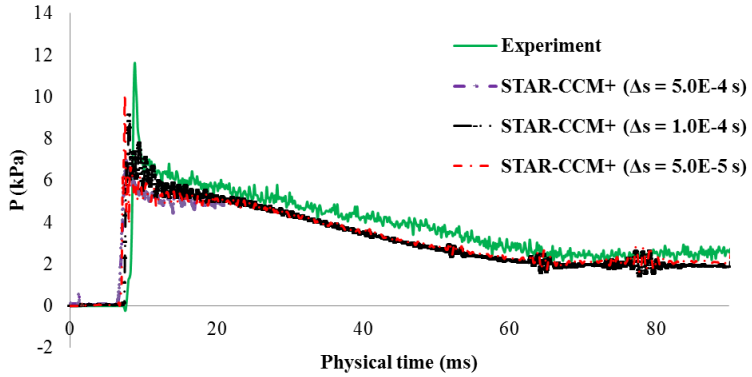

Fig. 2.7: The effect of time step (Δs) on the computed pressure at pressure transducer No.1.

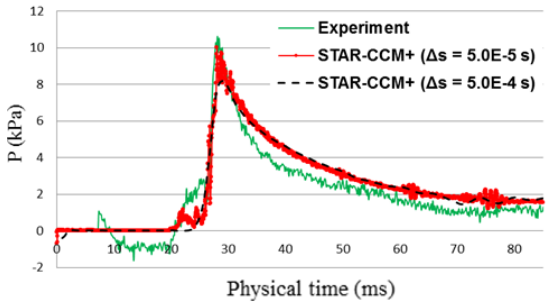

Fig. 2.8: The effect of two time steps in predicting P2.

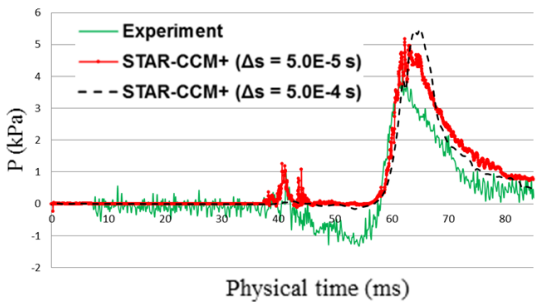

Fig. 2.9: The effect of two time steps in predicting P4.

The Courant number of tested simulations in the vicinity of pressure transducers was calculated as follows: "$\text{Courant number (CFL)} = \frac{1.35 \times 0.00005}{0.0075} = 0.1$". Thus, a Courant number of approximately 0.1 (based on the instantaneous impact velocity) is a good estimate for accurately predicting the slam peak pressures ensuring the independency of computed results on grid sizes.

2.3 SPH method

The results obtained using CFD were verified against simulations carried out by Shahraki et al. (2011), using the Smoothed Particle Hydrodynamics (SPH) technique. Shahraki et al. (2011) studied a range of coefficients of viscosity and speed of sound due to their significant effect on both computational time and accuracy of results. The study found that the optimal values for the numerical speed of sound[2], particle size and spacing among particles were 15m/s, 5 mm and 10 mm respectively.

In this study Shahraki ignored the influence of air in the simulations (i.e. the model was assumed to initially be located within a vacuum and then moved to impact a body of water).

2.4 Model tests

Whelan (2004) investigated the influences of geometry on slamming behavior of nine 2D 1/40-scale models entering still water under drop tests, see Fig. 2.10, at different conditions for varied wedge and catamaran geometries. Peak acceleration, velocity time record, average surface pressure and flow visualization were recorded and analysed. Various models were dropped vertically into still water using a drop test facility.

The University of Tasmania facility consisted of a 2.4m × 0.3m × 1.2m tank with a tower, main post, padded shock absorbers and two sets of adjustable bearings, (Figure 2.10). The bearings allowed for a free vertical translation motion without vibration. The gap at each end between the model and the wall of the tank in the 'y' direction set at 5 mm based on the results of a sensitivity study (Whelan, 2004).

Table 2-3: Details of Instrumentation (Whelan, 2004).

Sensor	Model	Range	Sensitivity	Resonant Frequency
Accelerometer	7290A-30	± 30 g	66 (±4) mV/g	1.5 kHz
Pressure Transducer	8510B-500	447 (± 0-3) kPa	4.1 kPa/Mv	500 kHz

[2] Numerical speed of sound which is always taken as less than the actual speed of sound in water and normally more than ten times the fluid maximum bulk velocity.

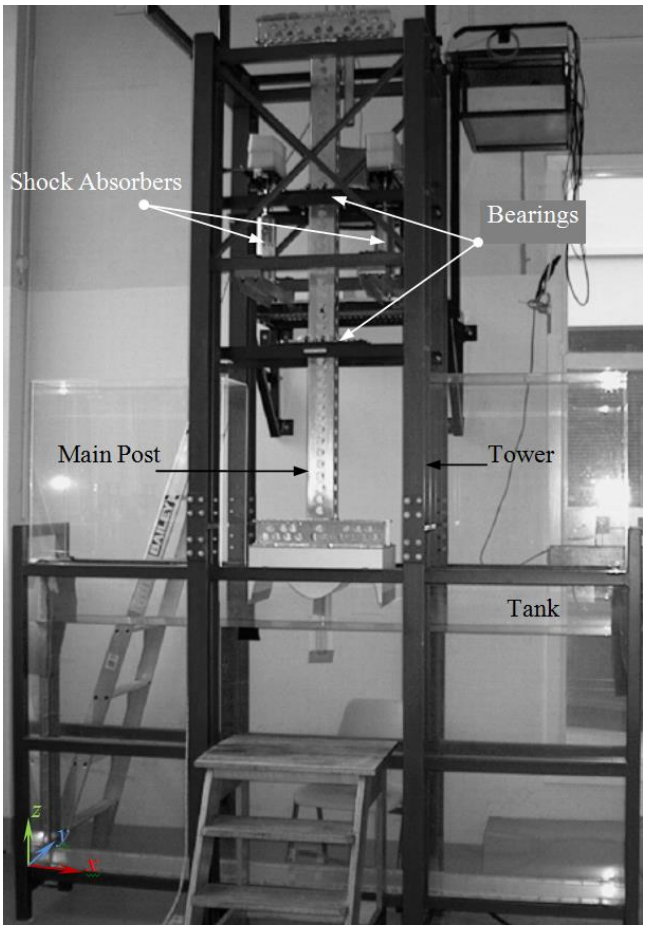

Fig. 2.10: Quasi-2D free-falling drop test tank at the University of Tasmania.

The data was recorded at a rate of 7042 Hz. In addition a high-speed camera was used to capture video images of the flow. The relevant specifications of the sensors used are given in Table 2-3.

2.5 Results and discussions

The results for wedge translation, velocity, vertical acceleration and pressure (using grid 2) are discussed both quantitatively and qualitatively. It was found that the computed pressures are very susceptible to the location of the pressure sensors and therefore a sensitivity study for the location of the pressure sensors was carried out in which a sensor's centre location in the simulation was varied to ±1.9 mm of the given location during experiments along the wedge side, see Fig. 2.11. The study was carried out on P3 transducer, which has a diameter of 3.8 mm.

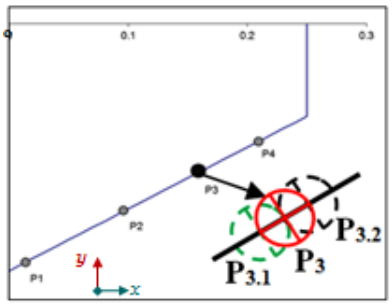

Fig. 2.11:Shifting positions of pressure transducer No.3 by ±1.9 mm.

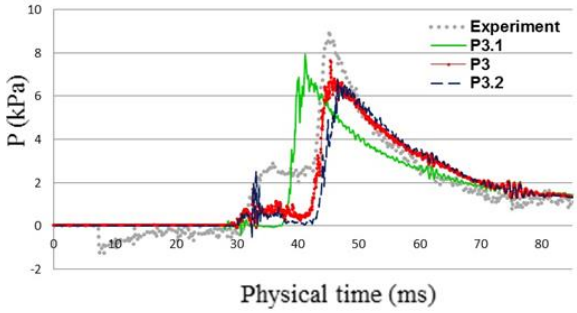

Fig. 2.12: The effect of the location of pressure transducers on the computed pressure.

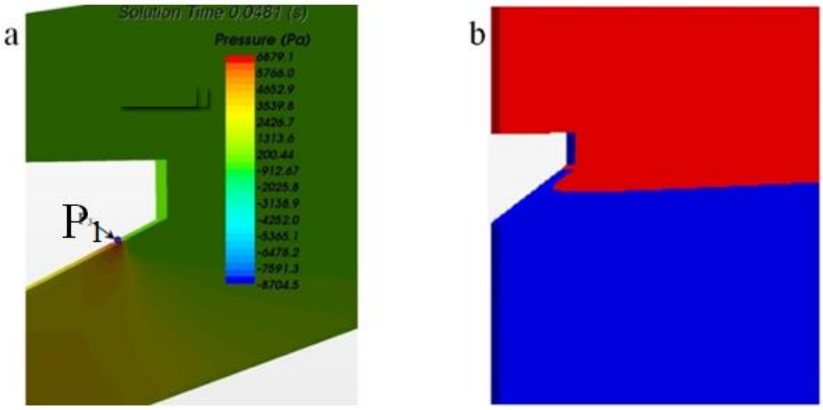

Fig. 2.13: 25° deadrise angle wedge shaped hullform during water-entry. Showing subplot (a) pressure contours and subplot (b) illustrates corresponding jet evolution that concurrent with P3 pressure peak.

The difference in the computed peak pressures due to changing the location of P3 was found to be approximately constant magnitude for P3.1 and result in a reduction in the magnitude of P3.2 (See Fig. 2.12). This emphasised the importance of validating the numerical results with high quality experimental data, as if there is a slight deviation in the position of the transducer, the error could be duplicated due to a sharp localized peak occurance on small sensing area, as shown in Fig. 2.9. Figs. 2.13-a and 2-13-b show the pressure contours concurrent with pressure peak at P3 and the corresponding jet formation respectively.

The wedge vertical translation during the drop is shown in Fig. 2.14. It is presented where time is set to zero when the wedge apex reaches the free surface with the same initial velocity as that measured in the experiments. The calculated vertical translations using SPH and CFD during wedge entry show excellent agreement with the experimental data, see Fig. 2-14. This is because the motion is predominantly dependent on the wedge's mass and buoyancy.

While SPH under predicts the drop velocity by approximately 8%, CFD shows excellent agreement with the experiments, see Fig. 2.15. Fig. 2.16 illustrates that the vertical acceleration is better predicted by CFD while SPH sustained unstable fluctuations.

The peak pressure is under predicted at P3 using CFD by 10%, as shown in Fig. 2.17. This emphasises that to accurately predict slam pressures a time step is needed (courant number around 0.1) and/or increased grid refinement. However this comes at the expense of reduced computational efficiency. However, the proposed verified CFD method using the same time step of the computed SPH results (i.e. Δs equal to 1.0E-4 s) shows better agreement with both pressure time-history trend and pressure peak measurement than using SPH in relation to the measured experimental data, as illustrated in Fig. 2.17.

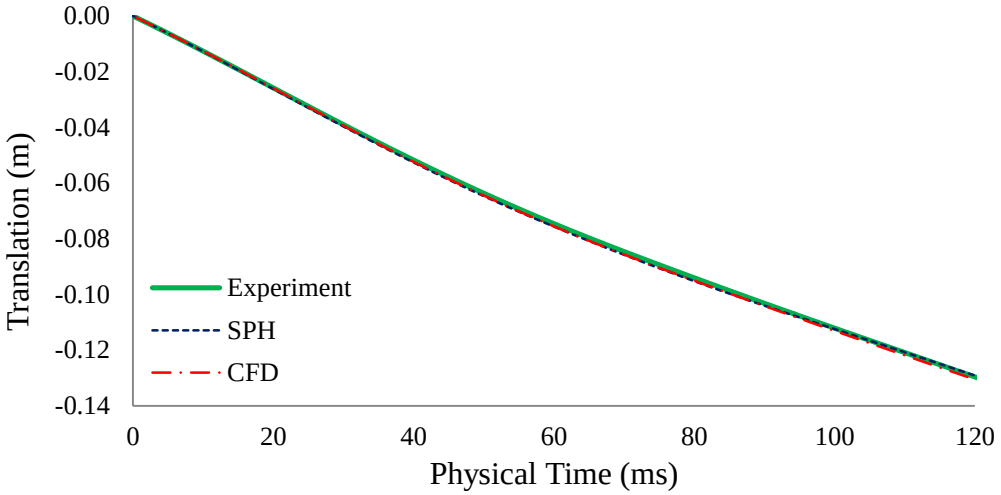

Fig. 2.14: Wedge vertical translation with respect to time.

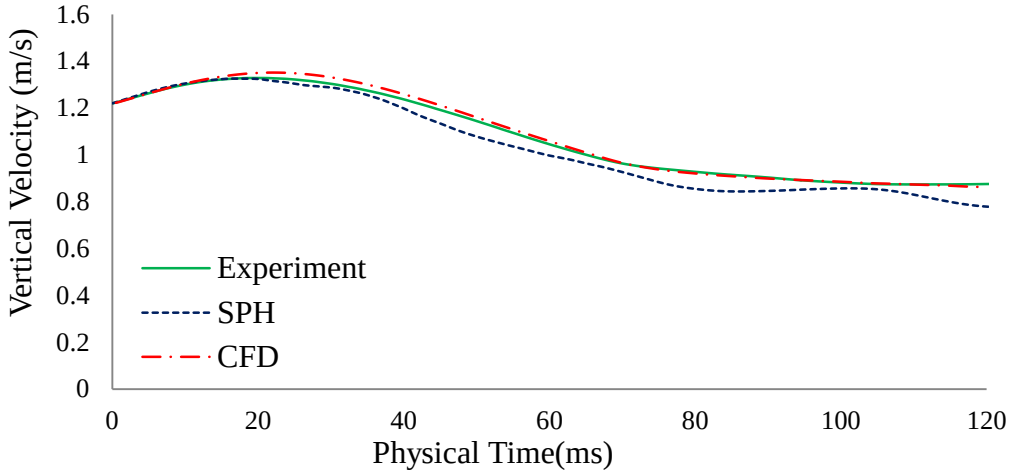

Fig. 2.15: Wedge vertical velocity with respect to time.

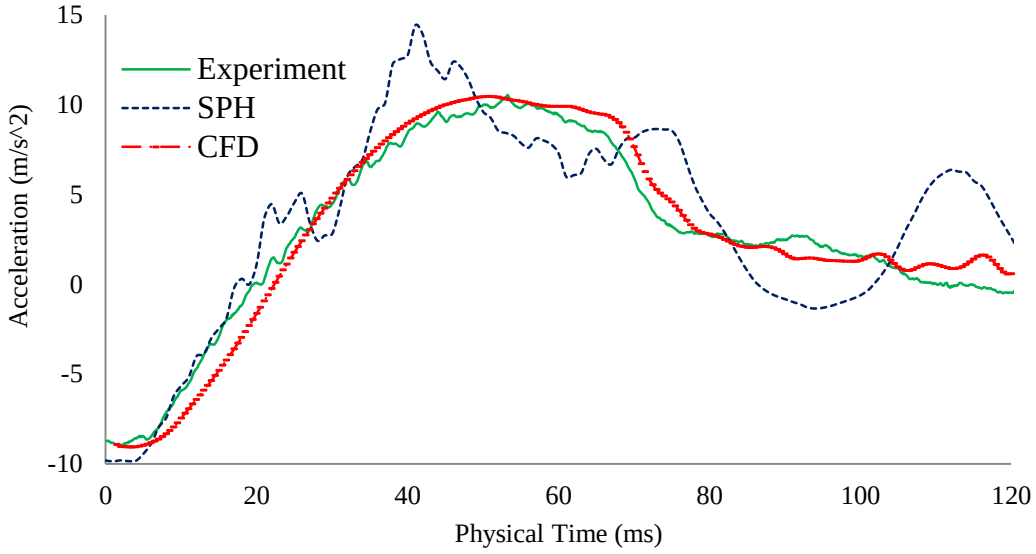

Fig. 2.16: Wedge vertical acceleration with respect to time.

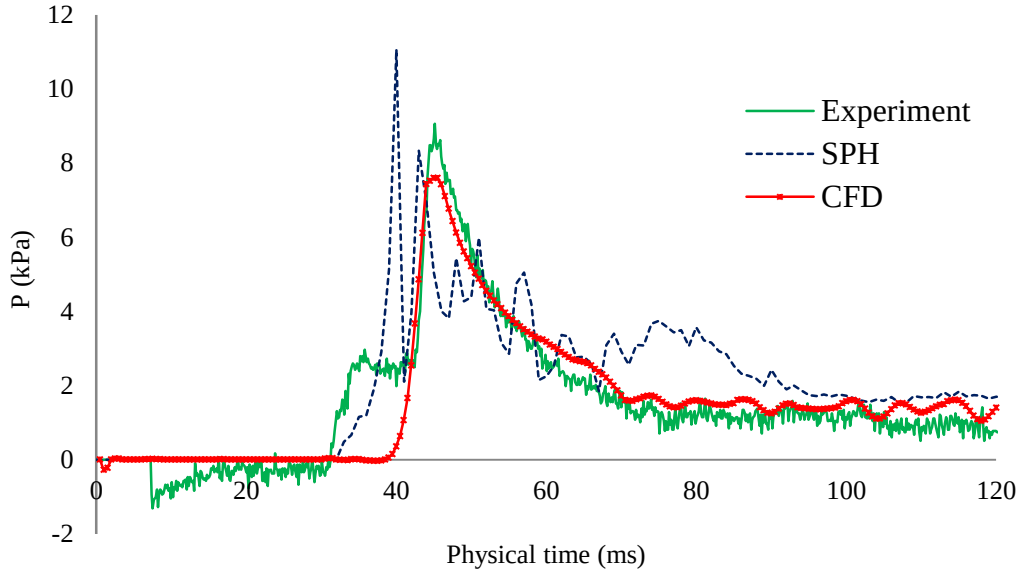

Fig. 2.17: Pressure time-histories at P3. Showing computed pressures using CFD and SPH (Shahraki et al., 2011) in relation to past experimental data recorded by Whelan (2004).

2.6 Conclusions

This chapter presented results of a comparative study for drop tests on symmetrical wedges. Numerical solutions using STAR-CCM+ CFD-code were compared with results from experimental drop test measurements. The simulations have illustrated the possibility of using CFD to accurately predict motion responses and local slamming pressures since excellent agreement was found with experimental data.

The location of the pressure transducers was found to have a significant effect on the numerical simulation results. Therefore much care and focus are needed when measuring the position of pressure transducers during experiments.

Relatively larger time steps can be used to accurately predict the wedge's motion responses, as well as the pressures distant from the wedge's apex.

Computing pressures near the wedge apex needs more focus due to the rapid increase of pressure in this particular zone. A Courant number of around 0.1 can be considered sufficient in predicting slamming pressures, particularly at the zone of large pressure change, as near the wedge apex.

The CFD results showed better agreement to the experimental results than available computed results using the 2D SPH technique, thus it is proposed that the work can be extended in the future to model slam loads of catamarans.

Air should be included within the simulation domain to improve the accuracy of the predictions for the slam pressure distributions and corresponding vertical acceleration, i.e. neglecting the air influences, such as done in the SPH simulations leads to inaccurate predictions.

2.7 Next steps

Having established the appropriateness of using CFD to predict 2D slam events for wedges, the next step is to extend the CFD simulations to predict impact pressures and corresponding motions of a quasi-2D wave-piercing catamaran model during water impact. This is a more complex situation than for the monohull wedge since the catamaran configuration provides restrictions for water and air movement from the impact region, so that the influence of including air compressibility also needs investigation.

Chapter 3

Predictions of quasi-2D wetdeck slam loads

This research was originally published, after peer-review, as:

Swidan, A., Thomas, G., Ranmuthugala, D., Penesis, I. & Amin, W. Numerical investigation of water slamming loads on wave-piercing catamaran hull model. In: 10th Symposium on High Speed Marine Vessels (HSMV), October 2014, Naples, Italy.

(http://www.hsmv.unina.it/conference%20proceedings/Papers/05.pdf)

For the avoidance of repetition the original paper has been modified for this thesis.

Chapter 4

Experimental investigation into wetdeck slamming loads

This research was originally published, after peer-review, as:

Swidan, A., Thomas, G., Ranmuthugala, D., Penesis, I., Amin, W., Allen, T. & Battley, M. Experimental drop test investigation into wetdeck slamming loads on a generic catamaran hullform. Ocean Engineering, vol. 117C, pp. 143-153. 2016a.

(http://dx.doi.org/10.1016/j.oceaneng.2016.03.059)

For the avoidance of repetition the original paper has been modified for this thesis.

4.1 Introduction

To date no three dimensional water impact tests of catamaran hull forms have been conducted and as such it has not been possible to validate 3D CFD predictions for these hull forms. This work was therefore motivated by the lack of data suitable for benchmarking catamaran vessels in a 3D flow regime.

The controlled-velocity water impact experiments reported here therefore focus on the characterisation of local slamming loads for a generic hull form of a wave-piercer catamaran during water entry. Direct measurements of hydrodynamic forces and pressure distributions are provided on an arched semi-closed wetdeck impacting water for a range of speeds and the three dimensionality of the water flow during the impact events is characterised.

4.2 Model and experimental setup

4.2.1 The controlled speed test system

Figure 4.1 illustrates the main components of the SSTS. The tank was filled to a depth of 1.15m with fresh water at a temperature of approximately 11°C.

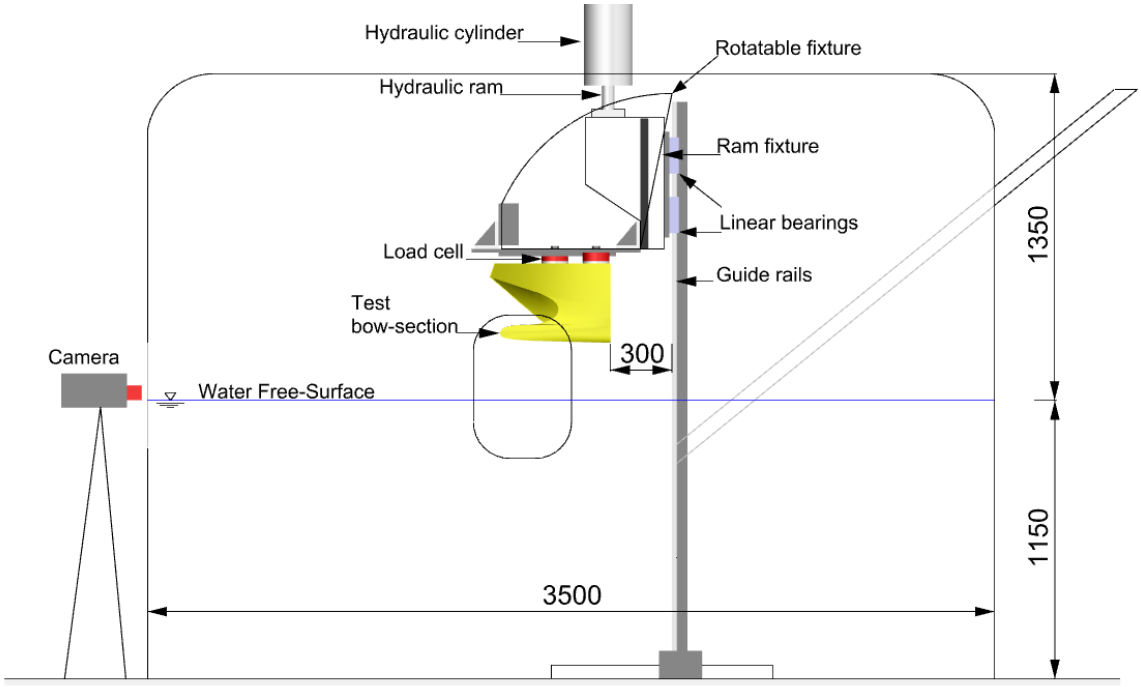

Fig. 4.1: Profile view of hydraulic test installation (dimensions in mm).

The water depth was considered sufficient as it was comparable with water depths used in previous controlled speed test experiments of similar or larger test specimens, such as those recently presented by Alaoui et al. (2015) and Tveitnes et al. (2008).

A sight window measuring 0.1m width x 0.4m height was cut into the side of the tank covered by 3 mm clear perspex in order to allow the high-speed camera's lens to face the model.

Although the test fixture can be used to set up different angles of trim for the model, from 0° up to 40° in 10° increments, based on results from previous full-scale trials and seakeeping tests for this particular type of vessel (for example those conducted by Jacobi et al. (2012) which showed slamming occurring at small pitch angles, all tests were conducted at zero trim angle.

4.2.2 The test model

A generic wave-piercer catamaran model was constructed at the Australian Maritime College (AMC), with the lines plan as shown in Fig. 4.2. The hull form is for a wave-piercer catamaran with a centrebow similar in style to those designed by Revolution Design Pty Ltd and manufactured by Incat Tasmania. The body lines of the generic wave-piercer catamaran hull form are presented (on the right hand side) with a 25 mm longitudinal spacing. On the left hand side of this diagram the transverse sections on which the pressure transducers were mounted are presented. This is to clarify the geometrical variations in the sections where the transducers were located.

The test model has a length (T) of 500mm, beam (L) of 638mm, height (H) of 327.6 mm and total mass of 14.8 kg. It was sized to ensure that there would be a gap between the model and the tank wall of double the model's overall beam. This was to minimise boundary condition effects and the possibility of wave reflections.

A three-dimensional Computer Numerically Controlled (CNC) router was used to cut the model out of 15 layers of glass reinforced plastic giving a total shell thickness of 10 mm with minimal surface roughness. This construction technique ensured high accuracy in positioning the pressure transducer locations (±0.1 mm). In addition the model was internally stiffened

by a grid of 12 mm thick plywood in both the longitudinal and transverse directions with a maximum spacing of 150 x 100 mm (see Fig. 4.3). All internal spaces were then filled with closed-cell expanding foam to avoid water ingress during the controlled speed tests.

A limited space around the pressure transducers was partially sealed using plastic sheeting and silicon to enable access to the transducers during the tests, if required. The model was installed on the centreline of the moving test fixture, as shown in Fig. 4.4.

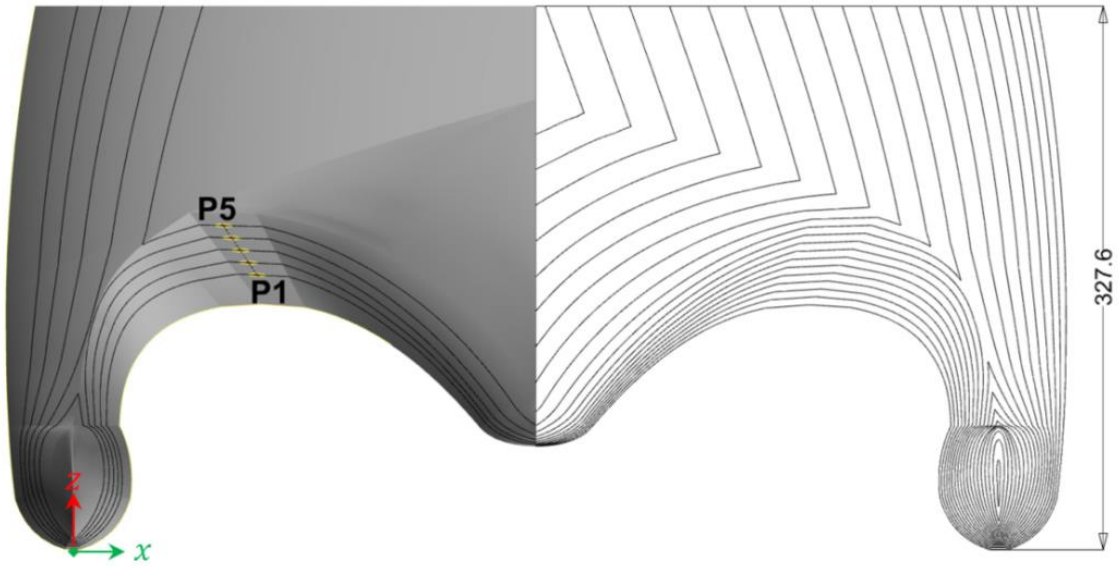

Fig. 4.2: Body lines of generic catamaran hull form, also showing the locations of the five pressure transducers.

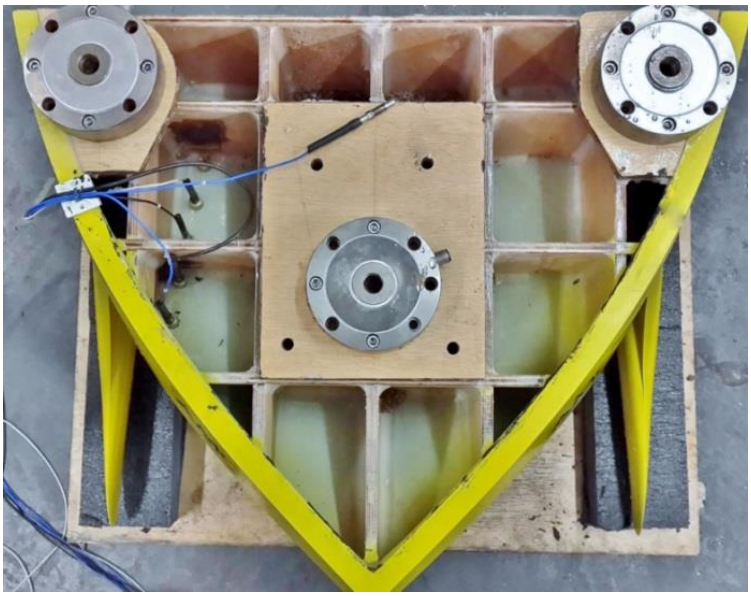

Fig. 4.3: Test model instrumented with three load cells and five pressure transducers. All spaces were filled with expanding foam prior to testing.

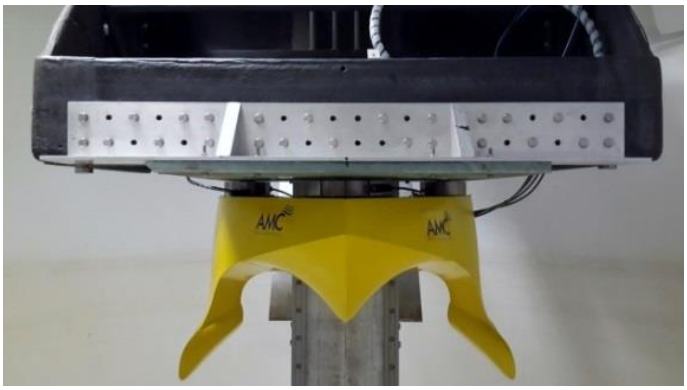

Fig. 4.4: Test model installed on the centreline of the moving test fixture.

4.2.3 Instrumentation

In order to characterise the response during impact the key parameters measured in the tests were vertical force and pressure. A summary of the instruments and signal conditioning hardware is given in Table 4-1.

Table 4-1: Details of Gauges.

Gauge	No. of Channels	Manufacturer	Model	Maximum Range	Signal conditioning
Load cell	3	Precision transducers	LPC-5 t	5000 kg	NI9237cDAQModule
Pressure Transducers	5	PCB-piezotronics	113B-26	68950 kN/m^2	NI9234cDAQModule
Position sensor	1	Vishay	REC-139L	3 m	PCB-483B0324vDCSupply

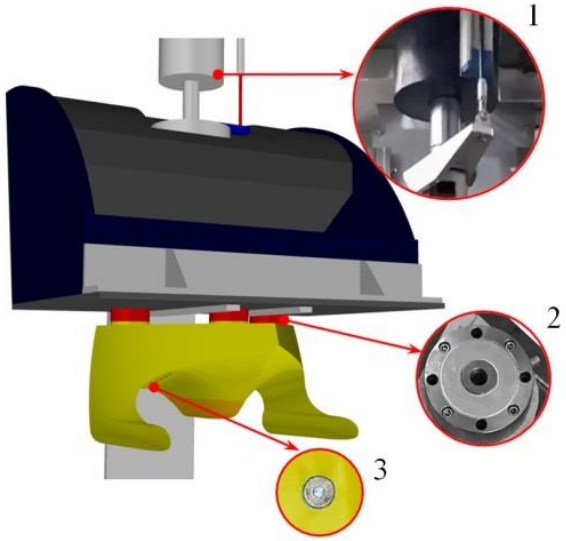

Fig. 4.5: The experimental test setup instrumentation; showing 1 = LVDT and hydraulic ram cylinder, 2 = Load Cell and 3 = Pressure transducer and fitting surface.

The total slamming loads acting on the model in the vertical direction were acquired directly by means of three full bridge load cells installed between the model and its stiffened support in the rig, as shown in Figs. 4.3 - 4.5. Three load cells were considered to be the minimum number sufficient to avoid moments during the impact phase based on recent drop-test experiments, such as those of Huera-Huarte et al. (2011). All the total impact force measurements presented in this paper are the sum of the three load cell outputs.

To measure the impact pressure on the model five Piezotronics transducers were mounted at selected positions equally distributed by 38.7 mm in the y direction along the highest points on the wetdeck arch at each transverse section, as shown in Figs. 4.2 and 4.5. Figure 4.2 also illustrates that the wetdeck arch surfaces in the vicinity of the fittings were designed to be flat to ensure the pressure transducer fittings were flush with the hull. Non-flush pressure sensors can cause separation in the flow, and hence affect the accuracy of measured pressures (Pistani & Thiagarajan, 2012; Van Nuffel et al., 2013). The exact locations of the pressure transducers are given in Table 4-2 and shown in Fig. 4.6, in relation to a fixed coordinate system as presented in Figs. 4.2 and 4.6 with the origin on the baseline at the bow of the starboard demihull.

A high-speed camera (Photron Fastcam SA5 model) with a maximum frame rate of 7500 fps and a 1 megapixel resolution was utilised to film the impact events at 3000 fps to preserve high resolution. This footage provided the opportunity to obtain an improved understanding of the flow behaviour beneath the arched wetdeck during the model water-entry. The time history of the moving model's position was measured using the servo-hydraulic system's linear displacement transducer. The velocity time history was obtained by differentiating the corresponding position to the corresponding time history.

Table 4-2: Location of Pressure Transducers.

Transducer/ Location	*x* (mm)	*y* (mm)	z (mm)
P1	111.06	96.82	165.62
P2	105.98	135.53	173.08
P3	100.9	174.25	180.53
P4	95.82	212.95	187.99
P5	90.74	251.67	195.45

The signals from all the instruments were acquired using a modular National InstrumentsTM compact data acquisition system (cDAQ 9178) with National Instruments LabVIEW software used to record the signals. Data recording was triggered once the model had travelled 50 mm from the start of each test. A sampling rate of 51.2 kHz was used; this is more than 2.5 times the sample rate used by Graczyk & Moan (2008) to reflect the real time histories of sloshing impacts, given also that the minimum recommended sample rate by the DNV (2010) is 20 kHz to provide sufficient density of data points, especially for the pressure peaks.

The measured data was automatically converted into its corresponding unit of measured data using the calibration factors that were input into the DAQ software prior to the tests.

4.2.4 Test conditions

The water impact experiments were conducted using the Servo-hydraulic Slam Testing System (SSTS). This system was originally developed at Callaghan Innovation, Auckland, New Zealand, and is now located at the Centre of Advanced Composite Materials, University of Auckland. This controlled-speed water impact facility consists of a circular polyethylene water tank measuring 3.5m in diameter and 2.5m in height. It has a servo-hydraulic system with a ram actuator supplied by pressure from two pre-charged accumulators. The velocity of the ram is controlled by a computer feed-back system and servo-valve, enabling constant or variable-velocity impacts to be achieved up to velocities of 10m/s. Attached to the end of the ram is a test fixture, which slides vertically on linear bearings. The motions of the fixture are therefore restricted in all degrees of freedom except for vertical motion. More details of the SSTS can be found in Battley & Allen (2012) and Stenius et al. (2013).

The water impact experiments were conducted at a range of controlled water-impact velocities as given in Table 4-3, with the speeds primarily being selected based on full scale impact values. A recent analysis of full-scale trials conducted by Jacobi et al. (2012) found that relative vertical velocities of up to 13m/s can occur. Consideration was also given to ensure that the ratio of measured loads to the maximum allowable load of the load cells (5 tonne) was sufficient to provide a good signal to noise ratio.

Table 4-3: Summary of Test Conditions.

Condition Units	v_{target} (m/s)	v_{impact} (m/s)	$v_{std\ x\ 100}$	$F_N = v_{impact}/\sqrt{gL}$
1	2.5	2.39	0.6	1.08
2	3	2.76	1	1.24
3	3.5	3.22	1.7	1.45
4	4	3.72	1.9	1.67
5	4.5	4.05	2.3	1.83
6	5	4.45	0.8	2.01

Additionally the test system needed to operate in a range that would minimise any velocity variations during the water-entry process, based on a study conducted by Battley & Allen (2012). The selected range of target velocities is given in Table 4-3. Also provided in this table are the corresponding average velocities that were achieved during the impacts, the corresponding standard deviation (v_{std}) of repeated tests and the corresponding Froude number based on the centrebow's length with a full scale value of L = 19m.

The SSTS was programmed to achieve the target velocity at a point at least 100 mm above the free surface. The driving ram continued to maintain a constant speed for at least 250 mm after the demihull keels touched the water, to ensure that the wetdeck was completely submerged. The maximum allowable distance to ensure the rig was stationary after a water impact was 810 mm from the datum, i.e. more than 600 mm from tank bottom.

After each controlled speed test the rig was returned back to its starting point by means of the hydraulic system. A time of at least 15 min was allowed between tests to ensure that the water free-surface was calm.

4.3 Uncertainty analysis

4.3.1 Random uncertainties

To confirm that the random uncertainty was within acceptable tolerances each condition was repeated for a minimum of three tests; this also provided confidence in the instrumentation and the recording DAQ system. The measured data from three controlled speed tests, for a target velocity of 4.5m/s, are presented in Fig. 4.7.

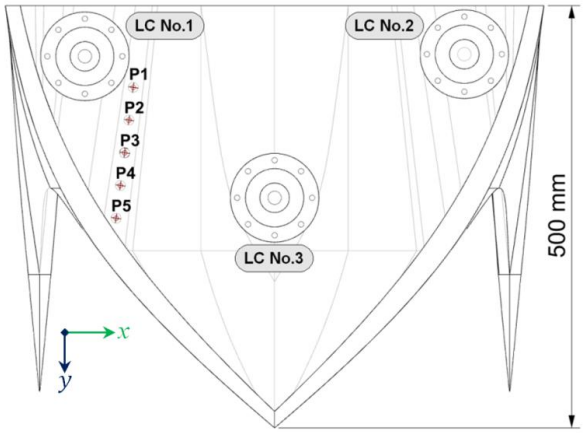

Fig. 4.6: The instrumented test model and spatial distribution of gauges (P = pressure transducer while LC = load cell).

The zero time and zero immersion refer to the instant at which demihull keels touch water, while the transducer positions used are illustrated in Fig. 4.6. Figure 4.7(a) shows excellent repeatability for the immersion data. In addition the velocity profile, illustrated in Fig. 4.7(b) (derivative of immersion), shows minimal variation between the three tests. The velocity magnitude drops by 6.5% for Test No.1 and 10% for Test No.2, in relation to the target velocity, during the impact phase. There is a direct correlation between the reduction in velocity and the development of the hydrodynamic loads between 28 and 45 ms, which is attributed to some lag in the response of the servo-hydraulic system.

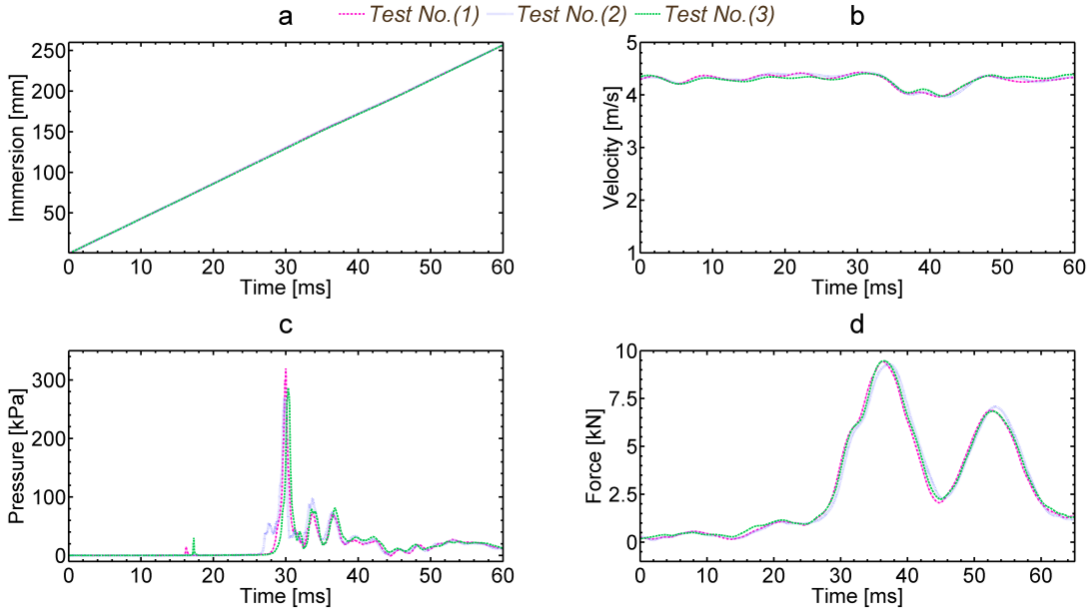

Fig. 4.7: Repeatability of three tests for target velocity of 4.5m/s; (a) immersion, (b) velocity profile, (c) pressure transducer and (d) hydrodynamic load.

The pressure peak at the transducer P1 is illustrated in Fig. 4.7(c), and was found to be uncertain by a maximum of ±5%, which is half the difference between the maximum and minimum values of pressure peaks (from repeated tests) divided by the mean value of pressure peaks. Fig. 4.7(d) illustrates excellent repeatability in the magnitude of the total impact force peak with uncertainty of approximately 2%.

Figures 4.8 - 4.10 confirm that the slam loads are strongly dependent on velocity profile. Thus it is more appropriate to compare the data with respect to instantaneous velocities rather than the target velocity, which can vary slightly due to the hydraulic system response and/or any change in the point where the ram starts to accelerate. Dismantling the model from the rig, then reinstalling it and repeating the tests confirmed the repeatability of the complete system set up. This was carried out at the target velocity of 4m/s, as presented in Figs. 4.9-11.

Not all of the uncertainty in force and pressure traces should be attributed to the instantaneous velocity; the velocity time series before impact can also influence jet formation and hence the amount of aerated water beneath the arched wetdeck during the impact phase.

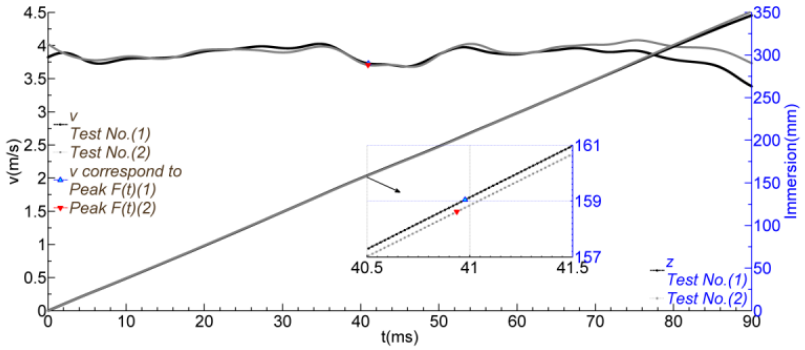

Fig. 4.8: Immersion and velocity time histories of repeated tests at target velocity equal to 4m/s.

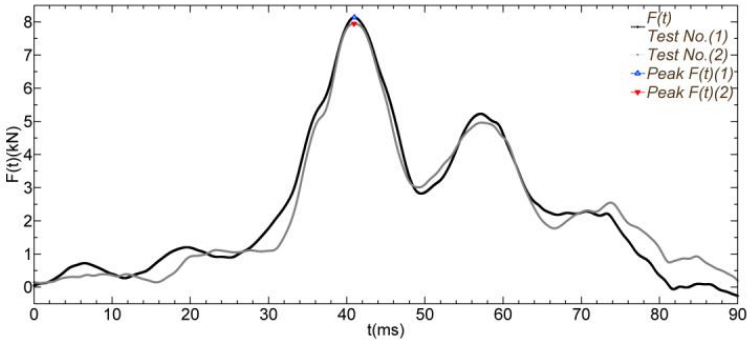

Fig. 4.9: Total hydrodynamic load time histories of repeated tests at target velocity equal to 4m/s.

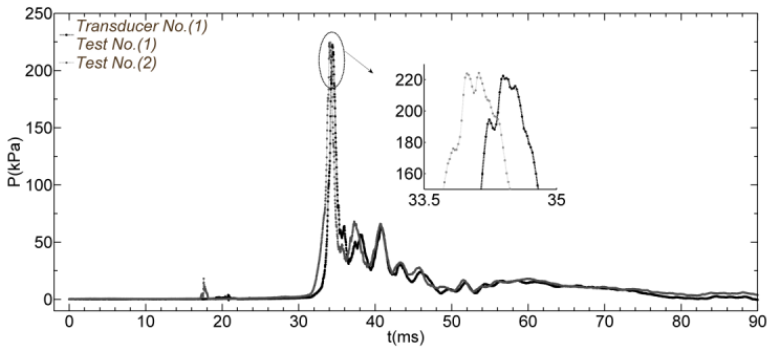

Fig. 4.10: Hydrodynamic pressure time-series of P1 at target velocity equal to 4m/s.

Figures 4.8 and 4.9 show that a change of 0.35% in impact velocity can affect the peak force magnitude by up to 3%. The subplot in Fig. 4.8 points to the immersion of the model during the impact phase and shows good repeatability between tests. Figure 4.10 illustrates excellent repeatability between measured peak pressures with uncertainty between the magnitude of peaks of 1.5%. Although there is slight temporal deviation between both pressures, the results correlate well with the velocity profiles.After each test some water droplets remained on the surface of the model. The effect of these droplets was determined to be negligible with no discernible difference in the results being apparent if the model was dried or not before a test. This was probably due to the two water-jets, from the entry of the demihulls and the centrebow, mixing at the top of the archway, as shown in Fig. 4.11, so that the wet deck is already wet when a slam event commences.

Fig. 4.11: Evolution of water-jets from the centrebow and demihull prior to wetdeck slamming event for a target velocity of 4m/s.

4.3.2 Systematic uncertainties

The systematic uncertainties were estimated for all of the instrumentation, based on technical data provided by the manufacturers, and this is summarised in Table 4-4. As stated in Section 4.4, the model was installed using a stiffened support in the rig through load cells to directly measure the vertical impact loads. This rigid support in the rig is inclined by less than 1° and hence considered horizontal.

Table 4-4: Summary of Systematic Errors.

Error source/ Gauge	Ram position	Load cell	Pressure transducer
Linearity error (%)	±1	0.05	1
Acquisition system (%)	1.2	1.2	1.9
Total (%)	2.2	1.25	2.9

4.3.3 Velocity variations

One of the principal factors affecting slamming loads is the impact velocity. Hence relating loads to the target velocity can be considered to be inaccurate when the measured velocity deviates from the target velocity.

Fig. 4.12 illustrates the maximum error bounds (Equation 4.1) in the measured velocity corresponding to the target velocity within the selected range of velocities, i.e. from 2.5m/s up to 5m/s in 0.5m/s increments.

Figure 4.12 shows that the uncertainty range can depend to some extent on the target velocity, i.e. around 4% reduction in target velocity at 2.5m/s, while the impact velocity decreased by approximately 11% for a target velocity of 5m/s. This is likely due to the direct correlation between the water entry velocity and the corresponding slam load, as will be discussed in Section 4.5.

$$Error\ bound = \frac{2(v_{target} - v_{impact})}{(v_{target} + v_{impact})} x100\% \qquad (4.1)$$

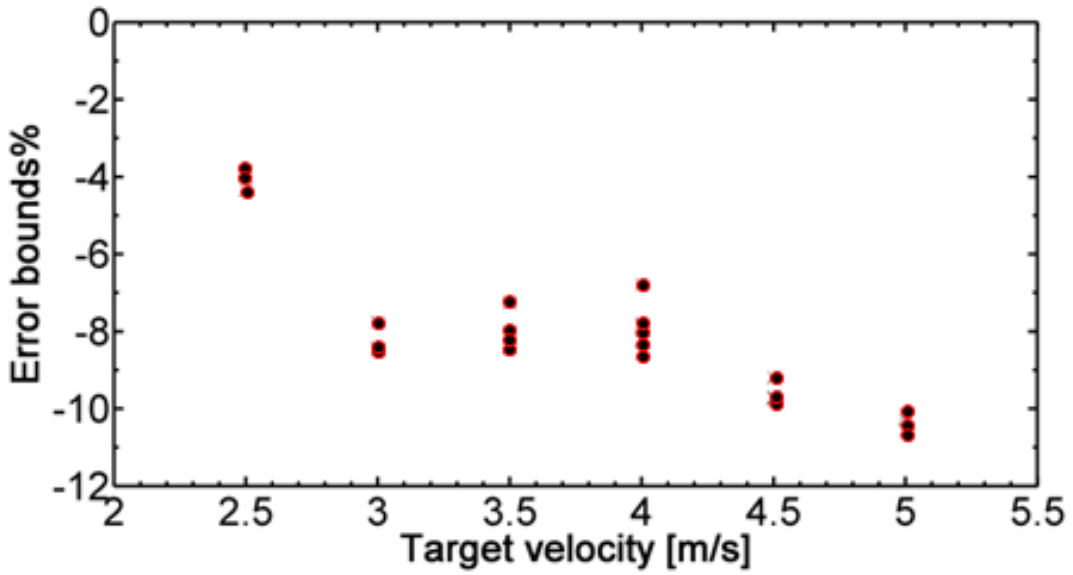

Fig. 4.12: Error bound of water impact velocity for the target velocity.

This variation was considered acceptable when compared with other facilities such as that used by Tveitnes et al. (2008) where the velocity varied by ±11% for a 5° wedge section during the impact phase at lower velocities than those used in the present work. To account for this slight change in velocity profiles all presented data in Section 4.5 corresponds to the instantaneous impact velocity rather than the target velocity.

4.3.4 Filtering

No filtering was applied to the pressure measurements during post processing to avoid the possibility of curtailing any peaks.

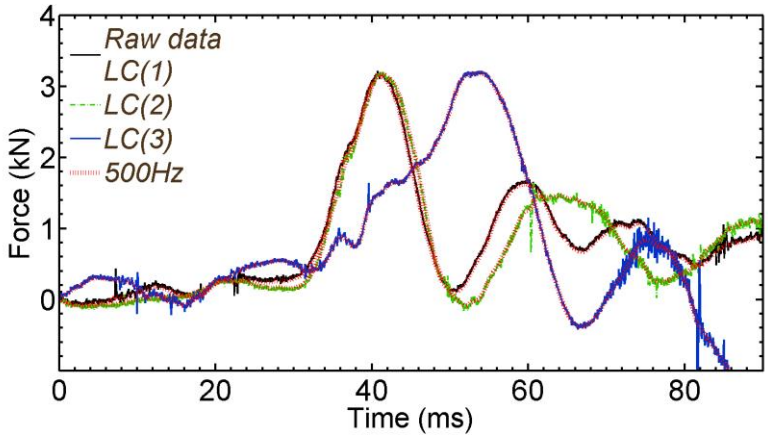

Fig. 4.13: Comparison of raw load signals from three load cells during 4m/s water-entry with filtered data with a cut-off frequency of 500 Hz.

The noise levels were seen to be negligible compared with the signal magnitude. The high sampling rate resulted in some noise in the hydrodynamic impact load signals, therefore a low-pass Butterworth filter was applied with a cut-off frequency of 500 Hz to all load signals during post processing. The results of this filtering on the loads can be seen in Fig. 4.13.

The filter was conducted using Matlab function named 'filtfilt' which is zero phase digital filtering, that preserves signal time-history in line with the original signal by processing current point in relation to both forward and reverse points in the frequency domain, further information can be found in Mitra & Kuo (2006).

4.4 Results and discussion

4.4.1 Time history results

The results from three model controlled speed tests at target velocities of 4, 4.5 and 5m/s are presented in this section. Figs. 4.14-4.16 include (a) immersion, (b) velocity, (c) vertical slam force and (d) pressure traces. The data presented starts at time instant t_o = 0 ms, which is the instant when the demihull keels touch the free surface. In these figures: subplots (a) illustrates the measured immersion time history, where the submergence of the model Z_o = 0m is concurrent with t_o; the calculated velocity time histories are presented in subplots (b); subplots (c) illustrate the three load cell outputs and their summation of the total vertical slam force acting on the entire model; subplots (d) represent the pressure traces at five selected points along the arched wetdeck corresponding to the pressure transducer location areas shown in Figs 4.2 - 4.6.

The results for an impact with a target velocity of 4m/s are now discussed in detail. The time history of the vertical immersion shows a linear water-entry process, as presented in Fig. 4.16(a). In Fig. 4.16(b) the velocity shows small variations of approximately 6% around a mean value of 3.85m/s. The most significant reduction in relative velocity corresponds to the time when the slam force is at a maximum at approximately t = 41 ms.

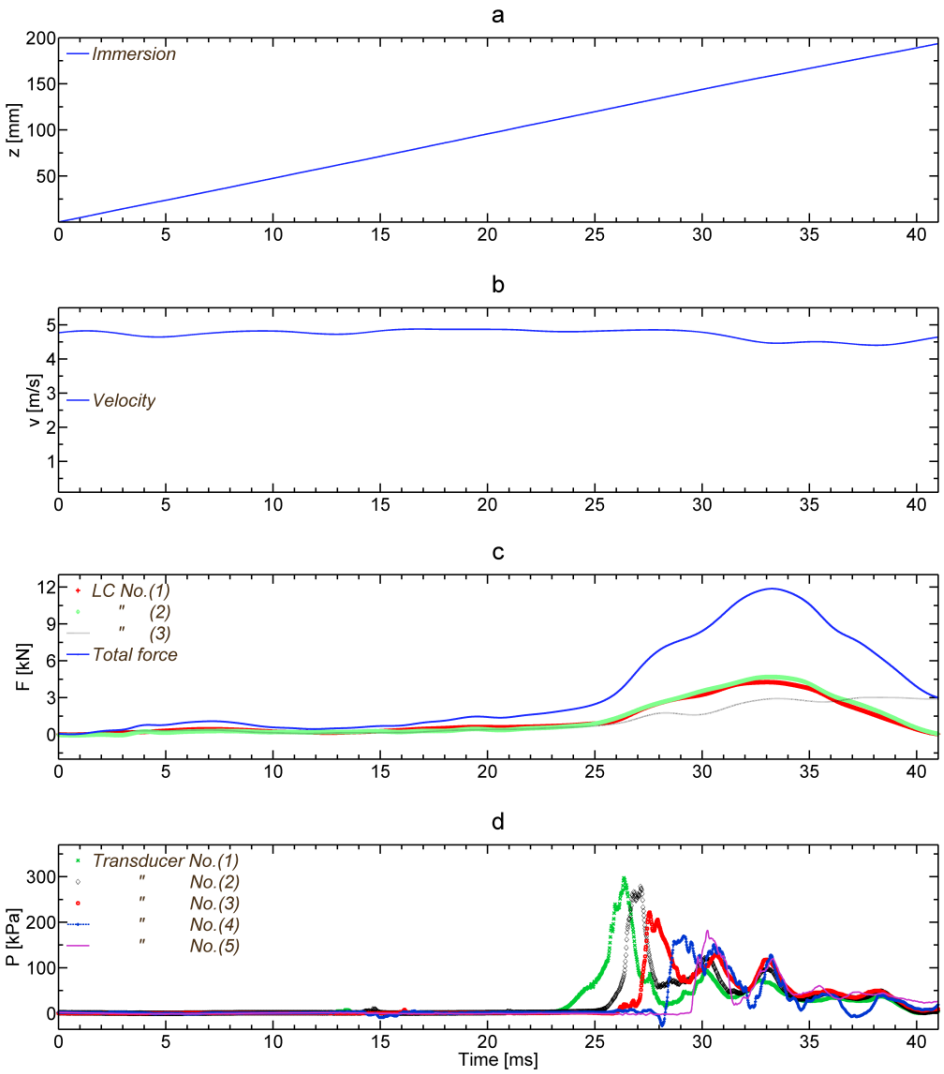

Fig. 4.14: Time-history of measured data (target velocity of 5m/s), (a) immersion, (b) velocity, (c) total hydrodynamic load and measured forces from three load cells, (d) pressure trace from P1 to P5.

Looking in detail at the total slam force results (Fig. 4.16(c)), the vertical force exhibits a series of peaks at 7, 19.5 and 41 ms, which correspond to different incidents in the overall slam event. These incidents are shown in the high-speed photographs presented in Fig. 4.17. The initial small peak in the slam force at 7 ms corresponds to an immersion of 26mm, when the broad section of the demihull keels start to displace water. At 19.5 ms the centrebow keel hits the free-surface, followed by an increase in slam force until it reaches the slam force peak at 41 ms, corresponding to 159 mm of immersion when the archway is filled with water and this followed by a rapid reduction in force, as presented in Fig. 4.16(c).

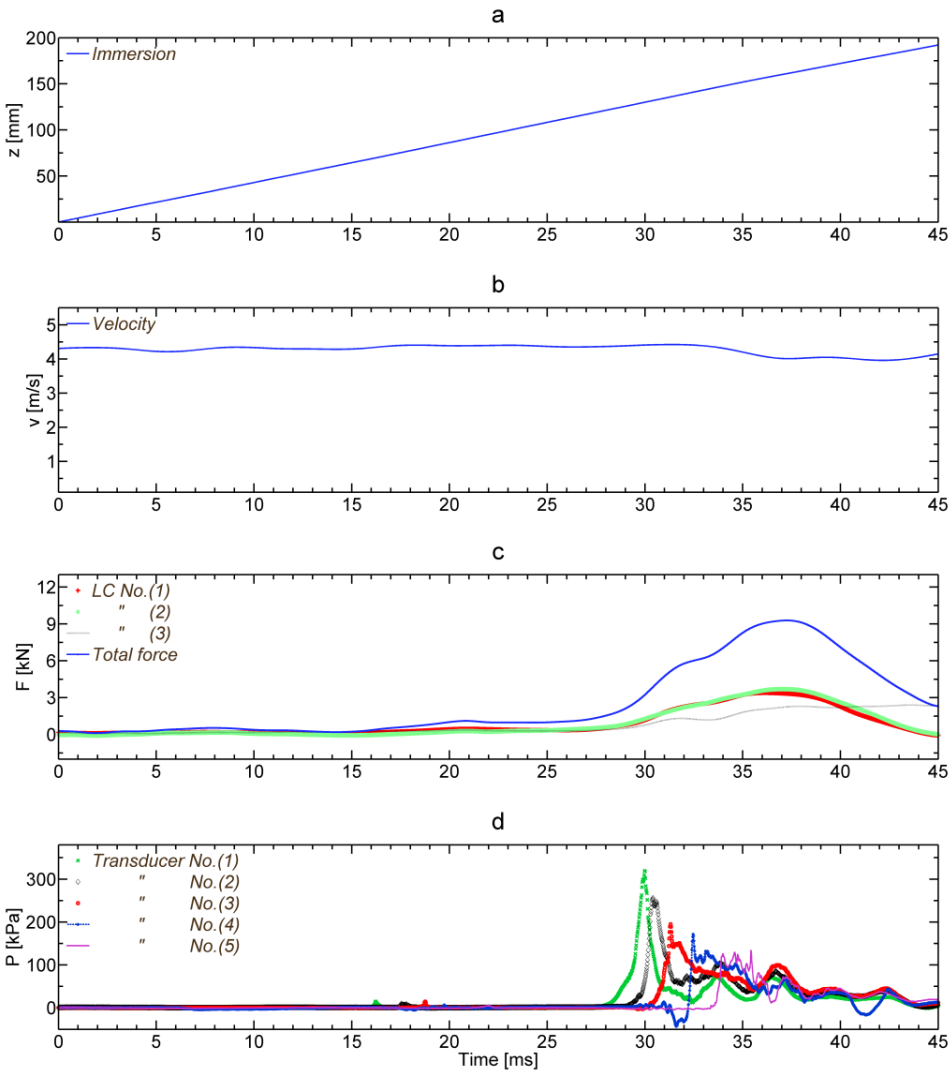

Fig. 4.15: Time-history of measured data (target velocity of 4.5m/s), (a) immersion, (b) velocity, (c) total hydrodynamic load and measured forces from three load cells, (d) pressure trace from P1 to P5.

In Figure 4.16(c) the individual signals from each of the three load cells are presented. The outputs of load cells LC1 and LC2, which are aligned transversely at the aft end of the model show good agreement with respect to rise time to peak load as well as the peak magnitude, indicating that the model enters the water symmetrically.

The resultant total force occurs mostly in the aft portion of the centrebow since the measured loads from the aft load cells have approximately double the magnitude of LC3 which is located close to the centre of the model.

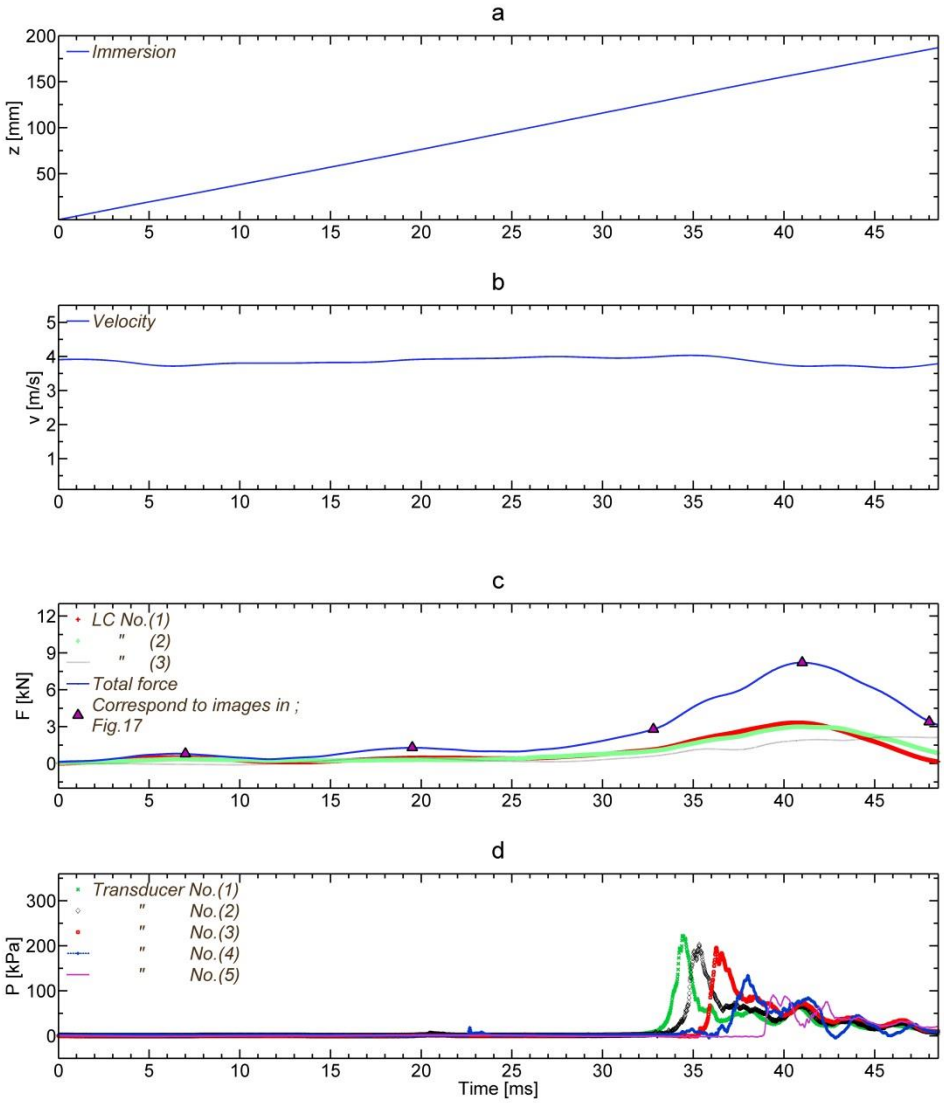

Fig. 4.16: Time-history of measured data (target velocity of 4m/s), (a) immersion, (b) velocity, (c) total hydrodynamic load and measured forces using three load cells, (d) pressure trace from P1 to P5, while '^' marker corresponds to images in Fig. 4.17.

The total vertical force indicates that the severity of the slam starts to increase rapidly at 33.8 ms, which relates to an immersion of 130 mm. This observation is important since it shows that for wetdeck slamming to occur, the archway does not need to be immersed to a level equivalent to the original free-surface. Instead the archway is filled before this amount of immersion occurs due to ingress of water displaced by the immersing demihulls (as shown in Fig. 4.17 at a time of 19.5 ms) and the centrebow.

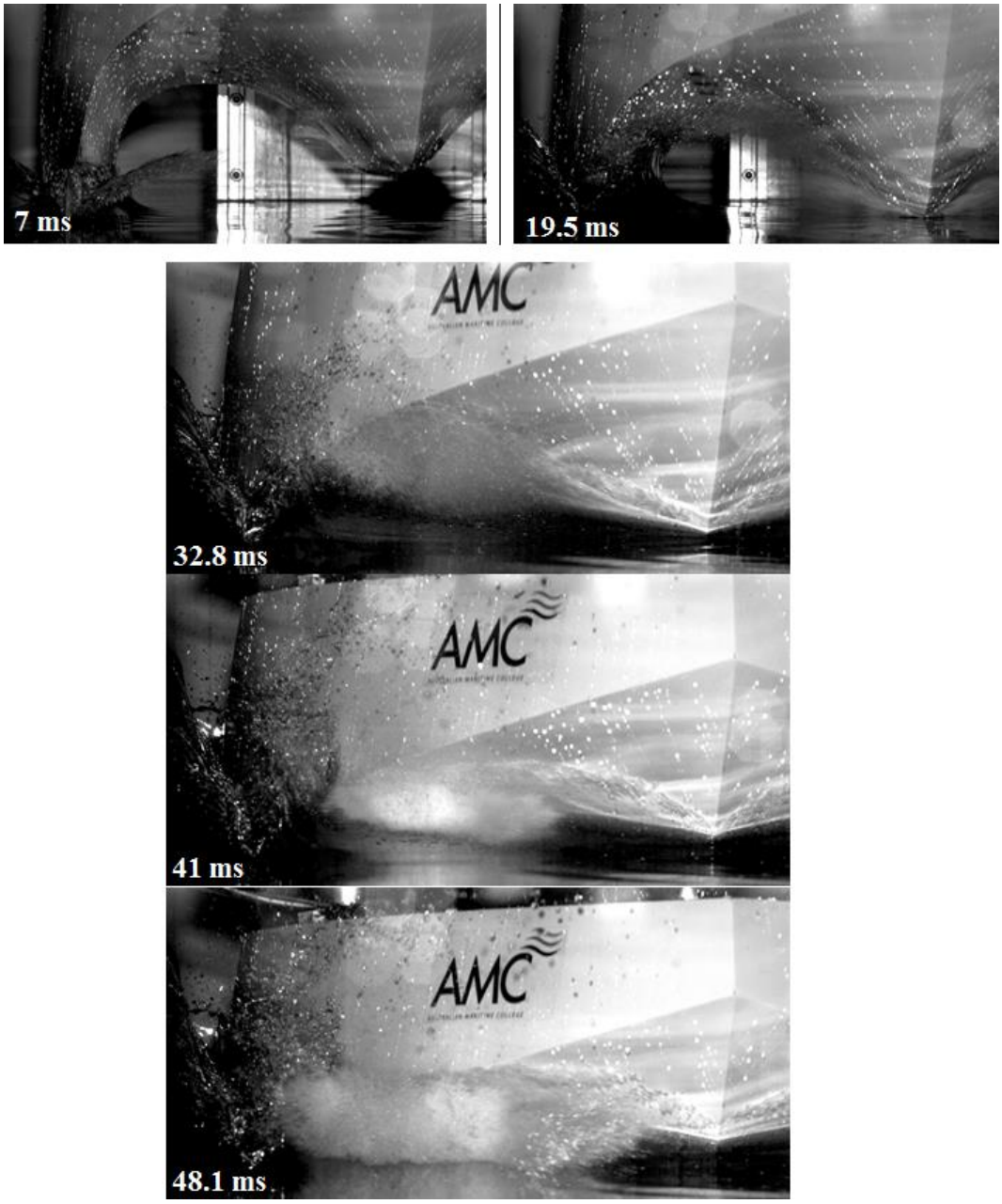

Fig. 4.17: Frames taken by high-speed camera 3000 fps (frame per second) correspond to 'Δ' markers in Fig. 16 (c).

This effect was previously proposed following model experiments of a wave-piercer catamaran in irregular waves by Thomas et al. (2011a). However, with no high-speed camera it was not possible to verify this phenomenon at that time. In these experiments it was confirmed through high-speed camera images, for example those taken at frames of 19.5 ms and 32.8 ms, as presented in Fig. 4.17. The images show an increase in water elevation in relation to the original free surface prior to the wetdeck water impact.

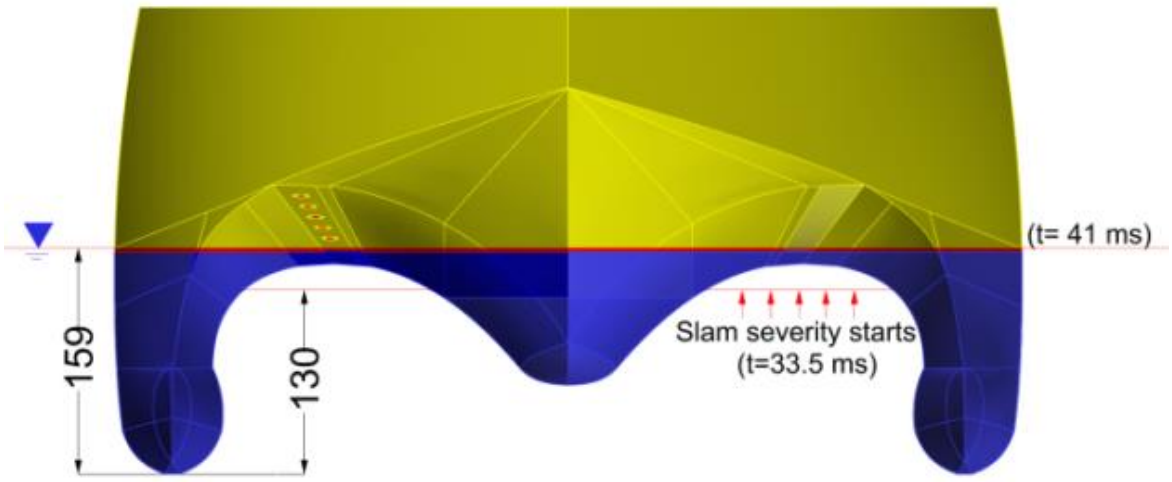

Fig. 4.18: Bow view of model showing immersions (130 and 159 mm) that correspond to the peaks of slam pressure and slam force respectively (4m/s water-entry) in relation to the original water-surface. Also shown on the starboard side are the locations of the five pressure transducers.

Thus designers should consider this in defining the air gap elevation, which is the minimal allowed distance between the calm water free surface and the wetdeck. This is illustrated in Figs. 4.18 and 4.23, where the equivalent calm water level for peak slam severity is shown.

The pressure results were obtained from the five pressure transducers located along the archway, with a constant relative angle of 11° between the flat panel where the pressure transducers were installed and the horizontal free-surface, as presented in Figs. 4.2, 4.18 and 4.23. It is interesting to note that P1 peaks at a time of approximately 34 ms for target velocity of 4m/s, confirming that the maximum local slam load occurred while the archway top is higher than the original undisturbed water surface. In addition there is a clear trend that the slam pressure moves towards the bow as the model becomes immersed further. As the slam pressure moves towards the bow, the peak magnitude decreases, despite a nearly constant relative velocity. These three dimensional effects are discussed in section 4.5.3.

The results for the other two impact velocities presented in Figs. 4.14 and 4.15 illustrate that the trends observed for 4m/s are consistent for the higher impact speeds of 5m/s and 4.5m/s respectively. These results therefore provide a full validation dataset for any future theoretical studies.

4.4.2 Influence of impact velocity

To study the effect of water-entry velocity on the slam force, tests were conducted for varying impact velocities. The slam force peak measurements of 25 successful controlled speed tests are plotted against the square of corresponding impact velocities in Fig. 4.19. From these measurements the following expression was derived for maximum slam force (F_{max}) based on impact velocity:

$$F_{max} = 571\ v^2 \qquad [\text{N}] \qquad (4.2)$$

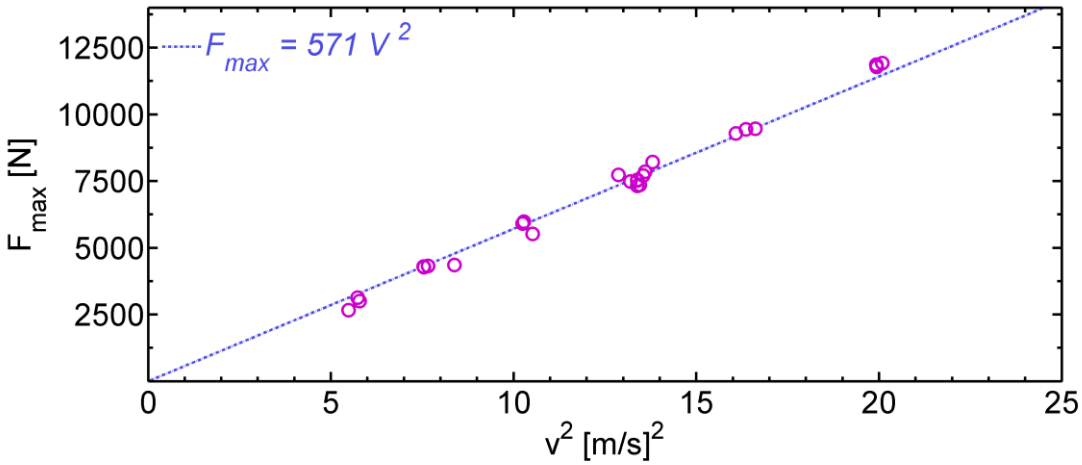

Fig. 4.19: Relationship between slam force peak and the square of the velocity at the instant of impact.

This was derived with an R-square confidence of 96.6 % and the trend line illustrates this strong dependency of total vertical force on impact velocity.

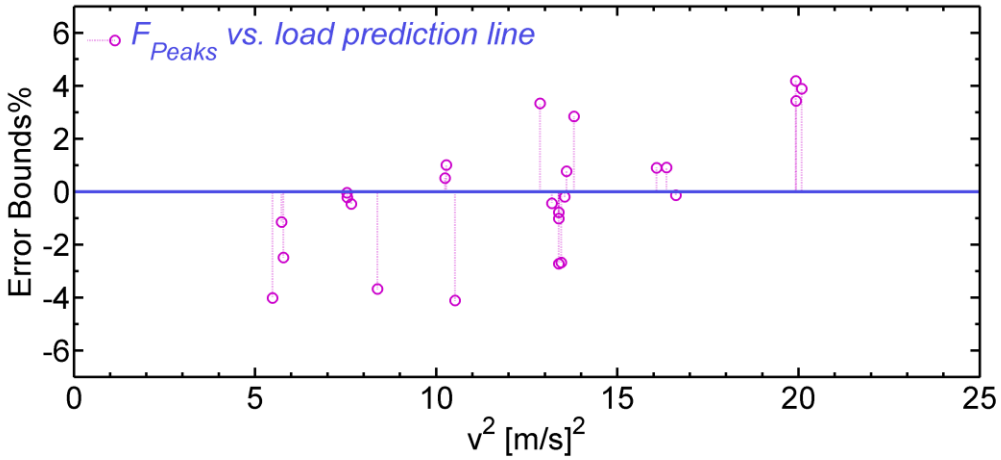

Fig. 4.20: The measured slam force peak error bounds corresponding to the square of instantaneous impact velocities against the slam load prediction equation, as illustrated in Fig. 4.19.

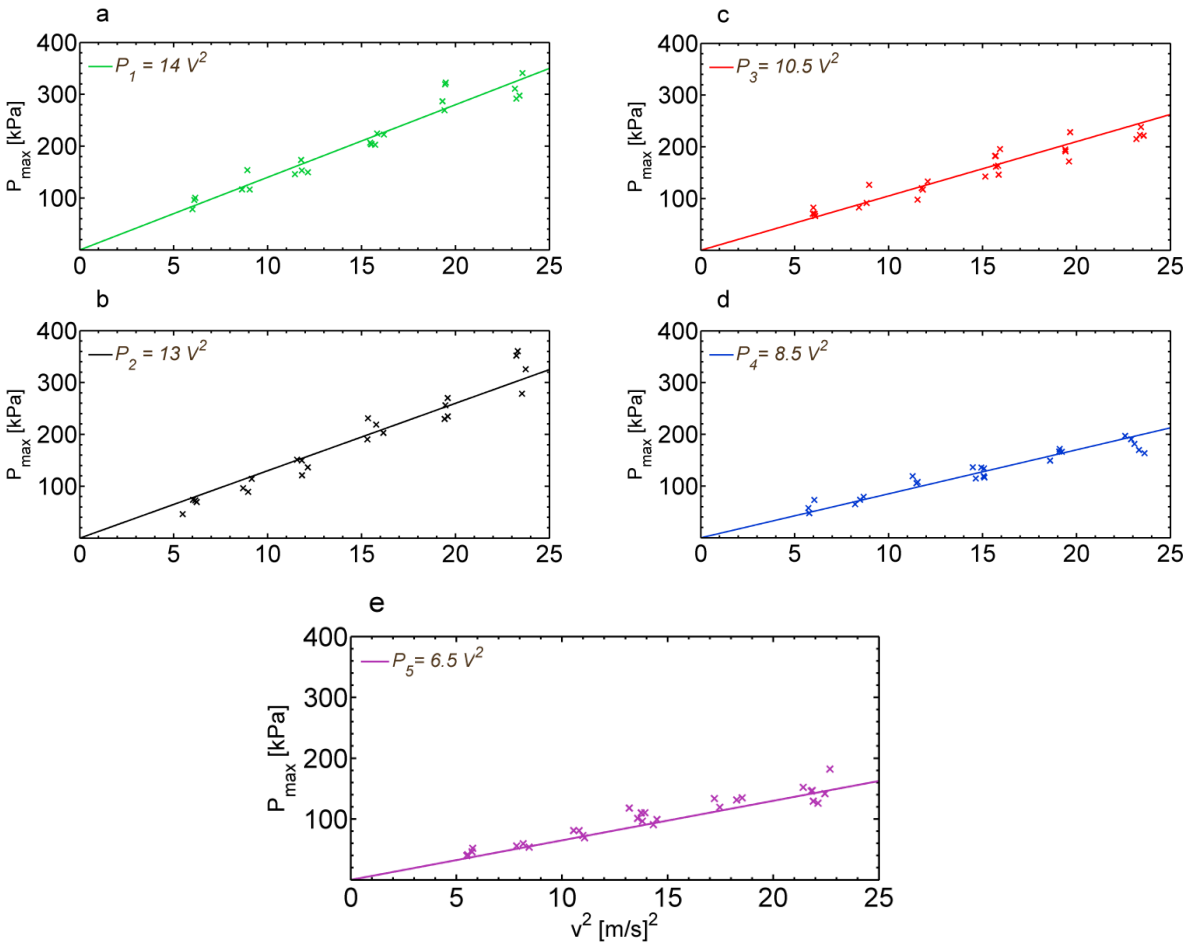

Fig. 4.21: Pressure peaks for the five pressure transducers plotted against the square of corresponding impact velocities. Subplots from (a) to (e) are for P1 to P5 respectively.

Fig. 4.20 illustrates the maximum error bounds in the total hydrodynamic slam force peaks corresponding to the square of the instantaneous impact velocities, against the load prediction equation. The variation of approximately ±4% gives further evidence in the veracity of the observed relationship of the measured data.

Figure 4.21 presents the pressure peaks for all the pressure transducers against the square of the corresponding impact velocities. The five subplots from (a) to (e) represent the measured peaks from P1 to P5 respectively, as well as the derived relationship expressions with a minimum confidence of 85%. Although the points generally fit well with the derived trend lines, the results suggest that the slamming pressures are more sensitive to slight changes in velocity profile than are the slam forces. This is probably due to the relatively small transducer sensor area (24.1 mm^2) making them sensitive to any small changes in the flow

behaviour; whereas such small changes are not discernible in the force measurements. The increased magnitude of the pressure towards the aft of the model is again shown in these plots and is likely due to the more confined nature of the archway here when compared to the bow region. It is worth mentioning that number of measured points varies due to failure of different transducers during tests. However, a minimum of three repeated tests were conducted for each measurement.

4.4.3 Three-dimensional effect

This section illustrates the importance of studying the wetdeck slamming problem as a three dimensional (3D) phenomenon. The 3D effect on slam peak pressures for varying impact velocities (from 2.5m/s to 5m/s in 0.5m/s increments) and the corresponding immersions and timings (occurrences) against the longitudinal locations of the five pressure transducers have been studied.

The mean values of slam pressure peaks of 25 controlled speed tests are plotted against the longitudinal locations of five pressure sensors (equally distributed in y direction) in reference to the centrebow's aft truncation, in Fig. 4.22. The pressures can be seen to be strongly location dependent, with the maximum pressures at P1 (located aft at a longitudinal distance equal to 96.8 mm) being approximately double that at the transducer furthest forward, P5 (at a distance of 251.6 mm). As the slam pressure moves towards the bow, the peak magnitude decreases, despite a nearly constant relative velocity per each trend line and constant relative impact angle of 11°, as presented in Fig. 4.23.

The mean values for the instantaneous immersion, corresponding to the slam peak pressures for varying water impact velocities presented in Figs. 4.23 - 4.24, illustrate that the slam pressure peaks at an immersion level approximately 10.5% lower than the level equivalent to the original water-surface. This is due to the wetdeck slamming phenomenon being characterised by pre-collapsed spray jets, together with large free-surface deformations in the semi-enclosed volume beneath the wetdeck. The presented plots also illustrate that the trends observed in Fig. 4.18 for 4m/s are consistent for the whole tested conditions with a variation of less than ± 2%. Fig. 4.23 illustrates also the slam peak pressure distributions along the arch way.

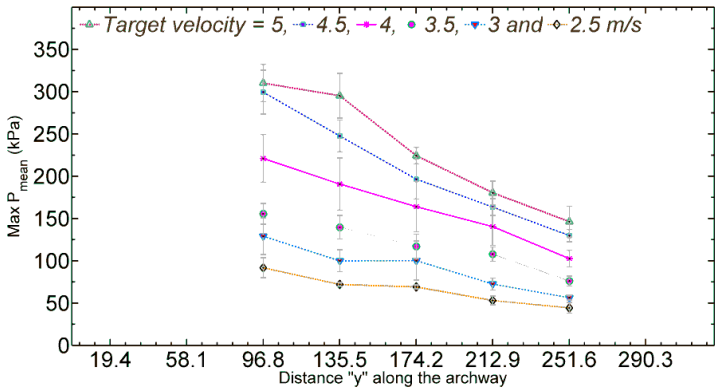

Fig. 4.22: Mean pressure peaks corresponding to six relative target velocities against the distance y in reference to the centrebow aft truncation. Vertical bars indicate standard deviation.

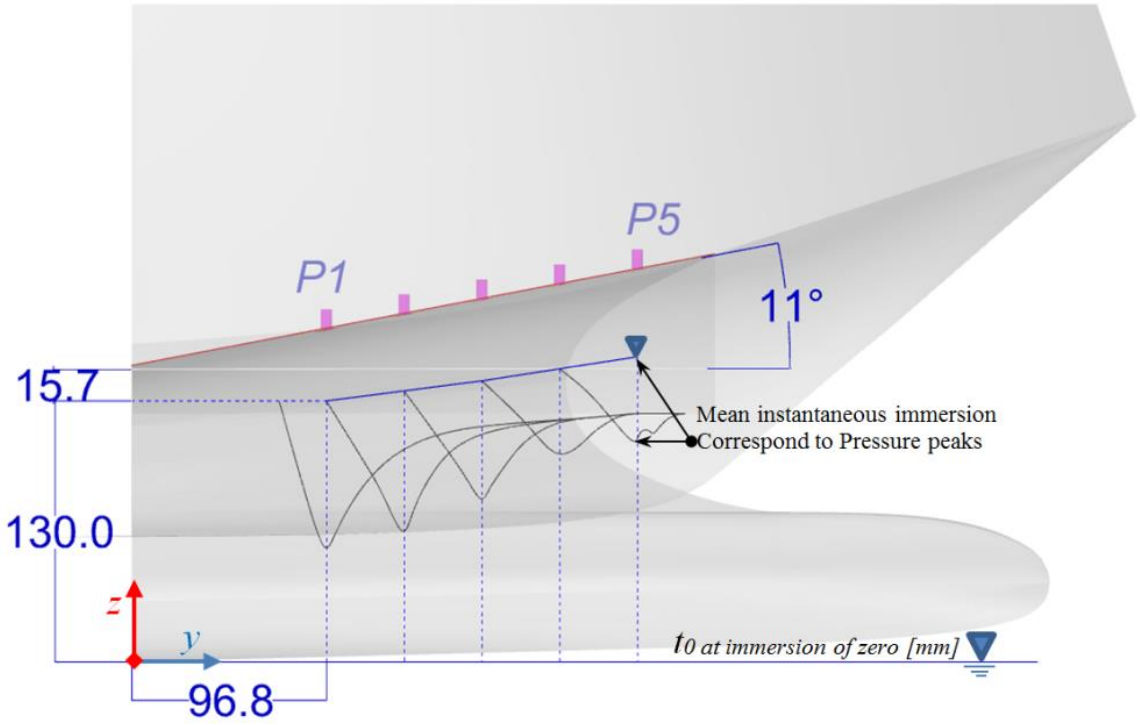

Fig. 4.23: Profile view of model showing immersions corresponding to the slam pressure peaks. Also shown on the archway are the locations of the five pressure transducers.

The three-dimensional effect has also been demonstrated by plotting the time variations between the slam pressure peaks in reference to t_o, as presented in Fig. 4.25, against the transducer longitudinal locations for all test conditions.

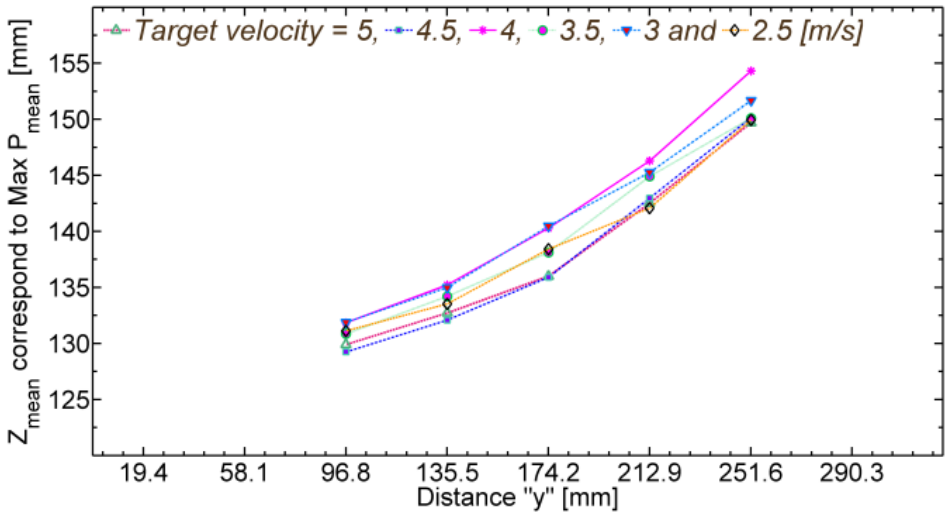

Fig. 4.24: Mean model immersions correspond to slam pressure peaks of all test conditions against the distance y in reference to the centrebow truncation.

A clear trend for the six impact velocities can be observed with the occurrence of the slam pressure peaks occurring later the further forward the transducer location is. The 3D effects presented and discussed here would not have been captured in the model experiments if the model had been simplified to purely two dimensional sections.

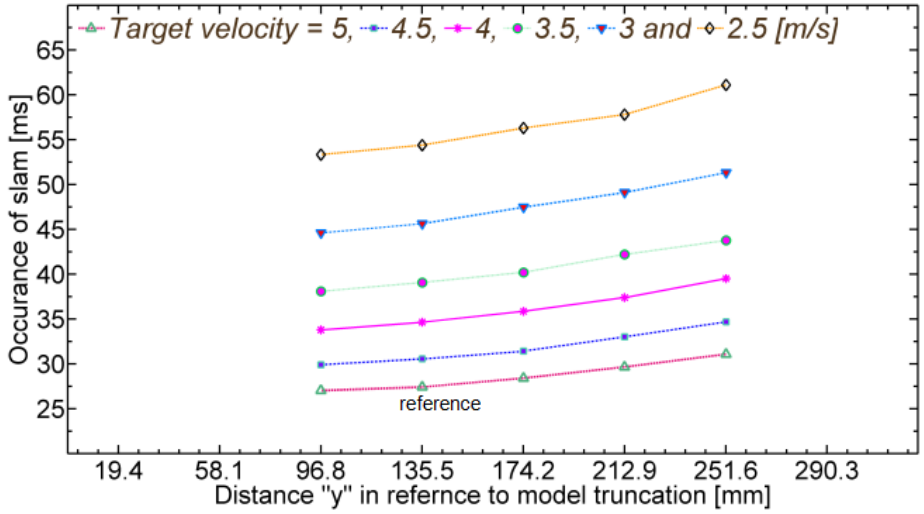

Fig. 4.25: Mean timings that correspond to the peak slam pressures of five pressure transducers at six relative velocities against the distance y in reference to the centrebow truncation.

4.5 Conclusions

This chapter reported on a series of water impact experiments to investigate the hydrodynamic loads and pressures experienced by a generic wave-piercer catamaran

hullform during water impacts. In contrast to previous model drop tests these experiments were conducted using a full three-dimensional catamaran model rather than two-dimensional sections, and with a controlled speed testing system. Since full details of the generic hull form are presented the results provide a comprehensive set of benchmarking data for use in the validation of numerical techniques to predict slam impact magnitudes of catamarans.

The systematic and random uncertainties associated with the controlled speed test results were quantified in detail and demonstrated the excellent repeatability of the tests; for example the uncertainty of the measured peak slam loads was found to be less than 5%.

The slam events were characterised by analysing the experimentally measured pressure, load and displacement and correlating this data with images from high-speed photographs. The maximum slam force was found to occur when the archway is filled with water, which occurs prior to the top of the archway reaching the original level of the water surface; thus suggesting that water builds up in the archway due to the immersion of the demihulls and centrebow. Designers should consider the increase in water elevation by approximately 10.5% in relation to the original water-surface prior to the wetdeck slamming event in defining the air gap elevation of catamarans.

A strong relationship between water-entry velocity and slam force was found and an empirical relationship is proposed to estimate the slam force magnitude as a function of the impact velocity: $F_{max} = \alpha\, v^2$ [N]. This relationship is of importance for further validation studies to provide an estimate of the slam force for a broader range of relative impact velocities.

The pressure results showed that the pressure increased the further aft the transducer was located, suggesting that the more contained the archway is the greater the pressure. Empirical relationships for the maximum slam pressures are presented in relation to the vertical velocity at impact.

The three dimensional effect on slam peak pressures and impact pulse timing has been investigated, showing that simplifying the wetdeck slam phenomenon as a quasi-2D problem can be considered to be an invalid assumption for such complex hull forms.

4.6 Next steps

The next step is to extend the experimental work on 3D catamaran hull forms by investigating the influence of flow separation (using an amended centrebow), the relative impact angle (between the wetdeck and the water-surface) and the relative vertical velocity on wetdeck slam load severity. As well as providing greater insight into the relationship between the impact pressure distributions and the slam load magnitude, the additional tests will give further data to enable the validation of 3D numerical methods.

Chapter 5
Characteristics of wetdeck slam events

This research was originally published, after peer-review, as:

Swidan, A., Thomas, G., Penesis, I., Ranmuthugala, D., Amin, W., Allen, T. & Battley, M. Wetdeck slamming loads on a developed catamaran hullform - Experimental investigation. Ships and Offshore Structures, vol. 1, pp.1-9. 2016b.

(http://dx.doi.org/10.1080/17445302.2016.1194555)

For the avoidance of repetition the original paper has been modified for this thesis.

5.1 Introduction

An initial experimental study into vertical water impact tests on a generic 3D catamaran model at a range of impact velocities and a fixed 0° angle of trim was presented in chapter 4 (see Fig. 5.1).

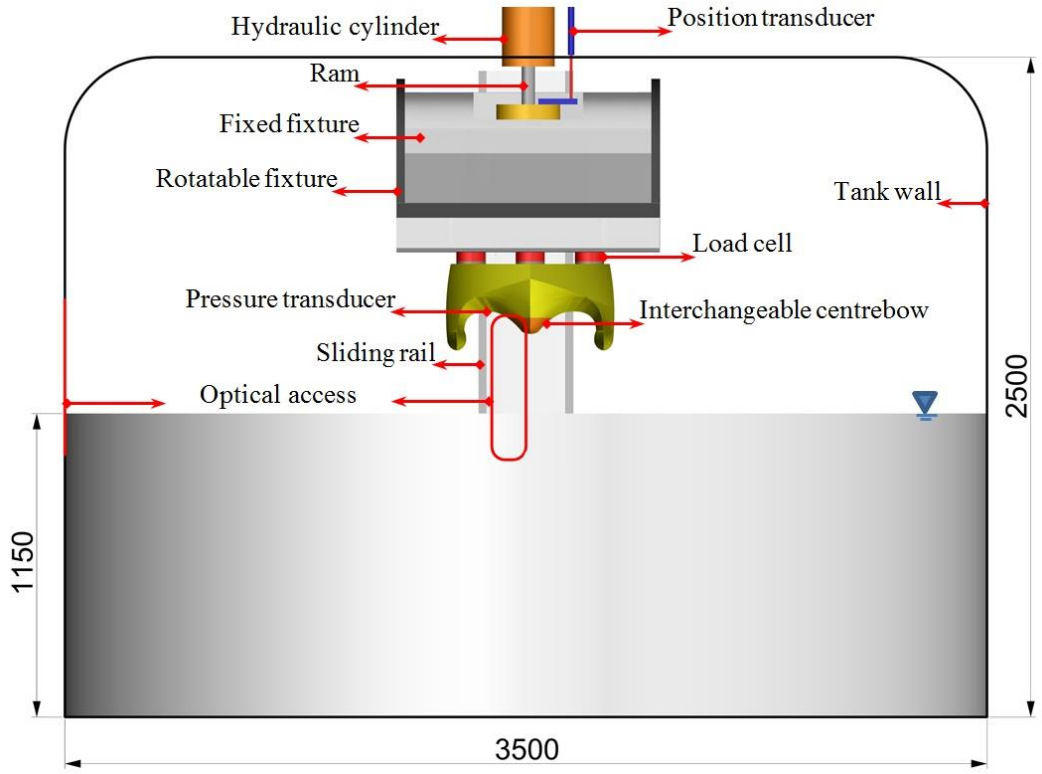

Fig. 5.1: General test arrangement. Showing the main components of SSTS and the instrumented model (dimensions in mm).

This chapter extends the work presented in chapter 4 by studying key elements influencing slamming load distributions and magnitudes on the catamaran wetdeck. In the next section the test setup is discussed, and a catamaran hull model with two interchangeable centrebows is presented. The pressure distribution along the wetdeck and the slamming forces on the entire model are measured directly during water-entry with two trim angles of 0° and 5° and at a range of vertical constant speeds (from 3 to 5m/s in 0.5m/s increments, to decrease noise to signal ratio effects). This allowed a study into the influence of the relative impact angle, velocity and water-flow separation on vertical force, slamming occurrence and pressure distributions.

5.2 Model and experimental setup

5.2.1 The test system

For the purpose of the present study, the impacts were conducted with the model at two fixed trim angles (θ) of 0° and 5°. To allow the model to trim by the bow by an angle θ of 5° a set of four wedges were fixed between the ram fixture (two stiffened 5mm Aluminium L-sections) and a stiffened plate that connected the load cells to the model, as illustrated in Fig. 5.2.

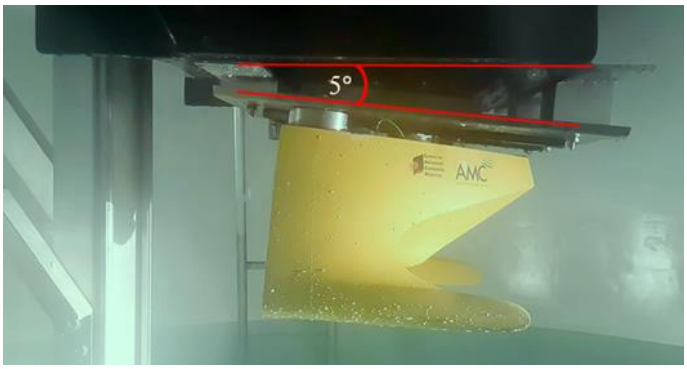

Fig. 5.2: Tested model installation at 5° angle of trim (bow-down), showing two wedges between the rig and a stiffened support.

5.2.2 Instrumentation

A summary of the instruments and associated systematic errors is given in Table 4.1. Further details on the instrumentation can be found in Allen (2013) and Battley & Allen (2012). The random uncertainties associated with the drop test results were quantified in detail and demonstrated the excellent repeatability of the tests, as presented in Appendix II.

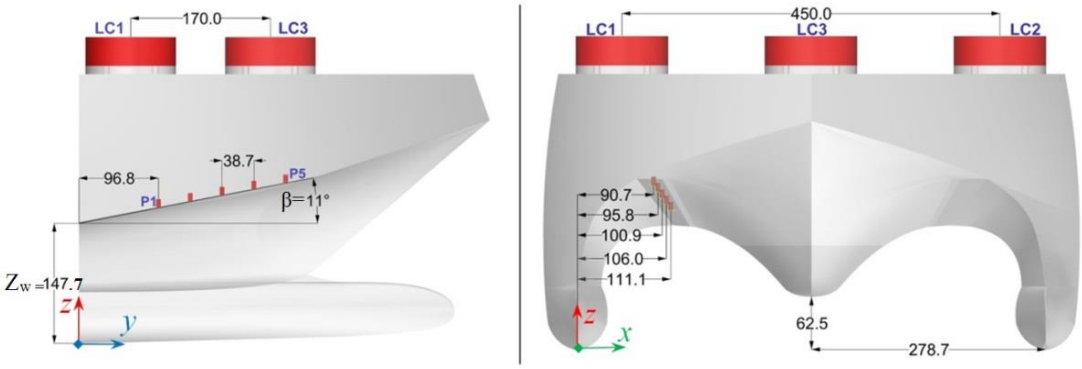

Fig. 5.3: Schematic diagram of profile and bow views of the parent model at θ = 0°, showing locations of the used pressure transducers and load cells (LCi).

In Fig. 5.3 the model is shown at zero trim ($\theta = 0°$) which corresponds to a relative impact angle β (between the archway of the wetdeck and the undisturbed water surface) of 11°. The figure also provides the locations of the five pressure transducers and three load cells.

5.2.3 The test model

The lines plan of a developed wave-piercer catamaran hullform model is illustrated in Fig. 5.4. This model was built with two interchangeable centrebows that can be attached to the main body, as shown in Figs. 5.4 to 5.6.

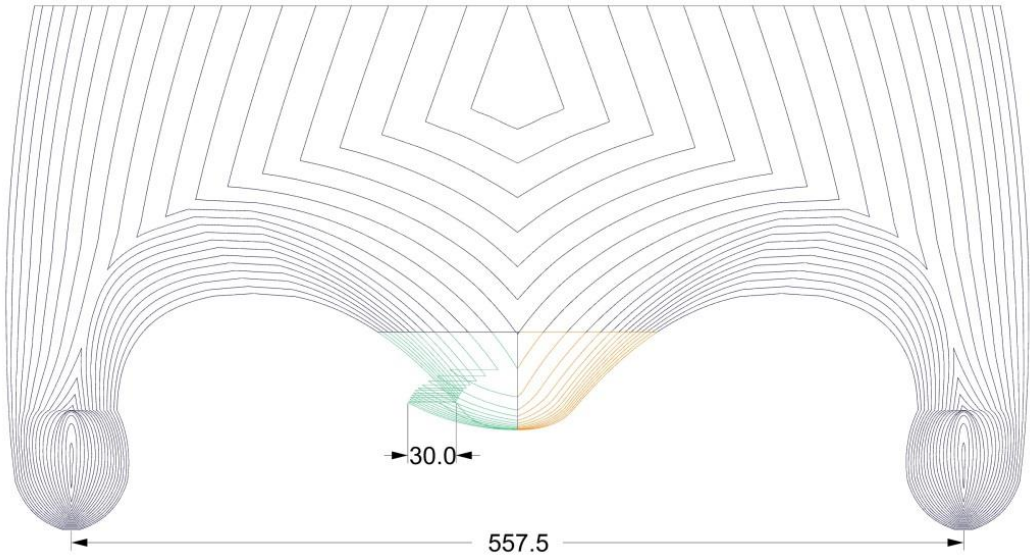

Fig. 5.4: Catamaran body lines with two interchangeable centrebows; showing the parent centrebow lines illustrated in orange on the right and the amended centrebow lines presented in green on the left.

Fig. 5.5: Catamaran test-model, showing the two interchangeable centrebows.

The main particulars of the test model are given in Table 5.1. The parent hull form is a generic wave-piercer catamaran (presented in orange lines in Fig. 5.4), similar in style to those designed by Revolution Design Pty Ltd and manufactured by Incat Tasmania. The second winged-centrebow (named in this study amended hull) is a proposed new design for the centrebow and aims to induce water separation at the tip of wings during water entry, as presented in Fig. 5.6. The objective of this early water separation is to generate an air cavity that can work as damper during wetdeck slamming.

Table 5-1: Test Model Main Particulars.

Length over all (mm)	500	
Beam (mm)	628	
Height (mm)	327.6	
Displacement (kg)	14.8	
Trim angle (θ°)	0	5
Depth to the wetdeck (mm)	147.72	168.3
Depth to the centrebow (mm)	62.52	71.75

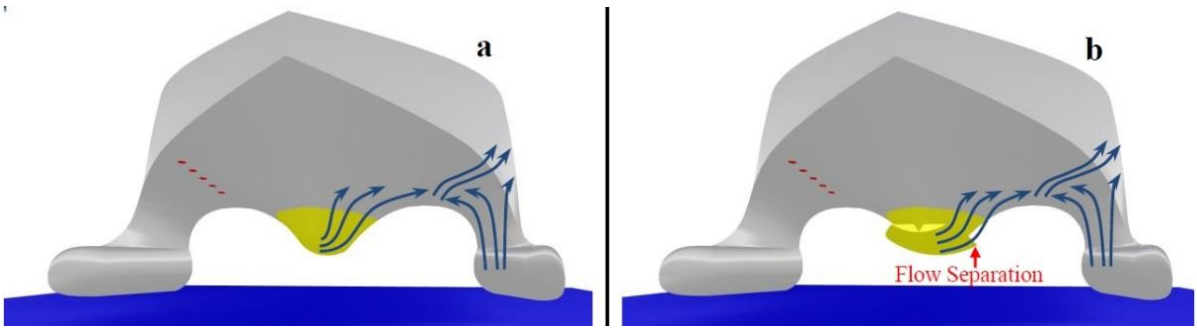

Fig. 5.6: Schematic chart showing the five pressure transducers (red surface) on the starboard side and the anticipated flow behaviour on one side during water penetration of; (a) parent centrebow and (b) amended centrebow.

Another feature is the larger exposed area of the winged centrebow with a reduced deadrise angle in order to provide greater resistance during water-entry and reduce the impact velocity (i.e. if tested in a more realistic slam scenario, i.e. full scale sea trials or sea-keeping model tests using towing tank). Additionally the winged shape of the amended centrebow is designed to increase the drag force during water-exit after slamming events, reducing the pitch motions.

5.2.4 Test conditions

A total of 20 test conditions for 64 water impact tests (i.e. some tests were repeated for four times due to failure of one or more transducers) discussed in the following sections are outlined in Table 5.2. The trim angle of 5° was selected on the basis of past model seakeeping tests conducted by Lavroff et al. (2013) on a 112m Incat catamaran, which showed that the peak pitch angle of a 2.5m catamaran model could reach a maximum of 5.1°

Table 5-2: Test Conditions.

Hull shape	v_{target} [m/s]	Trim angle	Condition No.
Parent	3	0	1
	3.5		2
	4		3
	4.5		4
	5		5
	3	5	6
	3.5		7
	4		8
	4.5		9
	5		10
Amended	3	0	11
	3.5		12
	4		13
	4.5		14
	5		15
	3	5	16
	3.5		17
	4		18
	4.5		19
	5		20

5.3 Results and discussion

This section presents and discusses the results of all test conditions given in Table 5.2. Table 5.3 presents the mean values of:

- impact velocities ($v_{\theta}°$), immersion ($Z_{F\theta°}$) (see Fig. 5.7) and timings ($\delta t_{\theta}°$) from t_0 = 0 s at which demi hull keels touch the free-surface to the timing at which slam force peaks;
- maximum force and pressure magnitudes.

The exact results and corresponding error bounds of all repeated tests are presented and discussed in sections 5.3.1 and 5.3.2. The measured immersion value ($Z_{F\theta°}$) given in Table 5-3 slightly increases or remains constant as the relative impact velocity increases, an exemption is for the amended hull at 0° trim angle. However, the reason of this is not clear to the author and it may need further investigations using CFD simulations.

Table 5-3: Summary of Results

Hull Model	v_{target} [m/s]	v_{impact} ($v_{\theta°}$) [m/s]		Immersion ($Z_{F\theta°}$)[mm]		$\delta t_{(\theta°)}$ [ms]		$F_{max(\theta°)}$ [kN]		$P_{max(\theta°)}$ [kPa]	
		$v_{0°}$	$v_{5°}$	$Z_{F\ 0°}$	$Z_{F\ 5°}$	$\delta t_{0°}$	$\delta t_{5°}$	$F_{0°}$	$F_{5°}$	$P_{0°}$	$P_{5°}$
Parent	3	2.8	2.7	157	163	52.86	55.4	4.3	5.73	129	162
	3.5	3.2	3.2	157	166	45.76	48.75	5.8	7.84	155	234
	4	3.7	3.7	157	171	40.4	43.84	7.6	10.3	210	277
	4.5	4	4	158	173	36.7	40	9.4	12.3	299	351
	5	4.5	4.4	160	177	33.5	37.2	11.9	14.3	316	406
Amended	3	2.75	2.8	161	164	54.74	56.5	4	5.1	154	197
	3.5	3.2	3.3	160	166	47	48.6	5.2	7.4	205	242
	4	3.7	3.7	154	169	39.66	43.5	7	9.7	248	313
	4.5	4.1	4.1	158	178	36.4	41	9.3	12.2	316	372
	5	4.5	4.5	162	179	34	37	11.2	14.1	376	457

5.3.1 Slamming force

This section discusses in detail the influence of the differing centrebows, vertical velocity and impact angle on the slamming force.

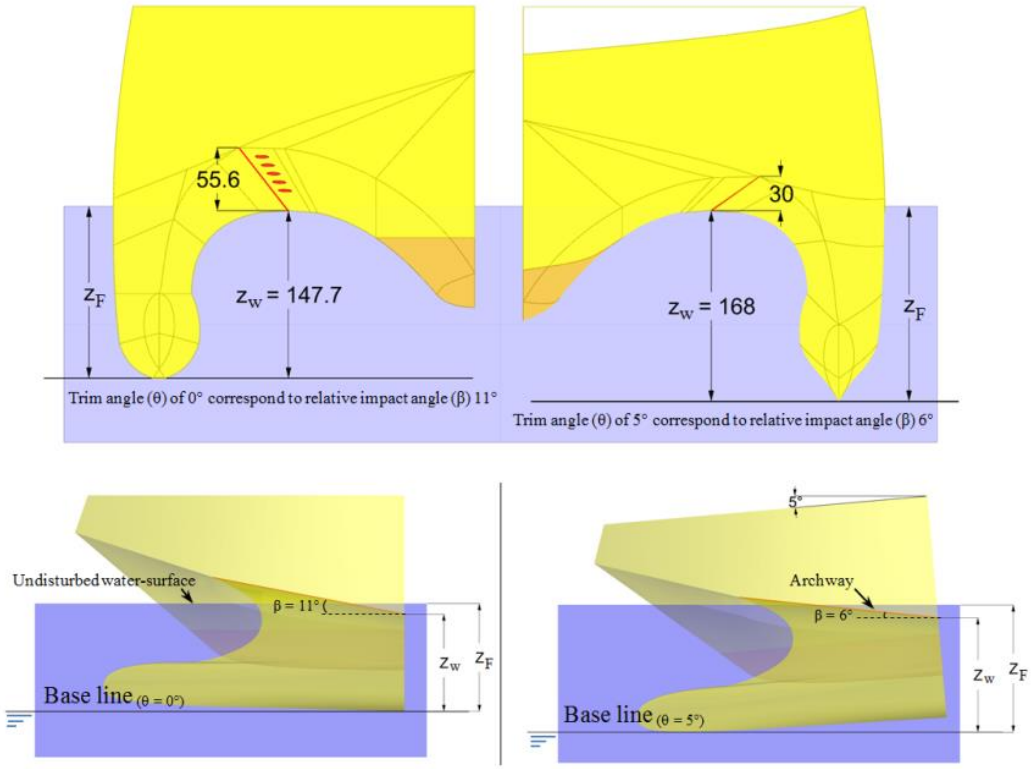

Fig. 5.7: Bow and profile views of model at trim angles of 0 and 5 degrees corresponding to two relative impact angles (β) of 11 and 6 degrees. It shows the red reference line on the archway that represents the highest section along the top of the arch way. z_w (θ°) is the vertical distance between the initial calm water-surface and the highest point on the wetdeck at the aft end of the centrebow and z_F (θ°) which corresponds to the immersion at which the maximum slam force occurs.

Slam force time-history

The results from two controlled speed tests at a target velocity of 4m/s using both centrebows at a fixed θ = 5° are compared and presented in Figs. 5.8 and 5.9. Fig. 5.8 includes; (a) vertical velocity and (b) total vertical slam force. In Fig. 5.8(a) the measured velocities for both the parent and amended models are shown to be in good agreement, with a maximum variation of approximately 6% (3.6m/s) around the mean value of 3.85m/s at an immersion of approximately 175 mm for both centrebows.

Fig. 5.8(b) illustrates a small drop in the force traces at an immersion of 55mm, attributed to the "internal knuckles" of demihulls, as illustrated also in Figs. 5.4 – 5.6. These knuckles cause water-flow separation, momentarily reducing the force. A similar effect for the amended centrebow can be seen at an immersion of 120 mm. This shows that any flow separation occurring during water-entry is followed by a reduction in the slamming forces.

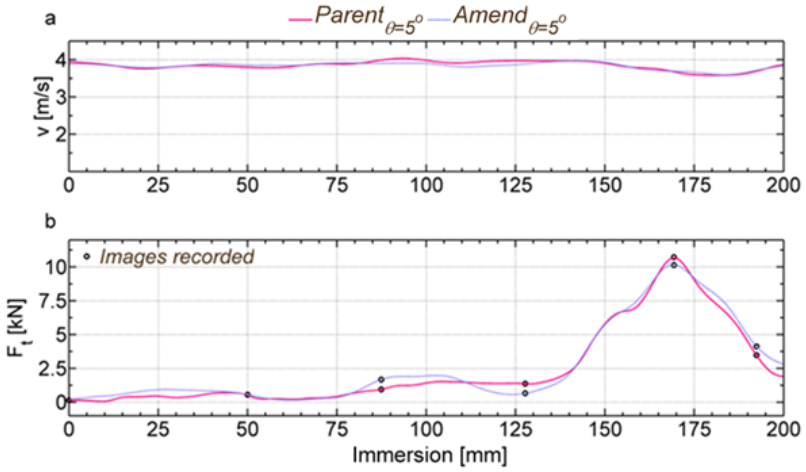

Fig. 5.8: Comparison between using parent against amended centrebows for a target relative velocity of 4m/s at θ = 5°. Subplots illustrate time histories of (a) measured velocities, (b) total slam force.

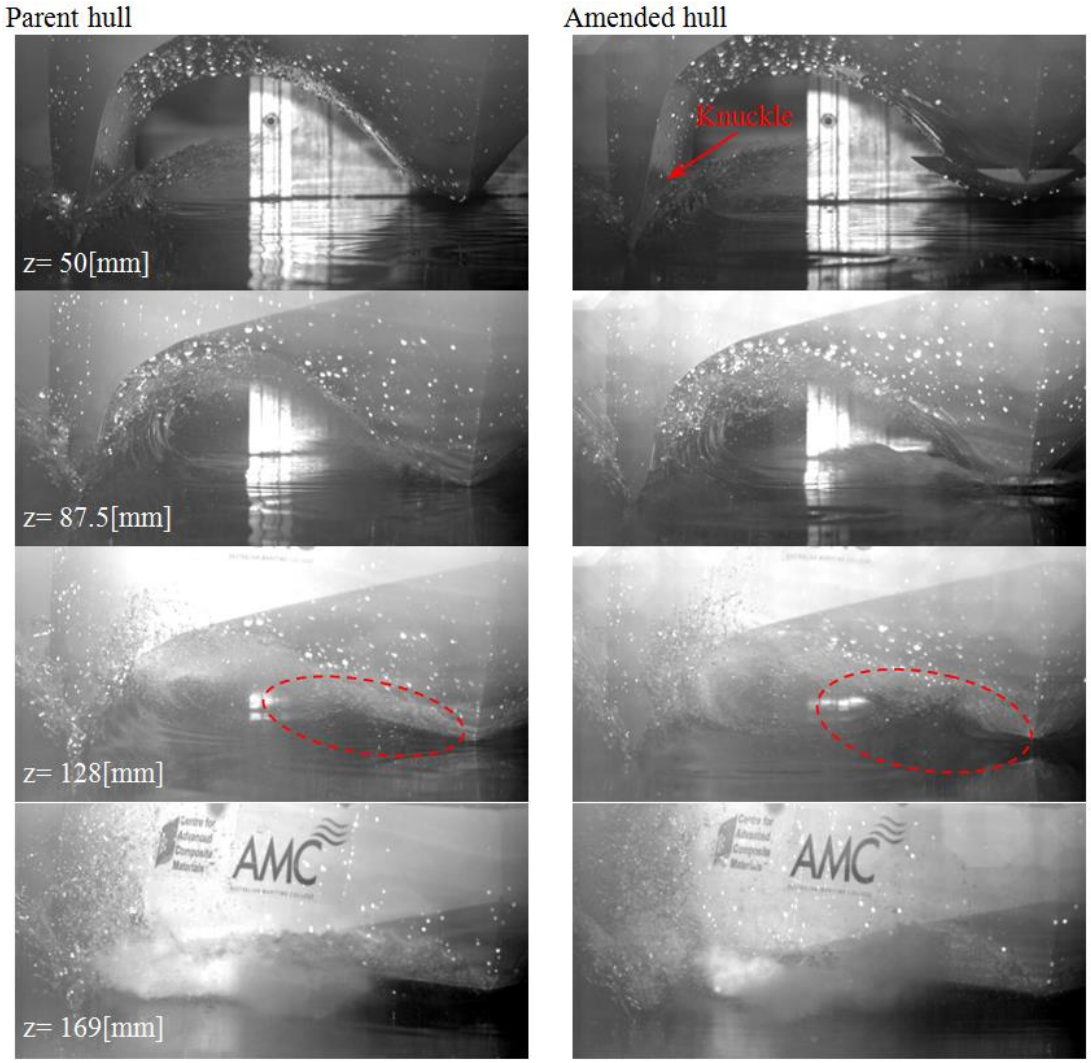

Fig. 5.9: Flow visualisation time history for; parent and amended centrebows hull at θ = 5° and impact velocity of 4m/s.

Fig. 5.9 shows greater disturbance of the water-surface for the entry of the amended centrebow than the parent at an immersion of 128 mm. Thus a larger air cushion beneath the wetdeck was expected during wetdeck-water impact for the amended hull. The most severe slam force occurs at 169 mm and 171 mm of immersion for the amended and parent hulls respectively, when the archway is filled with water.

Slam force magnitude

(Ge, 2002) observed that slam force could be considered as a function of the velocity squared. Fig. 5.10 presents the peak slam forces and the corresponding fitted linear curves for all conditions (given in Table 5.2) against the square of the instantaneous vertical velocity.

A strong correlation between the peak slam force and the relative water-entry angle and vertical velocities is observed. The measured slam force peak measurements collapse well along the fitted linear trend lines with a maximum variation of ±5%, as given in Table 5.4. This is attributed to the variations in the instantaneous impact velocities with a maximum variation of ±7%, as presented in Fig. 5.10.

The fitted relationships of slam force for θ = 5° is 30% higher than for θ = 0°, as given in Table 5.4. The increase in the slam force peaks was investigated through analysing the outputs of the used three load cells, as illustrated in Figs. 5.3 and 5.11.

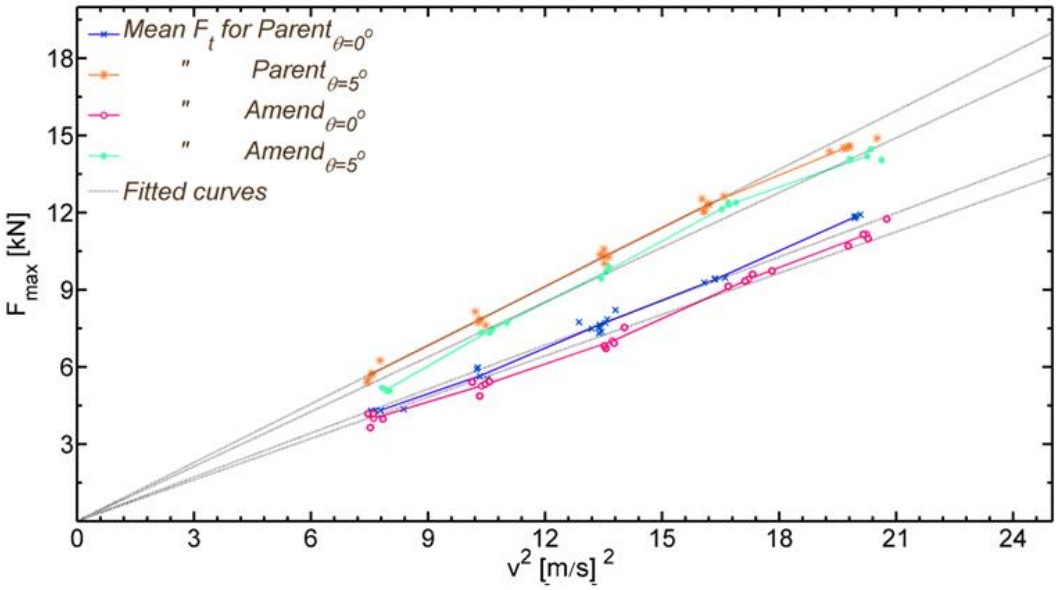

Fig. 5.10: Relationships of slam force peaks against the relative impact angles and the corresponding relative velocity for both centrebows.

Table 5-4: Summary of Expressions Derived for Maximum Slam Forces Based on Relative Impact Angles and Impact Velocities.

Trim angle (θ)	Hull model	Peak slam-force [N]	Deviation Bounds%
0°	Parent	$F = 571\ v^2$	±3.4%
	Amended	$F = 536\ v^2$	±3.7%
5°	Parent	$F = 760\ v^2$	±4.1%
	Amended	$F = 710\ v^2$	±5%

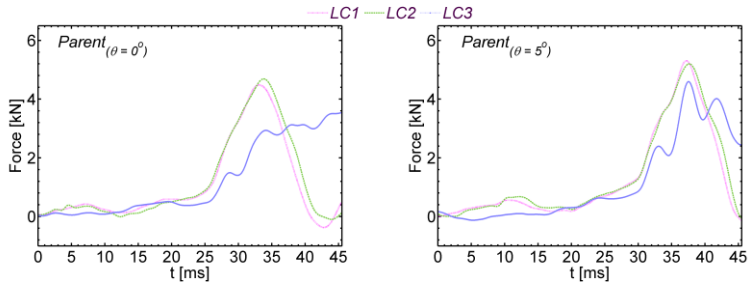

Fig. 5.11: Time histories of; LC1= load cell No.1, LC2 = load cell No.2 and LC3 = load cell No.3 for a target velocity of 5m/s and at two relative impact angles.

Figure 5.11 presents the outputs from three load cells for 5m/s impacts of the parent hull form at θ = 0° and θ = 5°. For the impact at θ = 5° the timing of the peak force at the bow of the model (LC3) closely correlates with the timing of the load cells at the rear of the model (LC1 and LC2). This indicates a more instantaneous peak force, supporting the traces seen in Fig. 5.12. The timing of the peak forces between fore and aft do not correlate for the impacts at θ = 0°, indicating the centre of pressure progresses across the model, i.e., the wetdeck slamming force magnitude depends strongly on the wetted area subjected to slam force. The results also demonstrate that the bigger the relative trim angle (θ), the sharper the total slam force trace and the more significant the force peak, as presented in Figs. 5.11 and 5.12. The mean slam force peak magnitude is of minimum of 6% lower for the amended hull with a maximum uncertainty of ±4.1% , as presented in Fig. 5.10 and given in Table 5.4. This is attributed to the higher air-cushioning effect from the amended centrebow and due to the difference in the rate of change of added mass during water-entry. Thus, it is proposed that one of the limitations of using constant speed water-entry systems to compare different hull forms is that the instantaneous impact velocity remains approximately constant all hull models, despite the variation in impact force time history during water-entry. If tested using seakeeping experiments, the relative instantaneous impact velocity would change as well as the corresponding hydrodynamic impact loads.

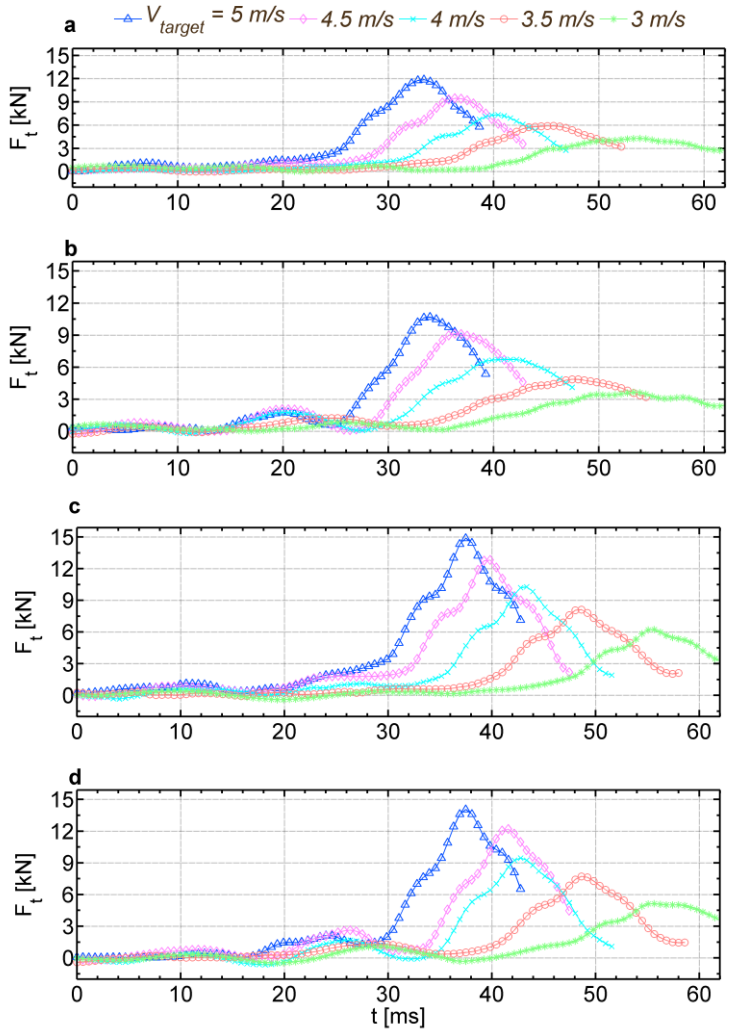

Fig. 5.12: Total hydrodynamic load time-histories for; (a) parent hull at θ = 0°, (b) amended hull at θ = 0°, (c) parent hull at θ = 5°, (d) amended hull at θ = 5°.

Occurrence of slam force

This section investigates the factors affecting the corresponding immersion to the slam force peak. Fig. 5.13 presents the total vertical slam forces acting on the entire model against both the non-dimensional ratio z_F/zw as defined in Fig. 5.7 and the velocity, where $z_{F/}z_w=1$ at which the lowest point of the wetdeck (at transom) touches the calm water-surface. The general trend is for an increase in impact velocity to delay the occurrence of the peak slam force to a deeper immersion.

For all impacts at θ = 0° the maximum slam force occurs while the wetdeck is partially submerged, i.e. $z_F/z_w>1$ as presented in Figs. 5.7 and 5.13. This figure also demonstrates that at θ = 5° while relatively low velocity impacts (3 and 3.5m/s) slam force peaks prior to theoretical immersion ($z_F/z_w<1$), this is likely due to water pile-up reaching the wetdeck prior to the theoretical immersion depth (i.e. $z_F/z_w=1$).

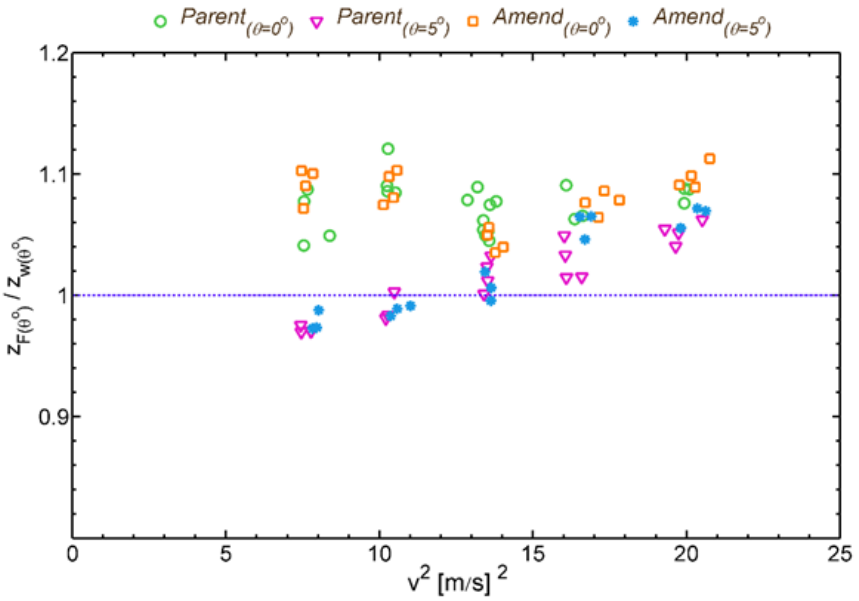

Fig. 5.13: Cross plot of slam force peaks against dimensional z_F/z_w for; (a) parent hull at θ = 0°, (b) amended hull at θ = 0°, (c) parent hull at θ = 5°, (d) amended hull at θ = 5°.

This agrees with the observations in Thomas et al. (2011a) that the immersion at which slam force peaks is a function of the water-entry velocity, however, does not agree with the proposed assumption of 2D filling by Lavroff (2009) and Thomas et al. (2011b). It can be considered therefore that if the relative impact angle is relatively small then the free-surface deformation beneath the wetdeck is high and the effect of the relative impact angle on the water surface deformation decreases as the relative vertical velocity increases. This could explain the conflict between previously conducted experiments using 2D free-falling technique (with 0° relative impact angle) and seakeeping tests with variable pitching angles, such as conducted by French (2012).

5.3.2 Pressure distributions

Fig. 5.14(a-e) presents the mean peak pressures for target velocities from 3 to 5m/s in 0.5m/s increments. For the parent hull at θ = 0° and 5°, and the amended hull at θ = 0°, the

maximum peak pressure is measured at P1. Then, as the slam pressure moves towards the bow, the peak magnitude decreases. For both hulls at $\theta = 0°$, big differences are shown in Fig. 14 (a-e) between pressure peaks at P1 and P5 of more than 50%. For the parent hull at $\theta = 5°$ the maximum pressure peak distribution differences is in the order of 34.5%, likely linked to the lower relative impact angle (dead rise angle) at the pressure transducers.

The maximum pressure magnitude at P5 is lowest for all test conditions. This is attributed to the location of P5 being out of the enclosed volume beneath the wetdeck where the water can escape in multiple directions, hence a low pressure field is observed in comparison with the rest of the transducers (P1-P4) that are located in the vicinity of the arch closure.

For the test conditions using amended hull at $\theta = 5°$ no clear trend can be observed. This is attributed to water flow separation during water-entry causing more aerated water content and smaller added mass.

Fig.14 illustrates the maximum and minimum peak pressures (error bounds) for all experiments. The repeated peak pressures show bigger error bounds than those of repeated force, velocity and displacement measurements with a range of maximum variations of 18%, 15% for parent hull at $\theta = 0°$ and $\theta = 5°$ respectively and in the order of 29% and 33% for the amended hull at $\theta = 0°$ and $\theta = 5°$ respectively. It is also interesting to note in Fig. 5.14 that using amended hull will lead increased maximum local pressure for both relative impact angles compared with the parent hull. Force analysis however, indicates the total vertical force decreases by approximately 6%. The big variations in peak pressures and between the amended and parent hulls are attributed to the change in jet evolution during water entry that influences the pressure fields along the pressure transducer region.

The disconnect between peak pressure and peak total force between the amended and parent hull forms highlights the necessity to accurately consider 3D pressure fields.

Integrating pressures can lead to in-accurate force predictions, unless complete pressure mapping is available. To accomplish this experimentally for 3D complex hull models is problematic. However calculation of the pressure coefficients using the traditional Wagner

formula (such as presented in Appendix III) can add an insight into calculation of pressure distributions.

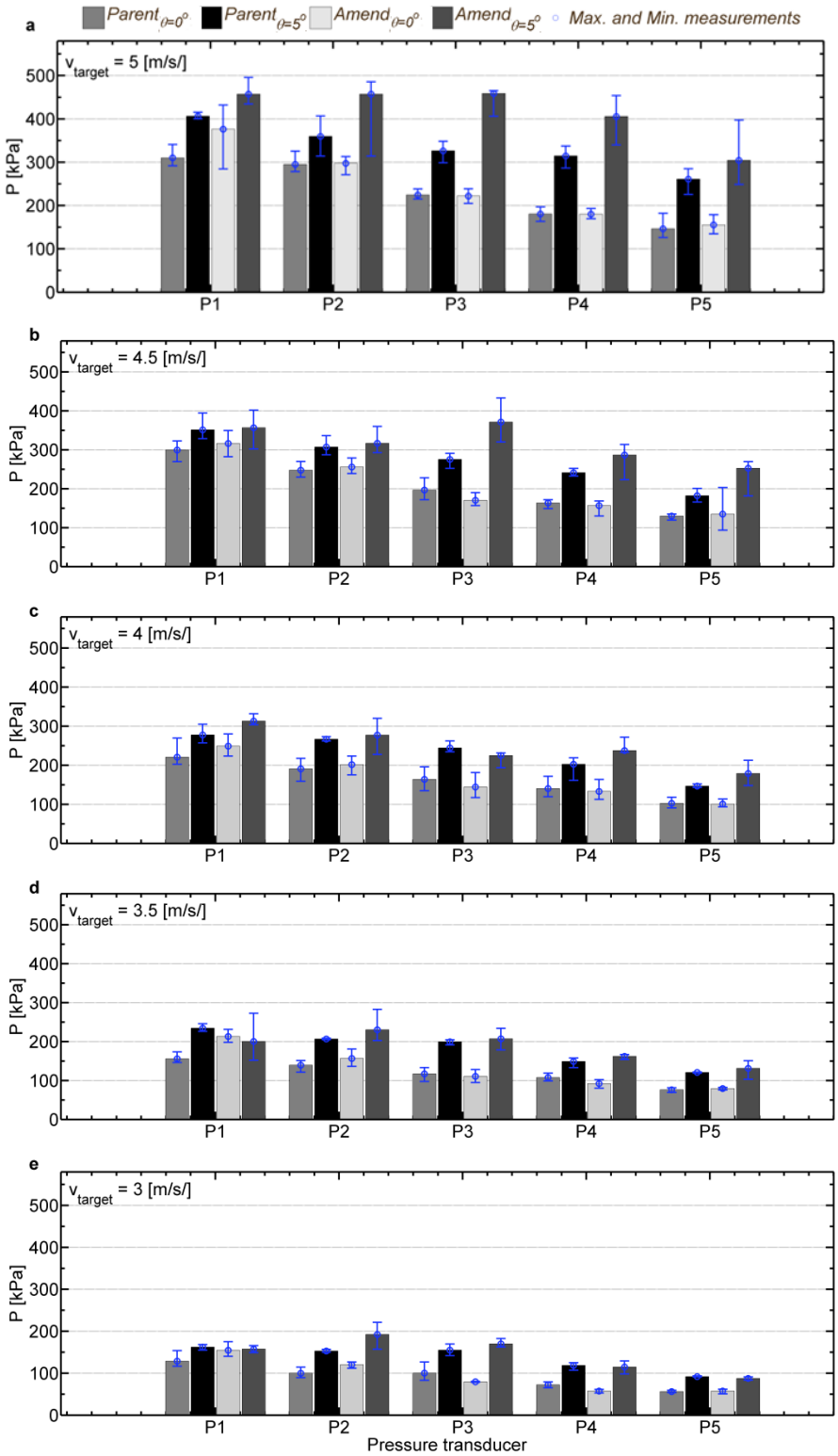

Fig. 5.14: The peak pressure distributions for all test conditions.

5.4 Conclusions

This work extended the three-dimensional water-impact tests using a controlled-speed servo-hydraulic slamming testing system to investigate the influence of centrebow geometry, relative impact angles and vertical velocity on hydrodynamic loads and corresponding pressure distributions.

A total of 64 successful water-impact tests were conducted on a catamaran hull model with two interchangeable centrebows at trim angles of 0° and 5° and at a range of vertical velocities of 3 to 5m/s in 0.5m/s increments.

The smaller the relative impact angle between water surface and wetdeck, the bigger the area of the wetdeck subjected to higher pressure fields and the more severe the vertical slam force. The results demonstrated that an increase of 5° trim by the bow can increase the vertical slamming force on the entire model by 30%.

The results also demonstrate that the smaller the relative impact angle, the sharper the total slam force trace and the more significant the force peak. This finding illustrates the importance of considering relative impact angle carefully, not only due to the increased slam force magnitude but also for its shorter duration.

A slight decrease in the resultant force magnitude by approximately 6% is achieved by using a winged amended centrebow. This is attributed to the larger air-cushioning between wetdeck and water (due to separation) and possibly due to variations in the added mass during slam between the two models.

Flow separation occurring during water-entry of a 3D body is followed by a reduction in the slamming forces. Local pressure concentrations in offshore/ships' structures can therefore be avoided by separating flow prior to impact with locations of concern.

The immersion corresponding to maximum slam force was found to be dependent on the relative impact angle and independent on the relative velocity for large relative angle (i.e. when the angle of trim is 0°). This finding is in contrast to previous studies by Lavroff (2009)

and Thomas et al. (2011b). However, both studies (past and present) agree that slam loads are strongly related to relative vertical velocity.

Strong relationships between impact velocity, water-entry angle, hull geometry and slam force were found and empirical relationships are proposed to estimate the slam force magnitude as a function of the impact velocity. These relationships are of importance for further validation studies to provide an estimate of the slam force for a broader range of relative impact velocities.

An increase in the pressure peak magnitudes in the vicinity of the semi-enclosed wetdeck void (surrounded by demihull and centrebow) for all conducted tests was observed, in comparison with the pressure transducer "P5" that is located out of that arch closure.

Larger slam pressure magnitudes do not necessarily lead to larger total forces. In addition pressure measurements at a limited number of points should not be used for comparing between two hull performances due to the possibility of changing flow behaviour. Thus directly measuring the entire resultant forces or using strain gauges for assessing local loads is recommended.

To decrease slamming forces on catamaran wetdeck structure, designers should look at increasing the relative impact angle between the arched wetdeck and water, decreasing the relative vertical velocity and/or avoiding arch closure by allowing water to easily escape from the archway closure.

5.5 Next steps

A significant data set of experimental results for 3D catamaran models entering water at prescribed velocities has been established. It is now possible to use this data to validate a 3D CFD method to predict wetdeck slamming loads and pressure distributions on a 3D wave-piercing catamaran model.

Chapter 6

Prediction of 3D wetdeck slam loads

This research was originally published, after peer-review, as:

Swidan, A., Thomas, G., Ranmuthugala, D., Penesis, I., Amin, W., Allen, T. & Battley, M. Prediction of Slamming Loads on Catamaran Wetdeck using CFD. In: The 13th international conference on fast sea transportation (FAST), 1-4 September 2015, Washington DC, USA.

For the avoidance of repetition the original paper has been modified for this thesis.

Chapter 7
Conclusions and Future work

7.1 Summary

The work in this thesis addresses the current limitations of ship designers to assess catamaran wetdeck slam loads, increases knowledge with regard to 3D wetdeck slam events and sheds light on key factors influencing wetdeck slam severity. This was achieved through the following:

1. The development of numerical CFD modelling commenced with a quasi-2D model progressing to a 3D numerical model using a dynamic meshing technique. One of the drawbacks in employing CFD techniques for solving 3D flow regime is the deformation of the free-surface, jet evolution and multi-phase flow which require significant computer power and time to accurately capture slam event details (such as the impact pressure peaks at localised points). To overcome this issue, the presented approach is recommended whereby simple hull shapes in a 2D flow regime are used to test key parameters influencing the numerical uncertainties as demonstrated in Appendix I. The 3D complex bodies can then be simulated with more confidence. The developed 3D CFD numerical model can accurately predict wetdeck slamming events and offers a feasible solution to the localised pressure distributions, total vertical force and flow behaviour around the bow section.

2. Two series of controlled-speed water impact experiments were conducted in collaboration with the University of Auckland using the SSTS system to characterise wetdeck slamming loads, define key-factors influencing their severity and to allow validation of the 3D impact predictions. A 3D bow section model of a generic wave-piercing catamaran was designed and built with two interchangeable centrebows. The direct measurements of pressure distributions, vertical force and corresponding immersions at two trim angles and a range of constant impact velocities gave new insight into the wetdeck slamming phenomenon. All the presented experimental results considered the slight variations measured in velocity profile by using the instantaneous impact velocity at the time of interest.

There are several improvements that can be made to the numerical model and the experimental setup presented in this study to widen the scope of their applications. These are discussed in section 7.4.

7.2 Conclusions

The verified and validated 2D and quasi-2D CFD simulations of catamaran wetdeck slam events using the overset meshing technique have clearly demonstrated their ability to adequately predict impact pressure distributions and corresponding vertical accelerations.

The computed flow structure matched well with experimental imagery that illustrates the existence of entrapped air pockets and entrained bubbles beneath the wetdeck during a quasi-2D slam event. The detailed flow structure and viscosity of the water should be considered within the simulation when flow separation occurs, while it was found that including the compressibility of the air leads to more accurate predictions when air cushions are created during wetdeck-water impact.

Modelling the corresponding motions under gravitational forces (free-falling) are difficult to predict during transient water impacts, as the simulation requires dynamic grid motions. Validated results demonstrated that utilising an overset meshing method (which was under development at the time of this work within STAR-CCM+) can accurately predict the corresponding vertical acceleration, follow an unsteady velocity trace and capture details of jet evolution and flow structure. This was achieved in relation to the applied hydrodynamic loads during water impacts with high accuracy and reasonable computational effort.

It is common in CFD water-impact simulations to use a fixed grid method (body remaining stationary) with an inlet flow at a given (steady or unsteady) velocity trace to simulate water impact scenarios. Although, this technique is simpler as it requires generating one fixed grid as well as using less computational effort, the comparative numerical results demonstrated that simulating the body's unsteady motion using an overset grid technique resulted in better predictions of slam load peaks, pressure distribution magnitudes and timings with a maximum deviation of ±5%. The work demonstrated the advantage of using a moving body sub-domain (i.e. overset grid technique) to accurately and efficiently predict slam events.

CFD predictions were more accurate than those obtained from SPH simulations when compared with experimental data. The 2D results showed that the maximum slam pressure peak magnitude occurs at the top arch of the arched wetdeck and then propagates aft (around the structure in the transverse direction) with lower magnitudes towards the demihulls and centrebow keel. The 3D simulations gave more insight into the impact pressure distributions, as results showed that slam pressure peaks slightly forward of the truncation (aft section) of the bow section. This was due to the rapid outflow and separation that occurs at the truncation leading to lower pressures in this vicinity.

This work has demonstrated that the 3D numerical model, developed with the CFD approach, would be reliable for naval architects, ship designers and classification societies to accurately predict impact pressure distributions and slam load components (such as the transverse splitting force) on complex hull geometries.

The experimental results provide a comprehensive set of benchmarking data for validation of numerical codes. The three dimensional effect on slam event was characterised and the results demonstrated that simplifying the wetdeck slam phenomenon as a quasi-2D problem is an invalid assumption that will cause errors in predictions of timing, corresponding immersion, magnitudes of pressure distributions and entire slam loads. An increase in the pressure peak magnitudes and loads at the enclosed vicinity of bow structure in relation to the open-sided structure for all conducted tests was observed. This indicates that the more contained the archway is, the greater the slam load.

A set of strong relationships between impact velocity, water-entry angle, hull geometry and slam force were found, and empirical relationships were developed to enable the estimation of the slam force magnitude as a function of the instantaneous impact velocity. Although no classification society rules consider the influence of pitch angle on wetdeck impact pressures severity, it was found that an increase of 5 degrees in trim angle can increase the vertical slamming force on the entire model by up to 30%.

As a result of using a winged (amended) centrebow, flow separation occurred on the tips of the wings during centrebow-water entry. Thus, the possible change in the rate of added mass

and the larger air-cushioning effect between the wetdeck and water surface showed a decrease in the resultant force by 6% in comparison to the parent centrebow.

The water elevation in the archway was found to increase by 10.5% in relation to the original water-surface. This observation adds an insight into defining the air gap of wave-piercing catamarans instead of the various recommended approaches for estimating the water elevation of traditional catamarans, presented by classification authorities (i.e. ABS, 2016; DNV, 2015; LR, 2016).A disconnect between impact pressure peak magnitudes and slam force peaks between the amended and parent hull forms highlights the need to accurately consider complete 3D pressure fields. It was observed that limited pressure distributions should not be used to assess slam loads due to the finding that localised pressure measurements are more dependent on flow behaviour than on the entire slam load magnitudes. Thus larger peak pressure magnitudes (at selected locations) do not necessarily lead to a larger total force.

7.3 Implications to the industry

This work provides original contributions to the field of catamaran performance, specifically, it adds knowledge that can be implemented within the industry in the following areas:

- CFD predictions of wetdeck slam events using overset meshing method were in better agreement with experimental data in comparison with other numerical techniques (e.g. SPH or fixed grid CFD technique).
- Validated CFD predictions present significant time and resource savings over experiments. The CFD tools developed are capable of accurately predicting slam forces, pressure distributions (both spatially and temporally), corresponding motions, and capturing flow structure details even in restricted water outflow conditions (i.e. semi-enclosed vicinity between the demihulls and centrebow).
- For assessing the performance of two different hull geometries, or even the same geometry subjected to unsteady flow behaviour during full-scale sea trials, load cells or strain gauges are recommended for measuring the applied slam loads, as the localised impact pressures are more sensitive to flow behaviour than to the applied hydrodynamic forces.

- The results of the experiments provide data that shed light on four main factors that can directly decrease the severity of wetdeck slam loads: 1. decreasing the relative impact velocity; 2. increasing the relative impact angle between water and wetdeck structure by either increasing the wetdeck longitudinal deadrise angle or by using an efficient ride-control system to decrease the corresponding pitch angle; 3. avoiding enclosed vicinities (i.e. enclosed by the adjacent structure from both sides) at the centrebow by allowing water to easily escape from the archway closure; and 4. facilitating flow separation prior to the wetdeck slam.
- The strong observed relationships between slam loads and corresponding impact velocities offer a method to estimate the slam force for a broader range of relative impact velocities and form a basis to study the issue of scaling for slam impacts. The study highlighted the important influence of the relative impact angle (between the wetdeck and the water-surface) on slam severity for design considerations.

7.4 Future work

Future research work could involve two general areas namely, CFD simulations and water-impact tests.

CFD simulations potentially provide an efficient tool for characterising wetdeck slam events. The verified and validated CFD method provided in this thesis is recommended for studying the influence of the following three design changes on slam severity.

- Increasing the longitudinal deadrise angle along the archway of the wetdeck in relation to the water-surface (i.e. decreasing the relative impact angle), was demonstrated to have had a significant effect on the slam load severity in an idealised still water case
- Providing venting holes in the two demihulls above the waterline (at the vicinity of the arch void) decreases the effect of the contained energy in the aerated-water in the arch enclosure and allows for a higher outflow rate. In addition this may affect the rate of change of the added mas of the hull further decreasing wetdeck slamming loads.
- Allowing the flow to separate immediately prior to the wetdeck slam event by improving the winged centrebow location and geometry.

The presented CFD approach could be extended to study the non-trivial issue of scaling of the hydrodynamic impact load magnitudes by simulating and comparing the model scale and full scale catamaran hull shapes. This would result in scaling factor coefficients for benchmarking catamaran vessels.

The experiments will never reproduce the behaviour of vessels in realistic sea conditions. However, they can illustrate factors influencing the problem of interest and add knowledge to the physics linked to wetdeck slamming.

The 3D water-impact experiments can be extended by implementing scaled-velocity traces recorded from full-scale sea trials rather than conducting constant-speed water impact tests. This will enable further investigation on the issue of scaling of slam loads.

The experiments in this work characterised slam loads using rigid models impacting still water. This was to focus on the influence of hydrodynamics on slam load severity, however it is recommended to extend the study to include the significance of hydroelasticity on slam events. In addition, including the significance of wave-height on slam load magnitudes will allow further numerical validation studies and will enrich the catamaran benchmarking dataset.

The proposed empirical relationships in this thesis (i.e. between the hydrodynamic impact loads, the velocity and the relative impact angle) are useful to provide an estimate of the slam force for a broader range of relative impact velocities for the same model. However, it is recommended that the study is ex-tended to include more factors that may influence the severity of slam loads such as the mass, added mass of the 3D model, deadrise angle and the volume of the enclosed vicinity between the centrebow and demihulls.

It would also be useful to propose a non-dimensional governing equation that implicitly includes the influence of the relative impact angle and added mass. This could be achieved by conducting a series of 3D CFD simulations based on the validated CFD method presented in this work.

References

ABS (2016). *Rules for building and classing high-speed craft*. American Bureau of Shipping.

Alaoui, A.E., Nême, A. & Scolan, Y.M. (2015). Experimental investigation of hydrodynamic loads and pressure distribution during a pyramid water entry. *Journal of Fluids and Structures*, vol. 54, pp. 925-35.

Alaoui, A.E., Nême, A., Tassin, A. & Jacques, N. (2012). Experimental study of coefficients during vertical water entry of axisymmetric rigid shapes at constant speeds. *Applied Ocean Research*, vol. 37, pp. 183-97.

Allen, T. (2013). Mechanics of Flexible Composite Hull Panels Subjected to Water Impacts. PhD thesis, University of Auckland, Auckland, NewZealnd.

Amin, W. (2009). Non-linear unsteady wave loads on large high-speed wave piercing catamarans. PhD thesis, University of Tasmania, University of Tasmania.

Batina, J.T. (1991). Unsteady Euler algorithm with unstructured dynamic mesh for complex aircraft aerodynamic analysis. *AIAA Journal*, vol. 29.

Battley, M. & Allen, T. (2012). Servo-hydraulic system for controlled velocity water impact of marine sandwich panels. *Experimental mechanics*, vol. 52(1), pp. 95-106.

Battley, M., Stenius, I., Breder, J. & Edinger, S. (2005). Dynamic characterisation of marine sandwich structures. In O.T. Thomsen, E. Bozehvlnaya & A. Lyckegaard (eds), *7th International Conference on Sandwich Structures*, Aalborg, Denmark, pp. 537-46.

Bertram, V. (2000). *Practical ship hydrodynamics*, Oxford: Butterworth Heinemann.

Bodony, D.J., Zagaris, G., Reichert, A. & Zhang, Q. (2011). Provably stable overset grid methods for computational aeroacoustics. *Journal of Sound and Vibration*, vol. 330, no. 17, pp. 4161-79.

Bozorgnia, M. & Lee, J.J. (2012). Computational fluid dynamic analysis of highway bridges exposed to hurricane waves. *Coastal Engineering Proceedings*, vol. 1, no. 33, p. 70.

Brizzolara, S., Curtin, T., Bovio, M. & Vernengo, G. (2012). Concept design and hydrodynamic optimization of an innovative SWATH USV by CFD methods. *Ocean Dynamics*, vol. 62, no. 2, pp. 227-37.

Campbell, I.M.C. & Weynberg, P.A. (1980). Measurement of parameters affecting slamming. *Final Report.Wolfson Unit for Marine Tech. Rep. No. 440, Technology Reports Centre No. OT-R-8042*.

Chen, H.C. & Yu, K. (2008). CFD simulations of wave–current-body interactions including greenwater and wet deck slamming. *Computers & Fluid*s, vol 38(5), pp.970-80.

Chuang, S.L. & Milne, D.T. (1971). *Drop tests of cones to investigate the three-dimensional effects of slamming* (No. NSRDC-3543). David W Taylor Naval Ship Research and Development Center Bethesda Md.

Chuang, S. (1966). Experiments on flat-bottom slamming. *Journal of Ship Research*, vol. 10, no. 1, pp. 10-7.

Davidson, G., Roberts, T. & Thomas, G. (2006). Global and slam loads for a large wavepiercing catamaran design. *Australian Journal of Mechanical Engineering*, vol. 3, no. 2, pp. 155-64.

Davis, M.R. & Whelan, J.R. (2007). Computation of wet deck bow slam loads for catamaran arched cross sections. *Ocean Engineering*, vol. 34, no.17, pp. 2265-76.

De Backer, G., Vantorre, M., Beels, C., De Pré, J., Victor, S., De Rouck, J., Blommaert, C. & Van Paepegem, W. (2009). Experimental investigation of water impact on axisymmetric bodies. *Applied Ocean Research*, vol. 31, no. 3, pp. 143-56.

Demirdzic, I., Lilek, Z. & Peric, M. (1993). A Collocated Finite Volume Method for Predicting Flows at all Speeds. *International Journal for Numerical Methods in Fluids, vol. 16, no. 12, pp. 1029-50*

Demirzic, I. & Peric, M. (1990). Finite volume method for prediction of fluid flow in arbitrarily shaped domains with moving boundaries. *International Journal for Numerical Methods in Fluids*, vol. 10, no. 7, pp. 771-90.

Dessi, D. & Ciappi, E. (2013). Slamming clustering on fast ships: From impact dynamics to global response analysis. *Ocean Engineering*, vol. 62, no. 0, pp. 110-22.

DNV (2010). *Environmental conditions and environmental loads*. Det Norske Veritas.

DNV (2015). *Rules for classification - High speed and light craft*. Det Norske Veritas. Retrieved February 30, 2016, from http://rules.dnvgl.com/docs/pdf/DNVGL/RU-HSLC/2015-12/DNVGL-RU-HSLC-Pt3Ch1.pdf.

Dobrovol'Skaya, Z. (1969) On some problems of similarity flow of fluid with a free surface. *Journal of Fluid Mechanics*, vol. 36, no. 4, pp. 805-29.

Dragomir, S.S., Pietro, C. & Anthony, S. (1998). Some Remarks on the Midpoint Rule in Numerical Integration. *RGMIA research report collection*, vol. 1, no. 2.

Engle, A. & Lewis, R. (2003). A comparison of hydrodynamic impacts prediction methods with two dimensional drop test data. *Marine Structures*, vol. 16, no. 2, pp. 175-82.

Faltinsen, O.M. (2005). *Hydrodynamics of high-speed marine vehicles*, Cambridge University Press.

Faltinsen, O.M. (2006). Hydrodynamic features of high-speed vessels. *Ships and Offshore Structures*, vol. 1, no. 1, pp. 13-23.

French, B. (2012). Slamming of high-speed catamarans in irregular seas. PhD thesis, University of Tasmania, Launceston, Australia.

French, B. & Thomas, G. (2014). Slam characteristics of a high-speed wave piercing catamaran in irregular waves. *Transactions. Part A. International Journal of Maritime Engineering*, vol. 156, no. 1, pp. A-25-A-36.

French, B., Thomas, G. & Davis, M.R. (2015). Slam occurrences and loads of a high-speed wave piercer catamaran in irregular seas. *In: Proceedings of the Institution of Mechanical Engineers, Part M: Journal of Engineering for the Maritime Environment*, vol. 229, no. 1, pp. 45-57.

Fricke, W. & Bronsart, R. (2012). Implusle Pressure Loading and Response Assessment. *In: Proceedings of the 18th International Ship and Offshore Structures Congress (ISSC)*, Hamburg, Germany, vol. 7, pp. 297-318.

Ge, C. (2002). Global Hydroelastic Response of Catamarans due to Wetdeck Slamming. PhD thesis, Norwegian University of Science and Technology, Trondheim, Norway.

Graczyk, M. & Moan, T. (2008). A probabilistic assessment of design sloshing pressure time histories in LNG tanks. *Ocean Engineering*, vol. 35, no. 8, pp. 834-55.

Hadler, J., Lee, C., Birmingham, J. & Jones, H. (1974). *Ocean Catamaran Seakeeping Design, Based on The Experiments of USNS HAYES. Annual meeting*, The Society of Naval Architects and Marine Engineerings.

He, W., Diez, M., Zou, Z., Campana, E.F. & Stern, F. (2013). URANS study of Delft catamaran total/added resistance, motions and slamming loads in head sea including irregular wave and uncertainty quantification for variable regular wave and geometry. *Ocean Engineerin*g, vol. 74, pp.189-217.

Hermundstad, O.A. & Moan, T. (2007). Efficient calculation of slamming pressures on ships in irregular seas. *Journal of Marine Science and Technology*, vol. 12, no. 3, pp. 160-82.

Hirt, C.W. & Nichols, B.D. (1981). Volume of Fluid (VOF) method for the dynamics of free boundaries. *Journal of Computational Physics*, vol. 39, no. 1, pp. 201-25.

Huera-Huarte, F.J., Jeon, D. & Gharib, M. (2011). Experimental investigation of water slamming loads on panels. *Ocean Engineering*, vol. 38. no. 11, pp. 1347-55.

Incat Tasmania (1986). *Earlier vessels*. Retrieved April 18, 2016, from http://www.incat.com.au/domino/incat/incatweb.nsf/0/22D59453CD047744CA2571AF001A37F9?OpenDocument

Incat Tasmania (2013). *112m high-speed wave-piercing catamaran (Kat Express 2)*. Retrieved May 12, 2016, from http://www.incat.com.au/domino/incat/incatweb.nsf/0/F53DF680FB0E2412CA257B39000A0B82/$File/0670137EH.jpg

ITTC (1999). Testing and Extrapolation Methods, High Speed Marine Vehicles, Sea Keeping Tests. in International Towing Tank Conference (ITTC) - Recommended Procedures and Guidelines. vol.7.5-02-05-04, 2002, p. 13.

Jacobi, G., Thomas, G., Davis, M.R. & Davidson, G. (2014). An insight into the slamming behaviour of large high-speed catamarans through full-scale measurements. *Journal of Marine Science and Technology*, vol. 19, no. 1, pp. 15-32.

Jacobi, G., Thomas, G., Davis, M.R., Holloway, D.S., Davidson, G. & Roberts, T. (2012). Full-scale motions of a large high-speed catamaran: The influence of wave environment, speed and ride control system. *International Journal of Maritime Engineering*, vol. 154, no. A3, pp. A143-A55.

Jalalisendi, M., Osma, S.J. & Porfiri, M. (2015). Three-dimensional water entry of a solid body: A particle image velocimetry study. *Journal of Fluids and Structures*, vol. 59, pp. 85-102.

Johannessen, S. (2012). Use of CFD to Study Hydrodynamic Loads on Free-Fall Lifeboats in the Impact Phase.: A verification and validation study. MSc. thesis, Norwegian University of Science and Technology, Trondheim, Norway.

Kaplan, P. (1987). Analysis and prediction of flat bottom slamming impact of advanced marine vehicles in waves. *International shipbuilding progress*, vol. 34, no. 391, pp. 44-53.

Kapsenberg, G. (2011). Slamming of ships: where are we now?. *Philosophical Transactions of the Royal Society A: Mathematical, Physical and Engineering Sciences*, vol. 369, no. 1947, pp. 2892-919.

Kvålsvold, J. & Faltinsen, O. (1995). Hydroelastic Modeling of Wet Deck Slamming on Multihull Vessels. *Journal of Ship Research*, vol. 39, no. 3, pp. 225-39.

Lavroff, J. (2009). The Slamming and Whipping Vibratory Response of a Hydroelastic Segmented Catamaran Model. PhD thesis, University of Tasmania, Hobart, Australia.

Lavroff, J., Davis, M., Holloway, D. & Thomas, G. (2011). Determination of wave slamming loads on high-speed catamarans by hydroelastic segmented model experiments. *International Journal of Maritime Engineering*, vol. 153, no. A3, pp. 185-97.

Lavroff, J., Davis, M., Holloway, D. & Thomas, G. (2013). Wave slamming loads on wave-piercer catamarans operating at high-speed determined by hydro-elastic segmented model experiments. *Marine Structures*, vol. 33, pp. 120-42.

Lewis, S.G., Hudson, D.A., Turnock, S.R. & Taunton, D.J. (2010). Impact of a free-falling wedge with water: synchronized visualization, pressure and acceleration measurements. *Fluid Dynamics Research*, vol. 42, no. 3, p. 035509.

Lewis, S.G., Turnock, S.R. (2008). Simulation of a free falling wedge into water using 2D CFD with applications in the prediction of high speed craft motions. Paper presented to ANSYS UK User Conference: Inspiring Engineering, UK.

LR (2016). *Rules and regulations for the classification of special service craft*. Lloyd's Register, Retrieved, March 20, 2016, from http://www.lr.org/en/RulesandRegulations/special-service-craft.aspx

Luo, H. & Soares, C.G. (2012). Review of model test techniques of local slamming on ships. *Electrical Measuring Instruments and Measurements*, p. 189.

Maritime Denmark (2013). *KatExpress 2 on its way to Denmark. Retrieved, May 2016, from* http://www.maritimedenmark.dk/?utm_source=uknyhedsbrev22-03-2013&utm_medium=email&utm_content=uknyhedsbrev2013&utm_campaign=uknyhedsbrev&Id=16757

Menter, F.R. (1994). Two-equation eddy-viscosity turbulence modeling for engineering applications. *AIAA Journal*, vol. 32, no. 8, pp.1598-1605.

Mitra, S.K. & Kuo, Y. (2006). *Digital signal processing: a computer-based approach*. vol. 2, Sections 4.4.2 and 8.2.5, New York: McGraw-Hill.

Mørch, H., Enger, S., Peri´c, M. & Schreck, E. (2008). Simulation of Lifeboat Launching Under Storm Conditions. In the proceedings of the *6th International Conference on CFD in Oil and Gas, Metallurgical and Process Industries*, Trondheim, Norway.

Mørch, H., Perić, M., Röper, J. & Schreck, E. (2009). CFD-Supported Design of Lifeboats. in *NAFEMS Seminar: Simulation of Complex Flows (CFD)-Applications and Trends*, Wiesbaden, Germany.

Ochi, M.K. & Motter, L.E. (1971). A method to estimate slamming characteristic for ship design. *Marine Technology,* vol. 8, no. 2, pp. 219-32.

Ochi, M.K. & Motter, L.E. (1973). Prediction of slamming characteristics and hull responses for ship design. *Transactions. Socciety of Naval Architecture and Marine Eng*ineering, vol. 81, pp. 144-76.

Oger, G., Doring, M., Alessandrini, B. & Ferrant, P. (2006). Two-dimensional SPH simulations of wedge water entries. *Journal of Computational Physics*, vol. 213, no. 2, pp. 803-22.

Okada, S. & Sumi, Y. (2000). On the water impact and elastic response of a flat plate at small impact angles. *Marine Science Technology*, vol. 5, no.1, pp. 31-9.

Paik, J. & Shin, Y. (2006). Structural damage and strength criteria for ship stiffened panels under impact pressure actions arising from sloshing, slamming and green water loading. *Ships and Offshore Structures*, vol. 1, no. 3, pp. 249-56.

Panahi, R. & Shafieefar, M. (2010). Towards a numerical hydrodynamics laboratory by developing an overlapping mesh solver based on a moving mesh solver; verification and application. *Applied Ocean Research*, vol. 32, no. 3, pp. 308-20.

Panciroli, R. & Porfiri, M. (2013). Evaluation of the pressure field on a rigid body entering a quiescent fluid through particle image velocimetry. *Experiments in fluids*, vol. 54, no. 12, pp. 1-13.

Payne, P.R. (1988). A discussion of the design pressures appropriate to the bottom of a planing boat. *Ocean Engineering*, vol. 15, no. 5, pp. 471-93.

Pistani, F. & Thiagarajan, K. (2012). Experimental measurements and data analysis of the impact pressures in a sloshing experiment. *Ocean Engineering*, vol. 52, pp. 60-74.

Razola, M., Rosén, A. & Garme, K. (2014). Allen and Jones revisited. *Ocean Engineering*, vol. 89, no. 0, pp. 119-33.

Roberts, T.J., Watson, N.L. & Davis, M.R. (1997). Evaluation of sea loads for fast ferry vessels. in SNAME (ed.), *4th International conference on Fast Sea Transportation (FAST)*, Sydney, Australia, vol. 1, pp. 311-6.

Rosén, A. (2005). Impact pressure distribution reconstruction from discrete point measurements. *International Shipbuilding Progess.*, vol. 52, no. 1, pp. 91-107.

Rothe, F., Sames, P.C. & Schellin, T.E. (2001). Catamaran wetdeck structural response to wave impact. in SNAME (ed.), 6th *International Conference of Fast Sea Transportation (FAST'01)*, Southampton, England, vol. 3, pp. 125-33.

Shahraki, J., Penesis, I., Thomas, G., Davis, M.R. & Whelan, J.R. (2011). Prediction of slamming behaviour of monohull and multihull forms using smoothed particle hydrodynamics. in RINA (ed.), *9th HSMV, High Speed Marine Vehicles*, Naples, Italy.

Starius, G. (1977). Composite mesh difference methods for elliptic and boundary value problems. *Numerische Mathematik*, vol. 28, no. 2, pp. 243–58.

Steinmann, P., Fach, K. & Menon, B. (1999). Global and Slamming Sea Loads Acting on an 86m High Speed Catamaran Ferry. in SNAME (ed.), *5th International Conference on Fast Sea Transportation*, Seattle, USA.

Stenius, I., Rosén, A., Battley, M. & Allen, T. (2013). Experimental hydroelastic characterization of slamming loaded marine panels. *Ocean Engineering*, vol. 74, pp. 1-15.

Stenius, I., Rosén, A., Battley, M., Allen, T. & Pehrson, P. (2011). Hydroelastic effects in slamming loaded panels. in SNAME (ed.), *11th International Conference on Fast Sea Transportation (FAST 2011), Honolulu, Hawaii, USA*, pp. 644-52.

Sun, H. & Faltinsen, O. (2009). Water entry of a bow-flare ship section with roll angle. *Marine Science and Technology*, vol. 14, no.1, pp. 69-79.

Sun, H. & Faltinsen, O.M. (2010). Numerical Study of Planning Vessels in Waves. *Journal of Hydrodynamics*, vol. 22, no. 5, Supplement 1, pp. 468-75.

Takashi, Y., Feng-Xiao, Y. & Takayuki, U. (2001). The Constrained Interpolation Profile Method for Multiphase Analysis. *Journal of Computational Physics*, vol. 169, pp. 556–93.

Tassin, A., Jacques, N., El Malki Alaoui, A., Nême, A. & Leblé, B. (2012). Hydrodynamic loads during water impact of three-dimensional solids: Modelling and experiments. *Journal of Fluids and Structures*, vol. 28, pp. 211-31.

Thomas, G. (2003). Wave Slam Response of Large High Speed Catamarans). PhD thesis, University of Tasmania, Hobart, Australia.

Thomas, G., Davis, M., Holloway, D. & Roberts, T. (2002). Extreme asymmetric slam loads on large high speed catamarans. in RINA (ed.), *6th Symposium of High Speed Marine Vessels*, vol. 8, pp. 15-23, Naples, Italy.

Thomas, G., Davis, M.R., Holloway, D.S., Watson, N. & Roberts, T. (2003). Slamming Response of a Large High-Speed Wave-Piercer Catamaran. *Marine Technology*, vol. 40, no. 2, pp. 126-40.

Thomas, G., Kibby, L., Ford, A., Binns, J., Finnie, I. & Kavanagh, N. (2011a). Experimental Investigation into Wave-Induced Design Loads on a Large Moored Catamaran. *Ships and Offshore Structures*, vol. 6, no. 4, pp. 273-95.

Thomas, G., Winkler, S., Davis, M., Holloway, D., Matsubara, S., Lavroff, J. & French, B. (2011b). Slam events of high-speed catamarans in irregular waves. *Journal of Marine Science and Technology*, vol. 16, no. 1, pp. 8–21.

Tveitnes, T., Fairlie-Clarke, A. & Varyani, K. (2008). An experimental investigation into the constant velocity water entry of wedge-shaped sections). *Ocean Engineering*, vol. 35, no. 14, pp. 1463-78.

Van Nuffel, D., Vepa, K. S., De Baere, I., Degrieck, J., De Rouck, J., & Van Paepegem, W. (2013). Study on the parameters influencing the accuracy and reproducibility of dynamic pressure measurements at the surface of a rigid body during water impact. Experimental Mechanics, vol. 53, no. 2, pp. 131-44.

Van Nuffel, D., Vepa, K.S., De Baere, I., Lava, P., Kersemans, M., Degrieck, J., De Rouck, J. & Van Paepegem, W. (2014). A comparison between the experimental and theoretical impact pressures acting on a horizontal quasi-rigid cylinder during vertical water entry. Ocean Engineering, vol. 77, pp. 42-54.

Veen, D., & Gourlay, T. (2012). A combined strip theory and Smoothed Particle Hydrodynamics approach for estimating slamming loads on a ship in head seas. Ocean Engineering, vol. 43, pp. 64-71.

Wacławczyk, T. & Koronowicz, T. (2008). Comparison of CICSAM and HRIC high-resolution schemes for interface capturing. *Journal of Theoretical and Applied Mechanics*, vol. 46, no. 2, pp. 325-45.

Wagner, H. (1932). Über Stross-und Gleitvorgänge an der Oberfläche von Flüssigkeiten', ZAMM, vol. 12, no. 4, pp. 193–215.

Wang, S. & Soares, C.G. (2013). Slam induced loads on bow-flared sections with various roll angles. Ocean Engineering, vol. 67, pp. 45-57.

Wendt, J.F. (2009). *Computational Fluid Dynamics*. Vol. 3, Library of Congress, Verlag Berlin Heidelberg.

Whelan, J.R. (2004). Wetdeck slamming of high speed catamarans with a centrebow. PhD thesis, Univesrsity of Tasmania, Tasmania, Australia.

Wilcox, D. C. (1998). Turbulence modeling for CFD. Vol. 2, pp. 103-217. La Canada, CA: DCW industries.

Yang, Q. & Qiu, W. (2012). Numerical simulation of water impact for 2D and 3D bodies. *Ocean Engineering*, vol. 43, pp. 82-9.

Yettou, E. M., Desrochers, A., & Champoux, Y. (2006). Experimental study on the water impact of a symmetrical wedge. Fluid Dynamics Research, vol. 38, no. 1, pp. 47-66.

Yettou, E. M., Desrochers, A., & Champoux, Y. (2007). A new analytical model for pressure estimation of symmetrical water impact of a rigid wedge at variable velocities. Journal of fluids and structures, vol. 23, no. 3, pp. 501-22.

Zagaris, G., Campbell, M. T., Bodony, D. J., Shaffer, E., & Brandyberry, M. D. (2010). A toolkit for parallel overset grid assembly targeting large-scale moving body aerodynamic

simulations. In Proceedings of the 19th International Meshing Roundtable (pp. 385-401). Springer Berlin Heidelberg.

Zhao, R. & Faltinsen, O. (1993). Water entry of two-dimensional bodies. *Journal of Fluid Mechanics*, vol. 246, pp. 593-612.

Zhao, R., Faltinsen, O., & Aarsnes, J. (1996). Water entry of arbitrary two-dimensional sections with and without flow separation. In Proceedings of the 21st symposium on naval hydrodynamics (pp. 408-423). Trondheim, Norway, National Academy Press, Washington, DC, USA.

Zhu, Z., Xulong, Y. & Yadong, W. (2012). Influence of Parameters Setting on Calculating Water-entry Flow Field at High Speed. In Proceedings of the 1st International Conference on Mechanical Engineering and Material Science. Atlantis Press.

Appendices

I CFD tested parameters

The first selected model was a wedge shaped hull form, for the following three reasons:

- The availability of published experimental data for wedge hull form drop tests.
- The availability of published SPH numerical predictions for wedge hull form drop tests.
- The reduced computational time and effort in creating the geometry and grid model for studying the influence of numerical parameters on predictions when compared with catamaran models.

The numerical study was then extended to simulate a quasi-2D Incat catamaran model impacting with water. To achieve stable numerical results, the parameters given in Table I.1 were selected.

Table I. 1: Parameters Tested in the Convergence Study for the Wedge and Incat Models

		Shape	Parameter	Tested	Selected
Physics	Segregated flow	CAT	Convection	1st/2nd -order	2nd-order
		Wedge		1st/2nd -order	2nd-order
	VOF	CAT		1st/2nd -order	2nd-order
		Wedge		1st/2nd -order	2nd-order
Solver	Implicit unsteady	CAT	Temporal discretisation	1st/2nd -order	1st –order
		Wedge		1st/2nd -order	1st –order
	6-DOF solver	CAT	Number of iterations	7. 10. 15	7
		Wedge		7. 10. 15	7
	Segregated flow	CAT	Velocity: under	0.5. 0.7. 0.8. 0.9	0.8
		Wedge	Velocity: under	0.5. 0.7. 0.8. 0.9	0.7
		CAT	Pressure: under	0.1. 0.2. 0.3. 0.5	0.2
		Wedge	Pressure: under	0.1. 0.2. 0.3. 0.5	0.1
Stopping criteria	Iterations	CAT	Number of inner	5, 10, 15, 20	10
		Wedge	Number of inner	5, 10, 15, 20	10
Flow model	Laminar, K-ε, K-ω,	CAT	Compressibility	Compressible air/	SST k-ω, Compressible
	Laminar	Wedge	Compressibility	Incompressible fluid	Laminar, Incompressible

Laminar flow was considered sufficient to predict the the localised loads for the wedge shaped hull form, while for the Incat model, using RANS-SST (shear-stress transport)

turbulence model leads to better results for simulating the fluids flow in a semi-enclosed void such as the volume of interest under the wetdeck (Menter, 1994; Wilcox, 1998), as illustrated in Figs. I.1(a) - I.1(c).

The preliminary predicted pressures of the catamaran model using the SST-model simulation were found to be promising. Although including the air compressibility effect shows better agreement for the maximum pressure magnitudes, while some oscillation occurs after the peak pressures, as illustrated in Figs. I.1(a) - I.1(c). These oscillations were attributed to the rapid change in the pressure fields beneath the wetdeck and hence changing the density correction value in the continuity and momentum equations may lead to such oscillations.

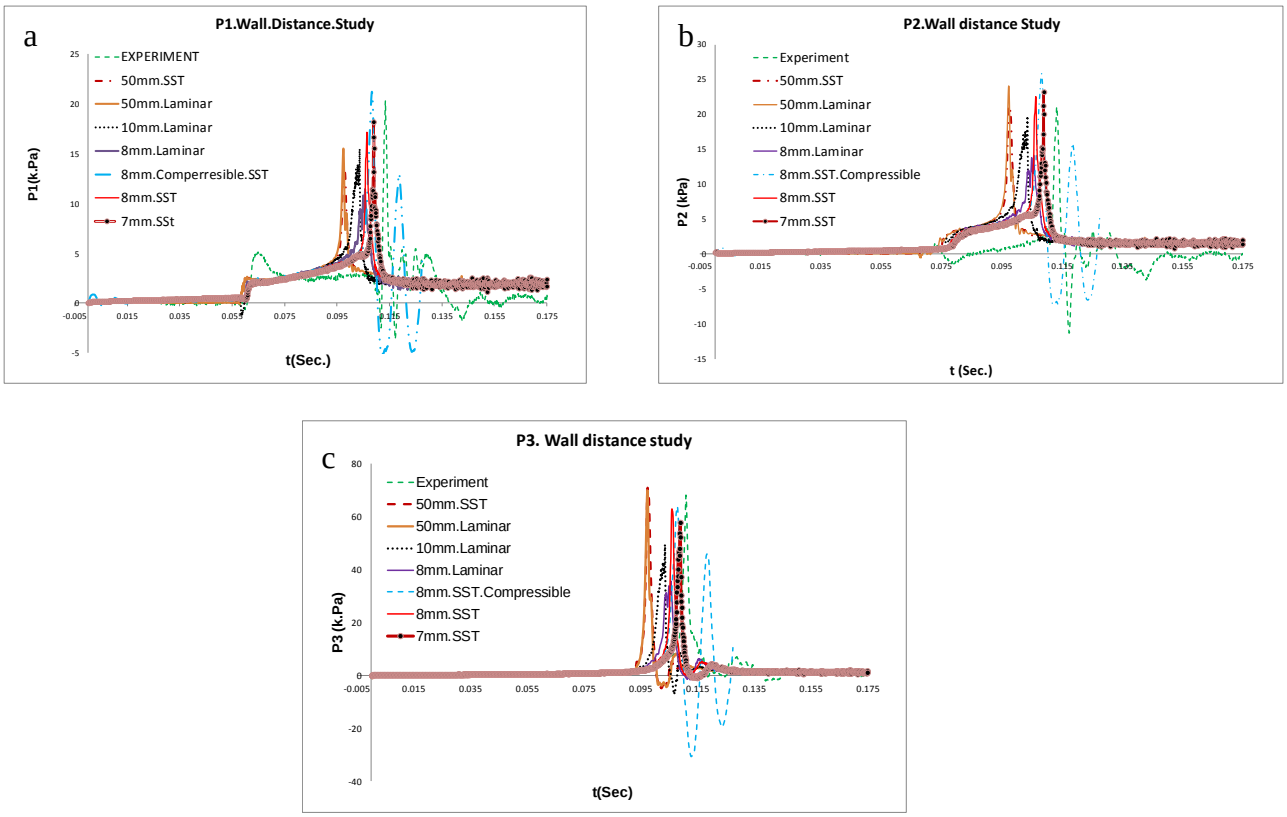

Fig. I 1: Validation study. Showing pressure time histories of three pressure probes located around the arched wetdeck of quasi-2D Incat hull model (P1 to P3, as illustrated in plots. I.a –I.c). Presented experimental pressure data were recorded by Whelan for mass number 0.29 and dimensionless drop height of 0.89 (Whelan, 2004).

II Repeatability

Each condition presented in chapter 5 was repeated for a minimum of three tests to provide confidence in the experimental setup. The measured data from three repeated water-impact tests using the parent hull model at 0 degree trim angle and at the maximum target velocity of 5m/s are presented in Figs. II.1- II.3. These figures demonstrate very good repeatability of velocity traces, hydrodynamic impact loads and pressure distributions at transducer P1, the location of this transducer is illustrated in Fig. 5.3.

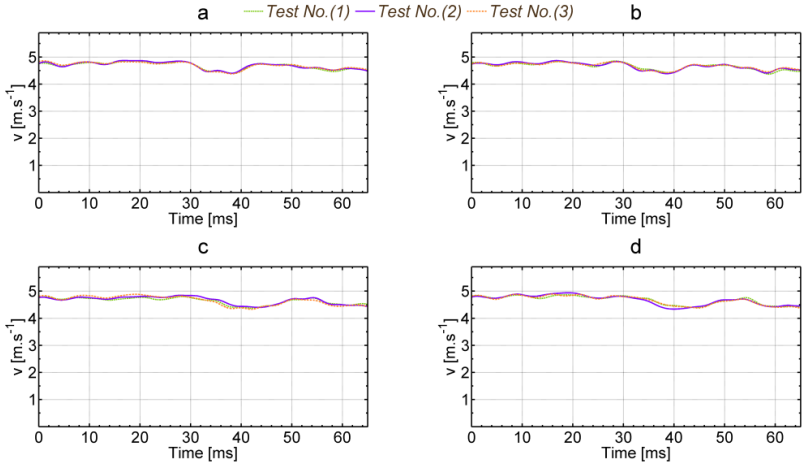

Fig. II 1: Velocity (a), load (b) and pressure (c) traces of three repeated tests the for conditions numbers 5 and 10 for (a) parent hull at θ = 0°, (b) amended hull at θ = 0°, (c) parent hull at θ = 5°, (d) amended hull at θ = 5°.

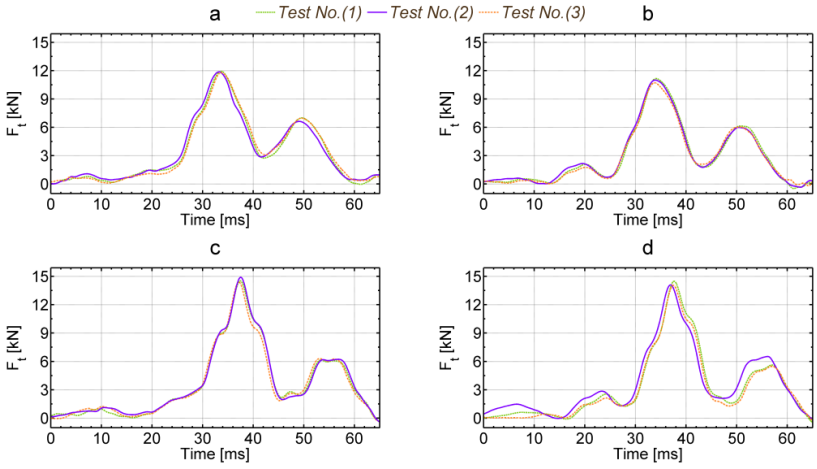

Fig. II 2: Total slamming force time histories of three repeated tests for conditions numbers 5 and 10 for (a) parent hull at θ = 0°, (b) amended hull at θ = 0°, (c) parent hull at θ = 5°, (d) amended hull at θ = 5°.

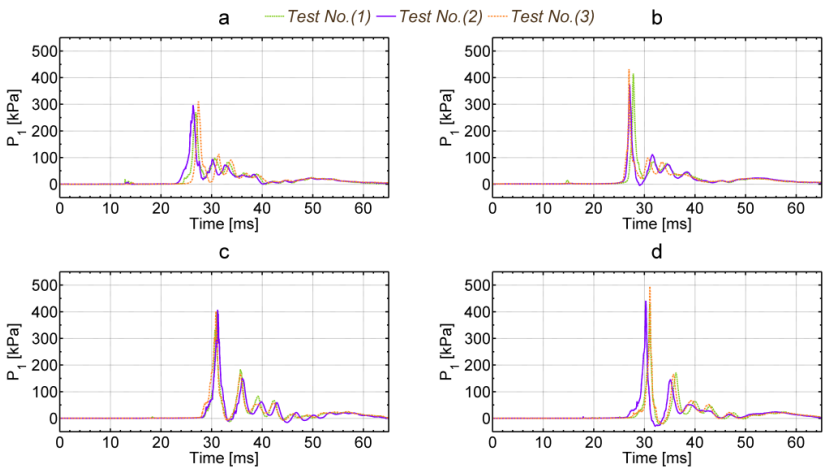

Fig. II 3: Maximum measured pressures of three repeated tests for conditions numbers 5 and 10 for (a) parent hull at θ = 0°, (b) amended hull at θ = 0°, (c) parent hull at θ = 5°, (d) amended hull at θ = 5°.

III Pressure Coefficients

The mean traces of maximum pressures at P1 (see Fig. 5.3) for a minimum of three water impact tests for the parent hull at trim angles of 0 and 5 and for all relative impact velocities mentioned in Table 5.2 are aligned using the cross-correlation function in Matlab that can detect and align the peaks of a number of signals. This allowed accurate calculation of the average of maximum pressure time histories for the three repeated tests per each condition. This enabled calculation of the pressure coefficients at the two relative impact angles using the traditional Wagner formula, as presented in Eq. C.1 and C.2 (The terms mentioned in Eq. C.1 and C.2 are defined in Fig. III.1).

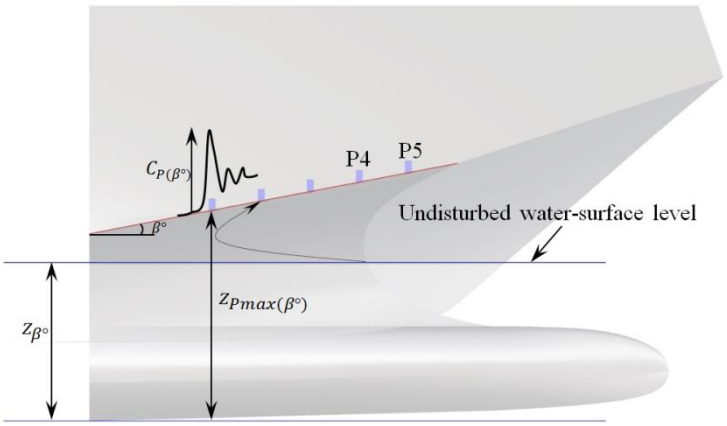

Fig. III.1: Schematic diagram defining the variables used to non-dimensionalized the catamaran wetdeck slamming pressure.

$$\xi_{\beta°} = \frac{z_{Pmax(\beta°)} - z_{\beta°}}{z_{\beta°}} \qquad \text{.... (C.1)}$$

$$C_{P(\beta°)} = \frac{2P_{max(\beta°)}}{\rho v^2} \qquad \text{.... (C.2)}$$

The repeatability of the experiments is acceptable since $C_{P(\beta°)}$ traces are in very good agreement. The maximum pressure coefficients of parent hull model at the two relative impact angles were found to be within approximately equal magnitudes of $C_{P(0°)max}$ = 26 ±2 and $C_{P(5°)max}$ = 34.5 ± 1.5. The traces of presented pressure coefficients are in good agreement. Thus the provided pressure coefficients can be used for validation of local pressures for this hull form at P1, which is independent on the impact velocity. This was

observed previously for other hull model shapes by Dobrovol'Skaya (1969), Lewis et al. (2010), Yettou et al. (2006), Zhao & Faltinsen (1993) and Zhao.R (1996).

Fig. III.2 illustrates also that the smaller the relative impact angle (β), the sharper the pressure coefficient trace, the more significant the pressure coefficient is $C_{P(\beta°)max.}$ and the shorter the peak duration.

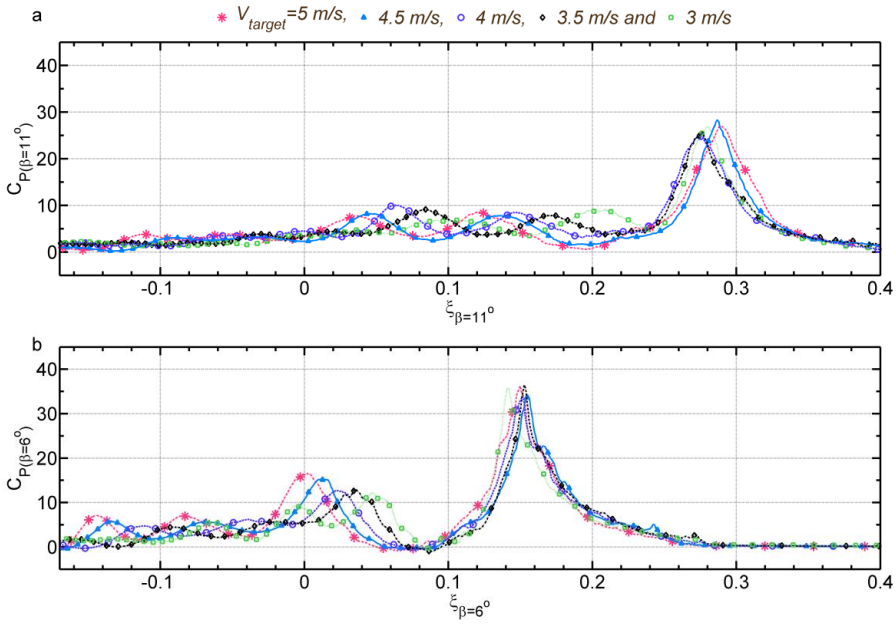

Fig. III.2: Catamaran pressure coefficients at two relative impact angles with non-dimensionalized catamaran entry-depth (as defined in Equation C.1); showing the pressure coefficients at; (a) trim angle of 0 degree (equivalent to relative impact angle of 11 degrees) and (b) a trim angle of 5 degrees (equivalent to relative impact angle of 6 degrees).

IV Simulated flow behaviour

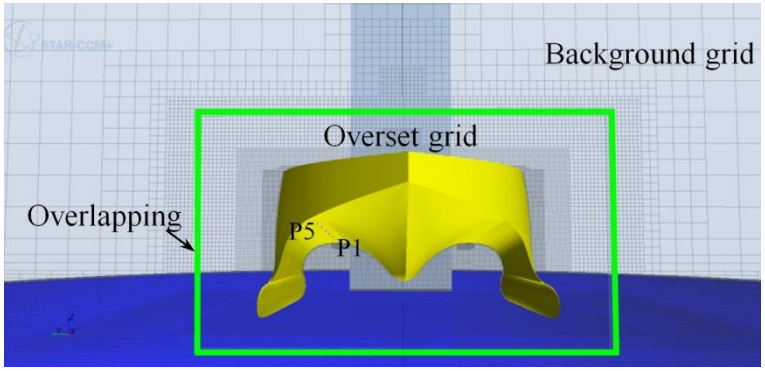

Fig. IV. 1: A symmetric plane of the generated overset grid and overlapping region to the numerical model developd in chapter 6.

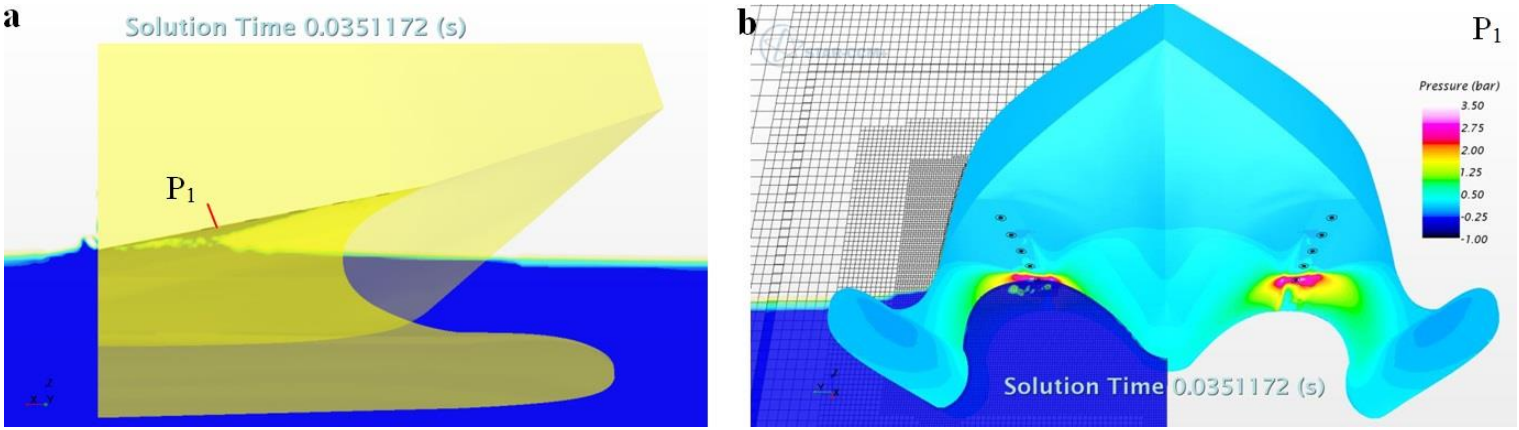

Fig. IV 1: Subplot (a) flow visualisation using a longitudinal section along the mid of transducer P1 (as illustrated in Fig.3.2), air inclusion has been captured around the vicinity of P1. Subplot (b) Pressure contours on the right hand sided of the figure as well as flow visualisation using a transverse section passing through the mid of transducer P1 on the left side, showing also the flow behaviour and existence of air entrapment.

Fig. IV.1 illustrates the numerical domain of the CFD simulations presented in Chapter 6. The overset meshing method was employed to implement a given velocity profile presented in Fig. 6.4. The CFD should be considered as appropriate to be part of the design process, as it can provide ship designers with detailed insight into wetdeck slam events. Fig IV.2 presents the flow visualisation and pressure contours of the simulation conducted in chapter 6.

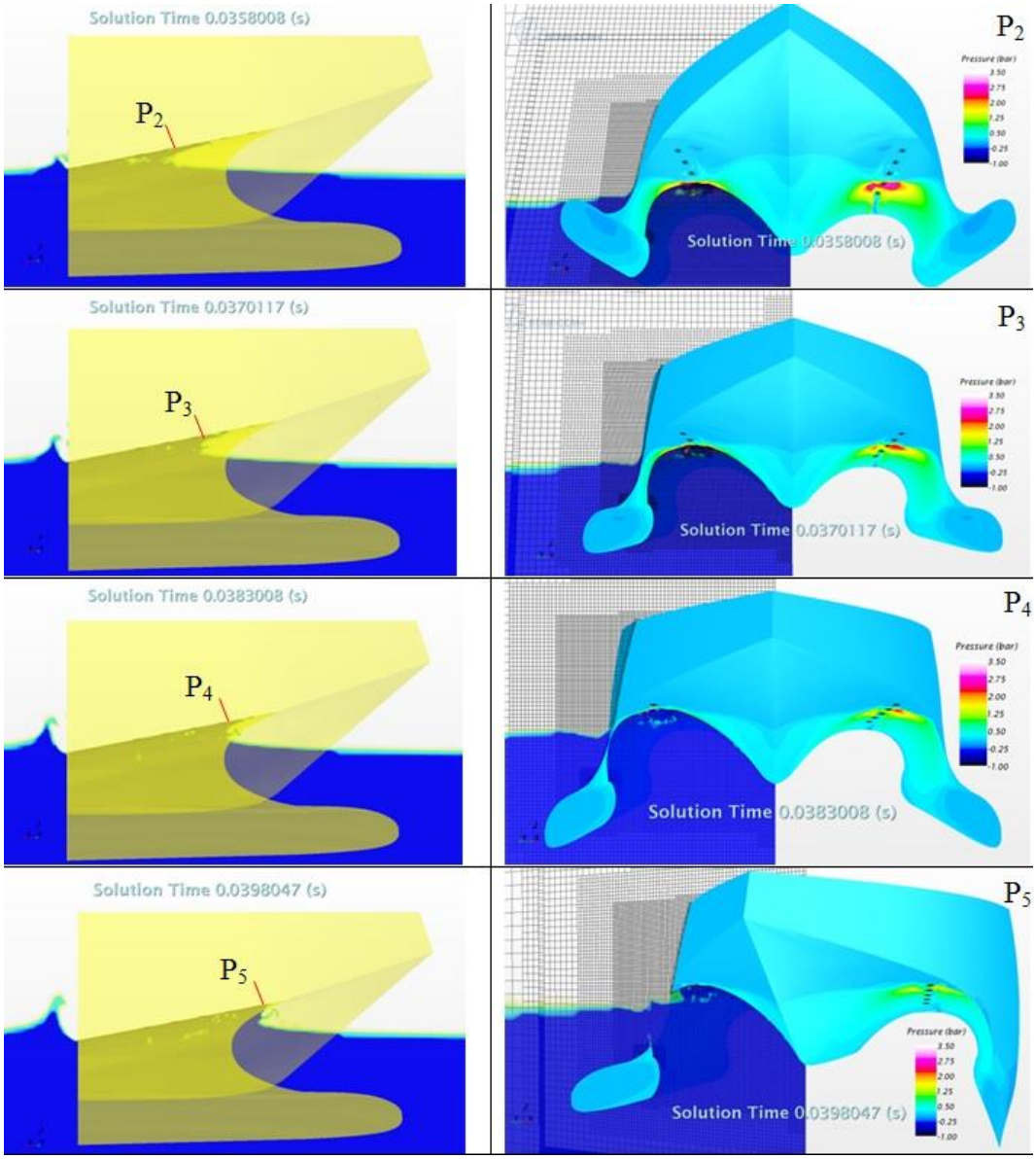

Fig. IV 2: Flow visualisation using both longitudinal sections across P2 to P5 on left hand side and transverse section with pressure contours on the right hand side.

V Instrumentation data sheets

Model LPC

LOW PROFILE UNIVERSAL LOAD CELL

A popular industry standard, universal low profile high accuracy load cell.

Compact in design, the LPC is eccentric load compensated, and temperature compensated -10 to 50°C.

Available in 7 different capacities from 1t to 100t.

Fully environmentally sealed and supplied with quality 6 core PVC screened cable.

Constructed in tool steel and corrosion resistant electroless nickel plated finish. The LPC directly replaces many International standard models and has a wide range of mounting accessories for both compression and tension applications.

Supplied with quality 6 core PVC screened cable.

Standard compression and tension accessories allow simple installation and enhanced lifelong accuracy.

APPLICATIONS

- Materials testing in compression or tension
- High capacity tension weighing, overhead weighing, cranes etc
- Low profile is idea for compression weighing of hoppers, tanks & silo weighers

FEATURES

- Low profile
- 0.05% accuracy
- Large capacity range 1t ~ 100t
- Comprehensive mounting accessory packages

Specifications

Note: All specifications are a maximum, as a % (±) of full load, unless otherwise stated.

Nominal Capacity	1t ~100t	Ultimate Load	300% of Rated Capacity
Signal Output at Capacity	2mV/V ± 0.1%	Input Resistance	820Ω Nominal
Linearity Error	< 0.05% FSO	Output Resistance	705Ω Nominal
Non-Repeatability	< 0.02% FSO	Insulation Resistance (bridge to ground)	> 5000 MΩ at 100V DC
Combined Error	< 0.05% FSO	Insulation Resistance (cable to ground)	> 1000 MΩ at 100V DC
Hysteresis	< 0.05% FSO	Excitation Voltage (Recommended)	5 ~ 20V AC/DC
Creep/Zero Return (30 mins)	< 0.03% FSO	Excitation Voltage (Maximum)	25V AC/DC
Zero Balance	< 2.00% Capacity	Storage Temperature Range	-50 ~ 70°C
Temperature Effect on Span/10°C	< 0.02% FSO	Cable Type	5.5mm, Screened, PVC Sheath
Temperature Effect on Zero/10°C	< 0.025% Capacity		6 Core x 0.24mm² (24 AWG)
Compensated Temperature Range	-10 ~ 50°C	Cable Length	3 Metres (1t ~ 5t) 5 Metres (10t ~ 25t)
Operating Temperature Range	-30 ~ 70°C		10 Metres (50t ~ 100t)
Service Load	100% of Rated Capacity	Material	Tool steel
Safe Load	150% of Rated Capacity	Finish	Electroless Nickel Plated

IP 67

Manufactured in New Zealand

PT Limited®
http://www.pt-global.com

Precision Linear Transducers, Conductive Plastic, up to 3000 mm

FEATURES

- Measurement range 25 mm to 3000 mm
- High accuracy ± 1 % down to ± 0.025 %
- Excellent repeatability
- Essentially infinite resolution
- Simple mounting
- Actuation tolerant to some misalignment
- Reduced bulk
- Material categorization: for definitions of compliance please see www.vishay.com/doc?99912

RoHS COMPLIANT

The 139 L is a robust industrial linear motion transducer with a side actuation, ideally suited for applications with very long travels.

QUICK REFERENCE DATA	
Sensor type	LINEAR, conductive plastic
Output type	Connector
Market appliance	Industrial
Dimensions	L x 36 mm x 61 mm (with L = TET + 169 mm max.)

ELECTRICAL SPECIFICATIONS	
Theoretical electrical travel (TET) = E	From 25 mm to 3000 mm in increments of 25 mm
Independent linearity (over TET) On request	≤ ± 1 %; ≤ ± 0.1 % ≤ ± 0.05 % for E ≥ 100 mm ≤ ± 0.025 % for E ≥ 200 mm
Actual electrical travel (AET)	AET = E + 1.5 mm min.
Ohmic value (R_T)	400 Ω/cm to 2 kΩ/cm
Resistance tolerance at 20 °C	± 20 %
Repeatability	≤ 0.01 %
Maximum power rating	0.05 W/cm at 70 °C, 0 W at 125 °C
Wiper current	Recommended: a few µA - 1 mA max. (continuous)
Load resistance	Minimum 10^3 x R_T
Insulation resistance	≥ 1000 MΩ, 500 V_{DC}
Dielectric strength	≥ 1000 V_{RMS}, 50 Hz

MECHANICAL SPECIFICATIONS	
Mechanical travel (MT)	See dimensions table 1
Housing	Anodized aluminum
Operating force	2.5 N typical
Coupling	Self alignment
Termination	Hydraulic type connector DIN 43650
Wiper	Precious metal multifinger
Sealed to	IP53
Mounting	Movable brackets

PERFORMANCE	
Operating life	40 million cycles typical/1 Hz/T° = 20 °C ± 5 °C/80 % TET
Temperature range	-55 °C to +125 °C
Sine vibration on 3 axes	1.5 mm peak to peak or 15 *g* - 10 Hz - 2000 Hz
Mechanical shocks on 3 axes	50 *g* - 11 ms - half sine
Speed (max.)	8 m/s for f < 2 Hz; 3 m/s for f < 5 Hz

Note

- Nothing stated herein shall be construed as a guarantee of quality or durability.

Model Number	ICP® PRESSURE SENSOR	Revision: C
113B26		ECN #: 40791

Performance	ENGLISH	SI	
Measurement Range(for ±5V output)	500 psi	3450 kPa	
Useful Overrange(for ± 10V output)	1 kpsi	6895 kPa	[2]
Sensitivity(± 10 %)	10 mV/psi	1.45 mV/kPa	
Maximum Pressure	10 kpsi	68,950 kPa	
Resolution	2 mpsi	0.014 kPa	[1]
Resonant Frequency	≥ 500 kHz	≥ 500 kHz	
Rise Time	≤ 1.0 µ sec	≤ 1.0 µ sec	
Low Frequency Response(-5 %)	0.01 Hz	0.01 Hz	
Non-Linearity	≤ 1.0 % FS	≤ 1.0 % FS	[3]
Environmental			
Acceleration Sensitivity	≤ 0.002 psi/g	≤ 0.0014 kPa/(m/s²)	
Temperature Range(Operating)	-100 to +275 °F	-73 to +135 °C	
Temperature Coefficient of Sensitivity	≤ 0.03 %/°F	≤ 0.054 %/°C	[1]
Maximum Flash Temperature	3000 °F	1649 °C	
Maximum Vibration	2000 g pk	19,614 m/s² pk	
Maximum Shock	20,000 g pk	196,140 m/s² pk	
Electrical			
Output Polarity(Positive Pressure)	Positive	Positive	
Discharge Time Constant(at room temp)	≥ 50 sec	≥ 50 sec	
Excitation Voltage	20 to 30 VDC	20 to 30 VDC	
Constant Current Excitation	2 to 20 mA	2 to 20 mA	
Output Impedance	<100 Ohm	<100 Ohm	
Output Bias Voltage	8 to 14 VDC	8 to 14 VDC	
Physical			
Sensing Geometry	Compression	Compression	
Sensing Element	Quartz	Quartz	
Housing Material	17-4 Stainless Steel	17-4 Stainless Steel	
Diaphragm	Invar	Invar	
Sealing	Welded Hermetic	Welded Hermetic	
Electrical Connector	10-32 Coaxial Jack	10-32 Coaxial Jack	
Weight(with clamp nut)	0.20 oz	6.0 gm	

CE[4]

All specifications are at room temperature unless otherwise specified.
In the interest of constant product improvement, we reserve the right to change specifications without notice.

ICP® is a registered trademark of PCB Group, Inc.

OPTIONAL VERSIONS

Optional versions have identical specifications and accessories as listed for the standard model except where noted below. More than one option may be used.

E - Emralon coating [5]

Coating	Emralon	Emralon
Electrical Isolation	10^8 Ohm	10^8 Ohm

Supplied Accessory : Model 065A08 Isolation ring 0.250"OD x 0.218" ID x 0.027" thk anodized aluminum (3)
Supplied Accessory : Model 065A22 Isolation Seal, .250" OD x .218" ID x .015", Torlon or Vespel (3)

H - Hermetic Seal [5]

Sealing	Welded Hermetic	Welded Hermetic

J - Ground Isolated [5][6]

N - Negative Output Polarity [5]

S - Stainless Steel Diaphragm [5]

Diaphragm	316L Stainless Steel	316L Stainless Steel

W - Water Resistant Cable [7][5]
Supplied Accessory : Model 060A03 Clamp nut, 5/16-24-2A thd, 1/4" hex, stainless steel (1)

WM - Water Resistant Cable [7][5]
Supplied Accessory : Model 060A05 Clamp nut M7 x 0.75-6g thd (1)

NOTES:

[1] Typical.
[2] For +10 volt output, minimum 24 VDC supply voltage required. Negative 10 volt output may be limited by output bias.
[3] Zero-based, least-squares, straight line method.
[4] See PCB Declaration of Conformance PS023 for details.
[5] For sensor mounted in thread adaptor, see adaptor installation drawing for supplied accessories.
[6] Used with optional mounting adaptor.
[7] Clamp nut installed prior to cable attachment

SUPPLIED ACCESSORIES:

Model 060A03 Clamp nut, 5/16-24-2A thd, 1/4" hex, stainless steel (1)
Model 060A05 Clamp nut M7 x 0.75-6g thd (1)
Model 065A02 Seal ring, sensor flush mount, 0.248" OD x 0.219" ID x 0.015" thk, brass (3)
Model 065A05 Seal sleeve sensor recess mount 0.248" OD x 0.221" ID x 0.240" thk 17-4 (1)

Entered: AP	Engineer: MJK	Sales: KWW	Approved: BAM	Spec Number:
Date: 3/19/2013	Date: 3/19/2013	Date: 3/19/2013	Date: 3/19/2013	40649

PCB PIEZOTRONICS
3425 Walden Avenue, Depew, NY 14043
Phone: 716-684-0001
Fax: 716-684-0987
E-Mail: info@pcb.com